REPORT DOCUMENTATION PAGE

AFRL-SR-BL-TR-98-

0342

1. AGENCY USE ONLY (*Leave Blank*)	2. REPORT DATE	3. REPORT TYPE AND DATES COVERED
	March 31, 1998	Final Technical 1 March 93 - 31 October 97

4. TITLE AND SUBTITLE
Improved Location, Green's Functions and Source Discrimination for Regional Events in Korea and Iran

5. FUNDING NUMBERS
F49620-94-1-0179

6. AUTHORS
Shelton S. Alexander

7. PERFORMING ORGANIZATION NAME(S) AND ADDRESS(ES)
The Pennsylvania State University
Department of Geosciences
University Park, PA 16802

8. PERFORMING ORGANIZATION REPORT NUMBER
N/A

9. SPONSORING / MONITORING AGENCY NAME(S) AND ADDRESS(ES)
Air Force Office of Scientific Research /NM
AFOSR/NP, Building 410
Bolling AFB, DC 20332

10. SPONSORING / MONITORING AGENCY REPORT NUMBER

11. SUPPLEMENTARY NOTES

12a. DISTRIBUTION / AVAILABILITY STATEMENT
Approved for Public Release; distribution unlimited

12b. DISTRIBUTION CODE

13. ABSTRACT *(Maximum 200 words)*

This study has developed new methods for improved discrimination of seismic events and improved hypocenter determinations using regional observations. Their implementation in a form suitable for near-real time applications was also carried out. Most of this research has been reported in technical articles and in three student theses (1 PhD; 1 MS, and 1 BS) completed as part of the project. Significant accomplishments in the research include: (1) Development and implementation of a new, trained artificial neural network method for rapidly identifying regional earthquakes and explosions using frequency-velocity seismic images of entire signatures; (2) Development and implementation of new cepstral stacking method (CSM) that can determine seismic source depth accurate to approximately 1 km using a single regional recording of an event of interest; (3) Extension of the CSM to allow a combination of individual stations and array or network recordings to be used to obtain accurate source depth estimates; (4) Application of these methods to: earthquakes and mining explosions in Scandanavia; Semipalatinsk nuclear explosions and a nearby earthquake; Chinese earthquakes and Lop Nor and Semipalatinsk nuclear explosions; and regional events in Iran and Korea.

14. SUBJECT TERMS
Source depth; region event identification; artificial neural networks; cepstral stacking; regional discriminants; CTBT monitoring

15. NUMBER OF PAGES
90

16. PRICE CODE

17. SECURITY CLASSIFICATION OF REPORT	18. SECURITY CLASSIFICATION OF THIS PAGE	19. SECURITY CLASSIFICATION OF ABSTRACT	20. LIMITATION OF ABSTRACT
N/A	N/A	N/A	SAR

NSN 7540-01-280-5500

Standard Form 298 (Rev. 2-89)
Prescribed by ANSI Std. Z39-1
298-102

IMPROVED LOCATION, GREEN'S FUNCTIONS AND SOURCE DISCRIMINATION FOR REGIONAL EVENTS IN KOREA AND IRAN

Final Report

Period Reported: 1 March 1993 - 31 October 1997

Sponsored By:

Department of the United States Air Force
Air Force Office of Scientific Research
Building 410
Bolling AFB, DC 20332
AFOSR Grant No. F49620-94-1-0179

Principal Investigator: Shelton S. Alexander

Telephone No.: (814) 863-7246

The Pennsylvania State University
Office of Sponsored Programs
110 Technology Center
University Park, PA 16802

March 1998

SUMMARY

This study has developed new methods for improved discrimination of seismic events and improved hypocenter determinations using regional observations. Their implementation in a form suitable for near-real-time applications was also carried out. Most of this research has been reported in technical articles and in three student theses (1 PhD, 1 MS, and 1 BS) completed as part of the project.

Significant accomplishments in the research include:

1. Development and implementation of a new,trained artifical neural network method for rapidly identifying regional earthquakes and explosions using frequency-velocity seismic images of entire signatures.

2. Development and implementation of new cepstral stacking method (CSM) that can determine seismic source depth accurate to approximately 1 km using a single regional recording of an event of interest.

3. Extension of the CSM to allow a combination of individual stations and array or network recordings to be used to obtain accurate source depth estimates.

4. Application of these methods to: earthquakes and mining explosions in Scandanavia; Semipalatinsk nuclear explosions and a nearby earthquake; Chinese earthquakes and Lop Nor and Semipalatinsk nuclear explosions; and regional events in Iran and Korea.

BRIEF DESCRIPTION OF RESEARCH RESULTS

This section provides in a condensed form a discussion of the most important advances resulting from this grant. Further details are provided in the publications based on this research that are listed at the end of this section and the Appendices to this report.

Depth Determinations

A major result of this study was to develop a Cepstral Stacking Method (CSM) for determining source depths reliably and accurately for shallow (crustal) earthquakes and explosions recorded at regional distances. If source depths accurate to about 1 km or better can be determined rapidly and routinely for all events larger than about magnitude 2.5, a major fraction of crustal earthquakes could be eliminated from further consideration under a CTBT, because only the shallowest events (less than about 5 km) will include possible explosions.

Focal depths from regional or teleseismic P-wave travel-time observations (hypocenters) typically are not accurate, especially when there are only a few stations, none of which is close to the epicenter. Because of the complexity of regional signals, direct identification of depth phases (pP - P and sP - P) usually is not feasible. Therefore, depth estimates made without any pP-P or

sP-P data may be biased and inaccurate. For example, teleseismic depth estimates for Iran appear to be systematically biased too deep by 5-10 km or more (Karl, 1995); thus shallow events less than 5 km deep could be mistaken for deeper events and eliminated from consideration as candidate explosions. The CSM overcomes this difficulty and provides reliable and accurate depth-phase delay times for small events for which reliable teleseismic depth-phase picks cannot be made.

Our earlier work on source depth in this study was focused on the development and testing of the CSM for application to single regional stations (e.g. Alexander, et al., 1995; Karl, 1995; Alexander, 1995). The most-recent research (e.g. Alexander and Yang (1997), Yang (1996)) has been focused on further developing the CSM approach and taking advantage of combined single-station stacking and stacking over new IMS monitoring arrays (Alpha arrays) and distributed regional stations. Details can be found in the references cited above (all based on this grant research).

Using only a single station, the CSM enhances depth phases, because each sub-window in the P and P-coda total window contains the same, or nearly the same, (pP - P) and (sP - P) delay times, whereas delay times for distinct crustal phases appear in at most a few sub-windows, as illustrated schematically in Figure 1. By stacking the cepstra (product or sum) of these sub-windows the depth-phase delay times common to all sub-windows are enhanced while crustal-phase delay times are not.

Figure 2 illustrates how the method works for a magnitude 4.6 regional earthquake in central Iran recorded at the ILPA array station IR1 at a distance of 639 km; the prominent depth-phase cepstral peak at 7.1 seconds is verified by 6 independent teleseismic pP - P delay times reported in the ISC Bulletin that agree within 0.1 seconds of this time. The corresponding depth is approximately 21 km (assuming an average crustal velocity of 6 km/sec), clearly identifying this event as an earthquake. Details can be found in Karl (1995) and Yang (1996).

As another illustration of the method, the results of single-station CSM cepstral stacking for a Soviet Test Site (Degelen) magnitude 5.2 underground nuclear explosion and a nearby magnitude 5.1 earthquake recorded at the regional SRO station MAIO at a distance of approximately 2100 km are shown in Figures 3 and 4 respectively. There is a prominent cepstral peak for the earthquake at a delay time between 5 and 5.5 seconds corresponding to a source depth of approximately 15 km if the depth phase is pP, and somewhat less if it is sP; in contrast, the cepstral peak for the explosion occurs at a small delay of less than 1 second (possibly not distinguishable from the large peak at zero delay time, because of the limited signal bandwidth), indicating a shallow depth. Figure 5 shows the seismic images (frequency-velocity) for these two events and two other Degelen explosions; the relative exitation of Lg and P for the event of March 20, 1976 is distinctively different (larger) compared to that of the explosions, as expected, further confirming that this event is an earthquake. This distinction can also be clearly seen in the band-pass-filtered signals shown in Figures 3 and 4.

Extension of the CSM by stacking individual-station stacked cepstra over a local array (Alpha array) or regional network of individual stations was found to result in significant further

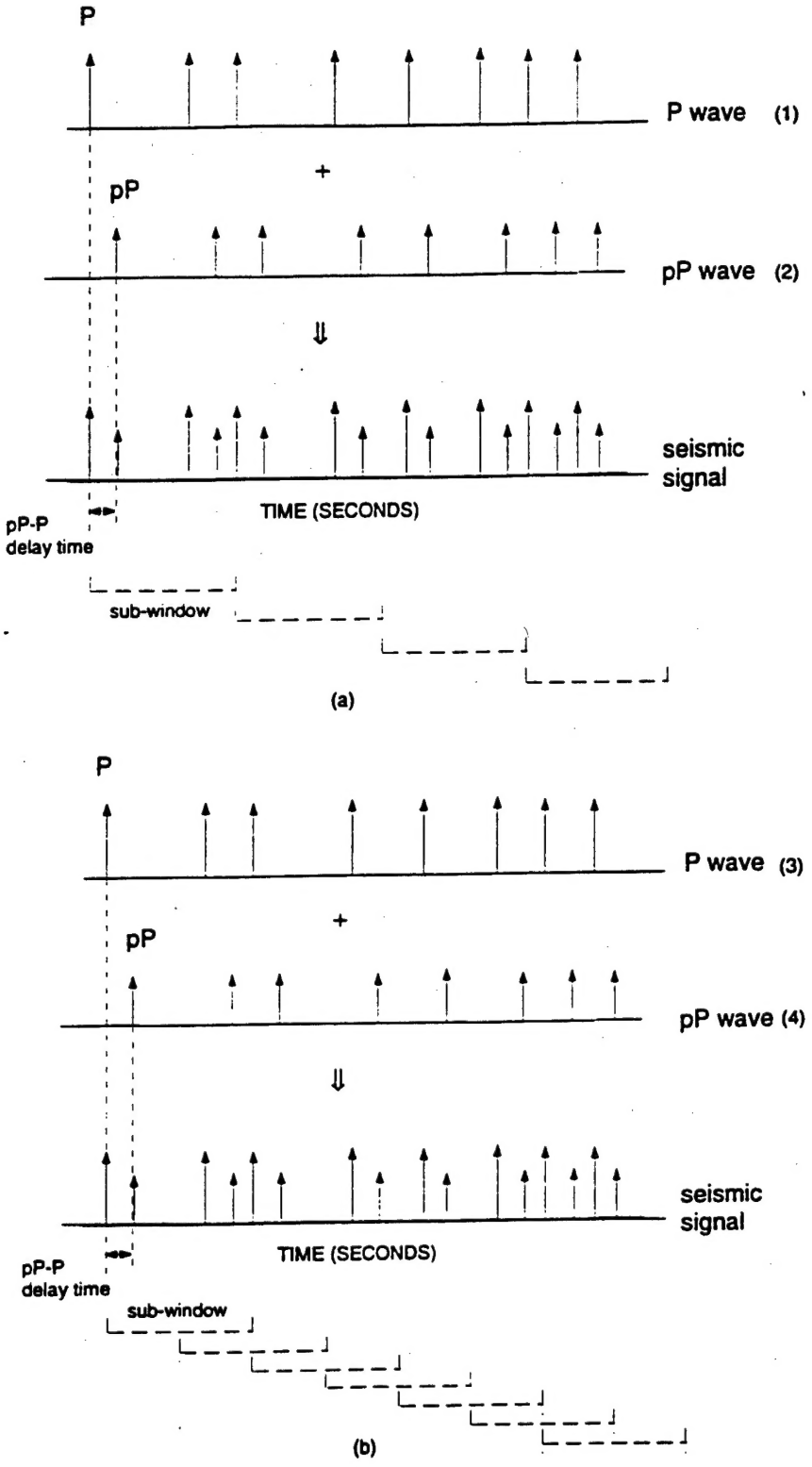

Figure 1. Schematic diagram depicting non-overlapping (a) and overlapping (b) sub-windows spanning the S-P window. Note that the panel pP doublet is present one or more times in every sub-window. The polarity of pP can be the same or opposite that of P (shown here as the same).

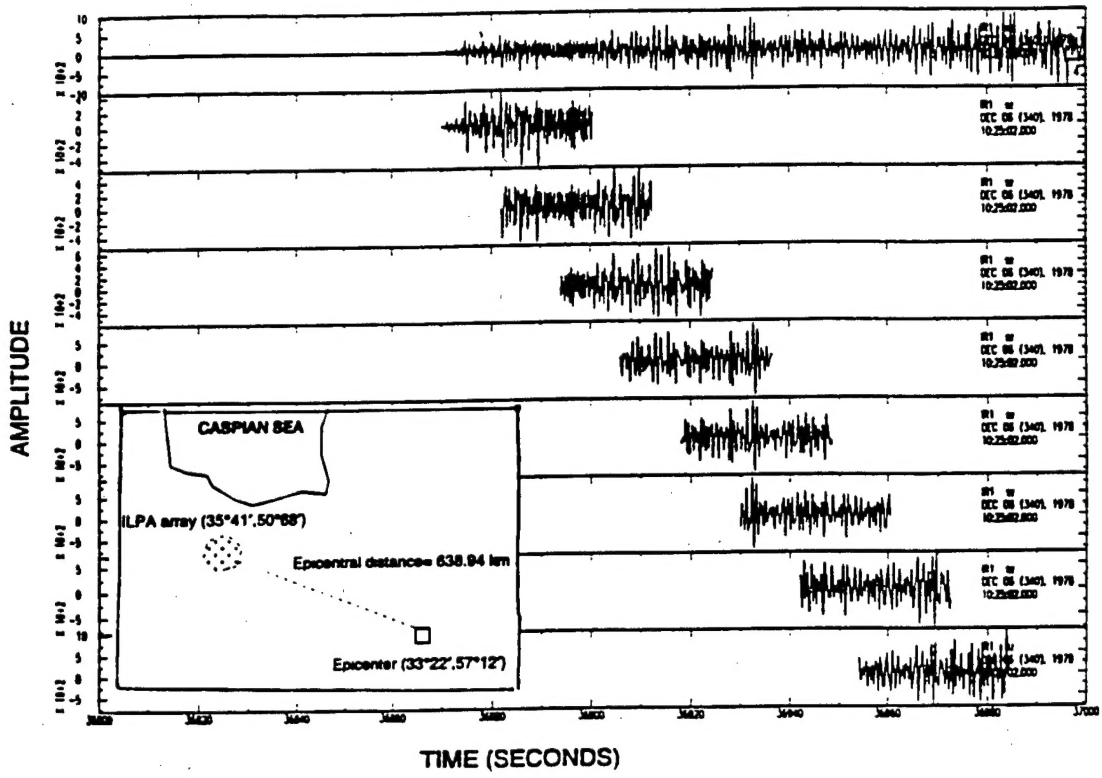

Figure 2a. Iranian earthquake recorded regionally by ILPA array station IR1 with sub-windows (30 seconds) and overlaps (60 percent) used for cepstral stacking.

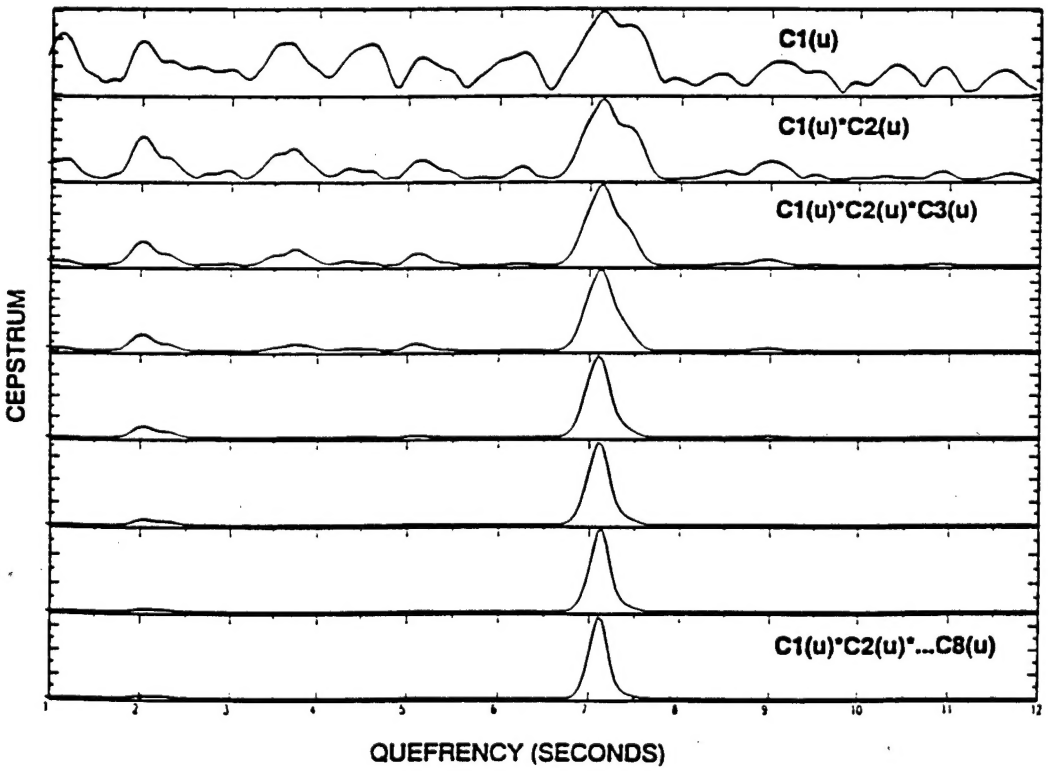

Figure 2b. Step by step product stacking of cepstra for successive sub-windows shown in Figure 2a illustrating how the depth-phase delay time of 7.1 seconds is enhanced.

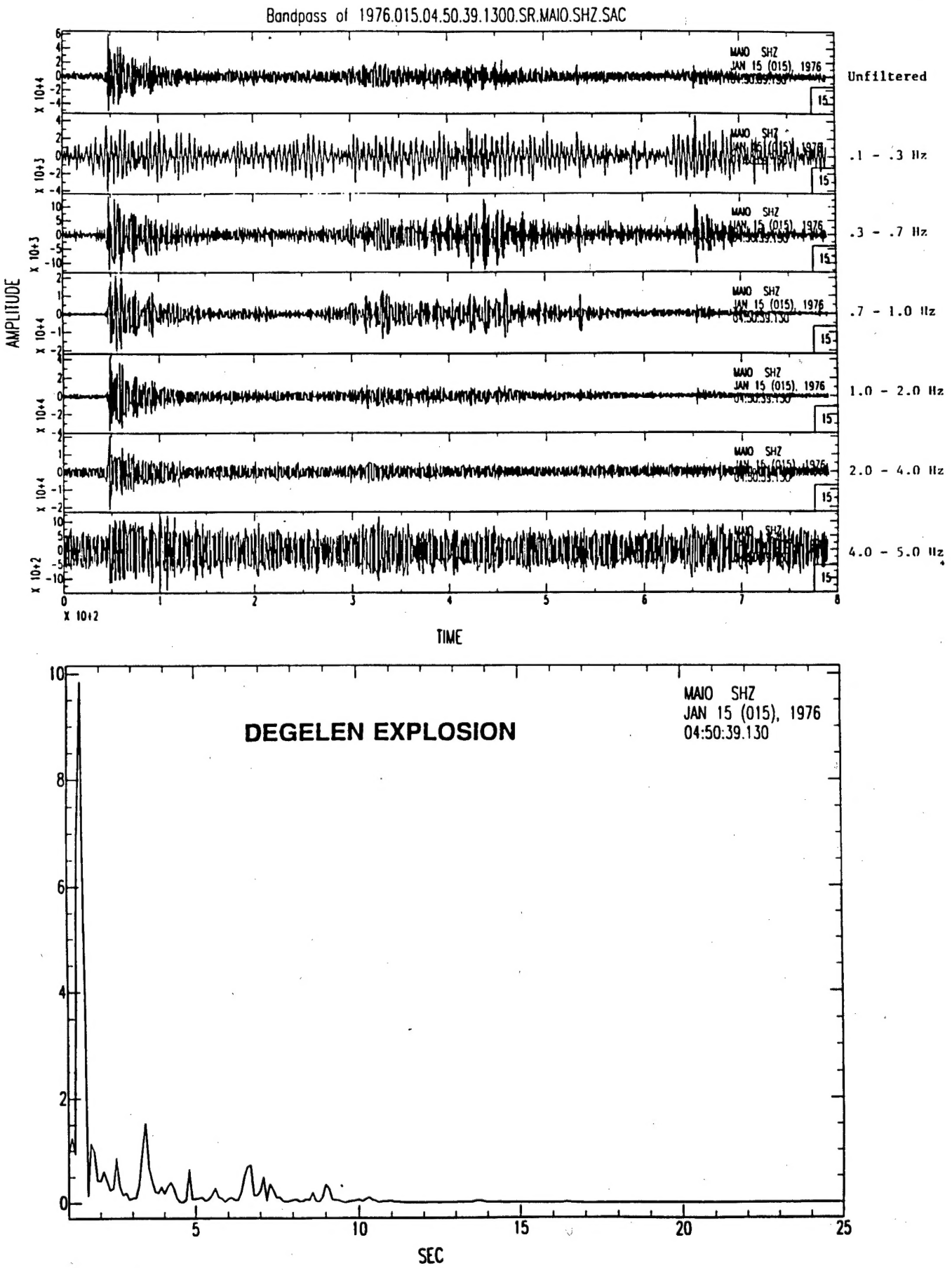

Figure 3. Cepstral stacking result (bottom panel) for the magnitude 5.2 Degelen nuclear explosion shown in the top panel. Distance is approximately 2100 km.

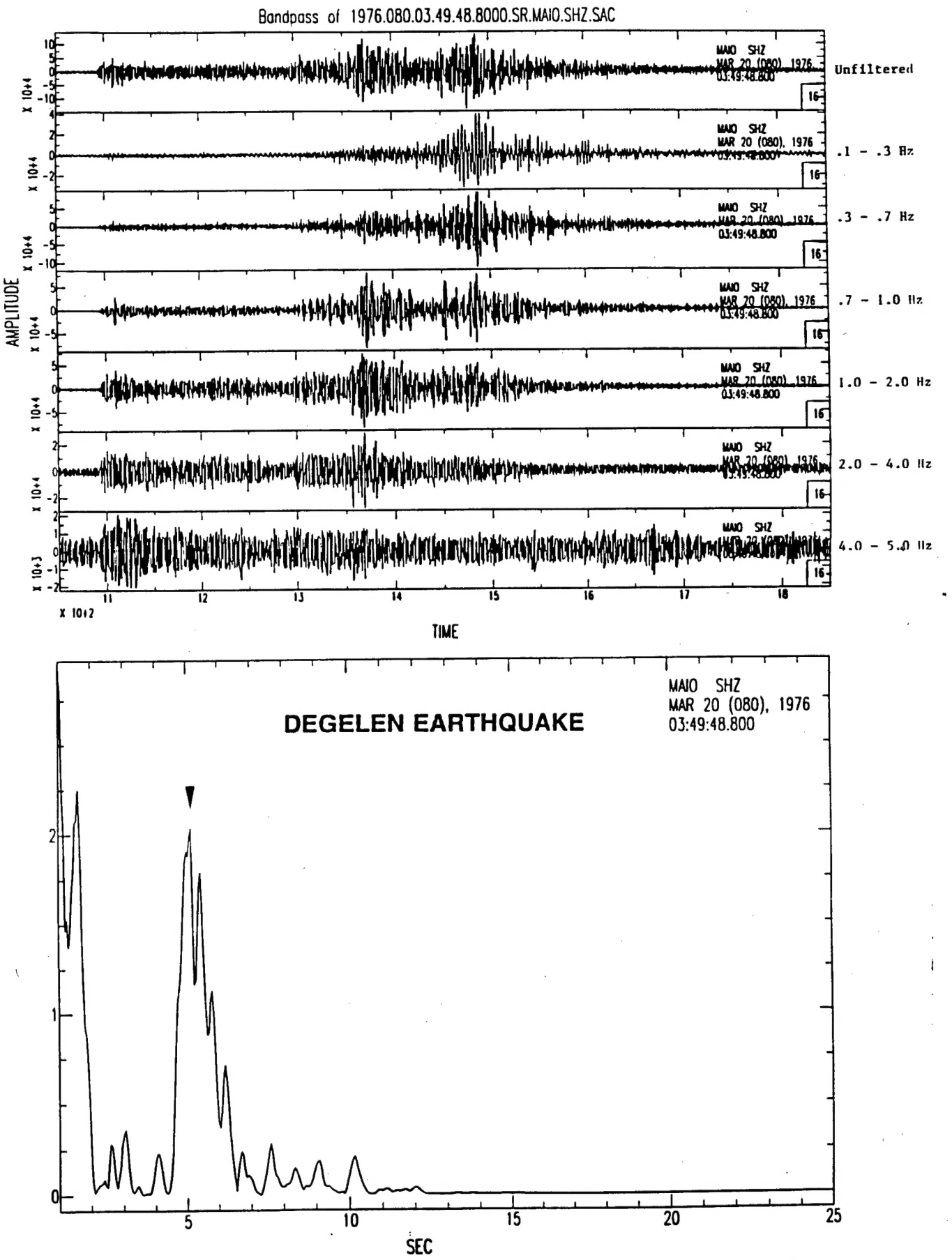

Figure 4. Cepstsral stacking result (bottom panel) for the magnitude 5.1 Degelen earthquake shown in the top panel. Distance is approximately 2100 km.

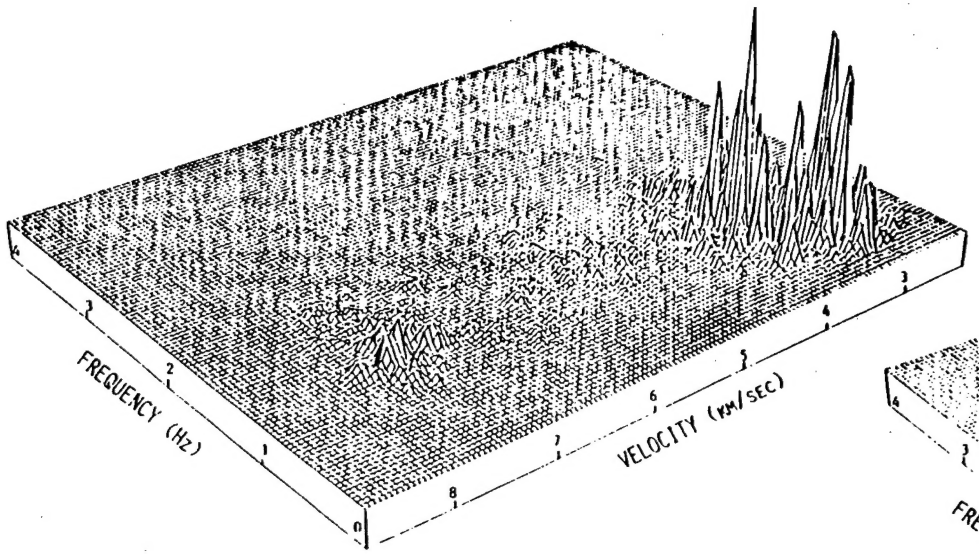

Event of 03/20/76, m_b 5.1, recorded at SRO station MAIO

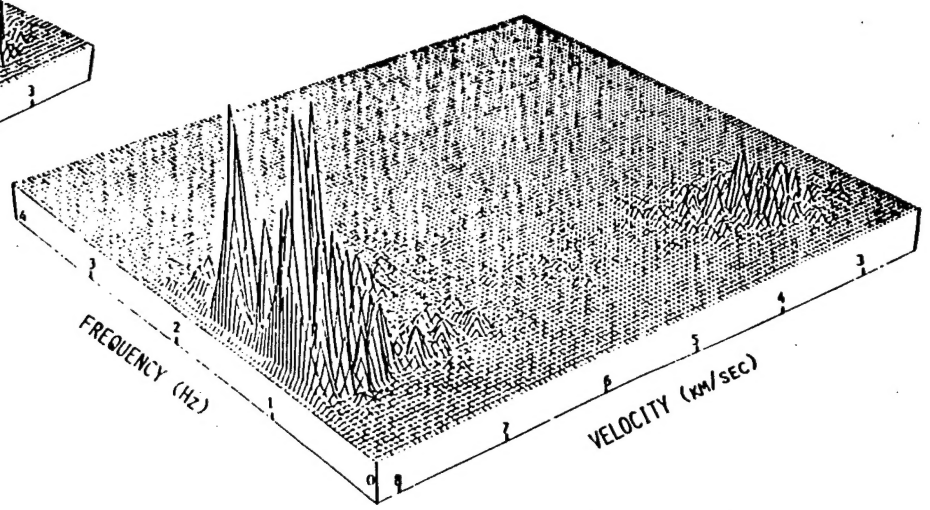

Event of 11/23/76, m_b 5.8, recorded at SRO station MAIO

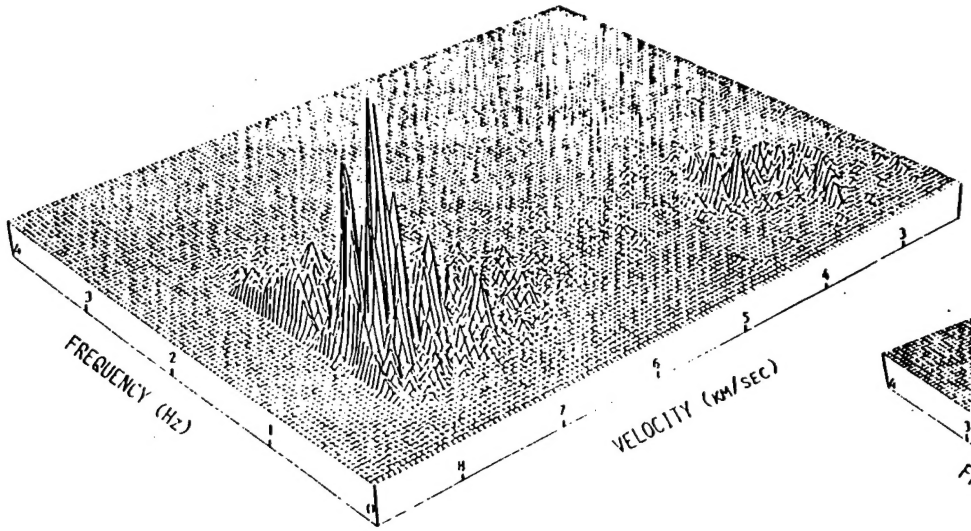

Event of 01/15/76, m_b 5.2, recorded at SRO station MAIO

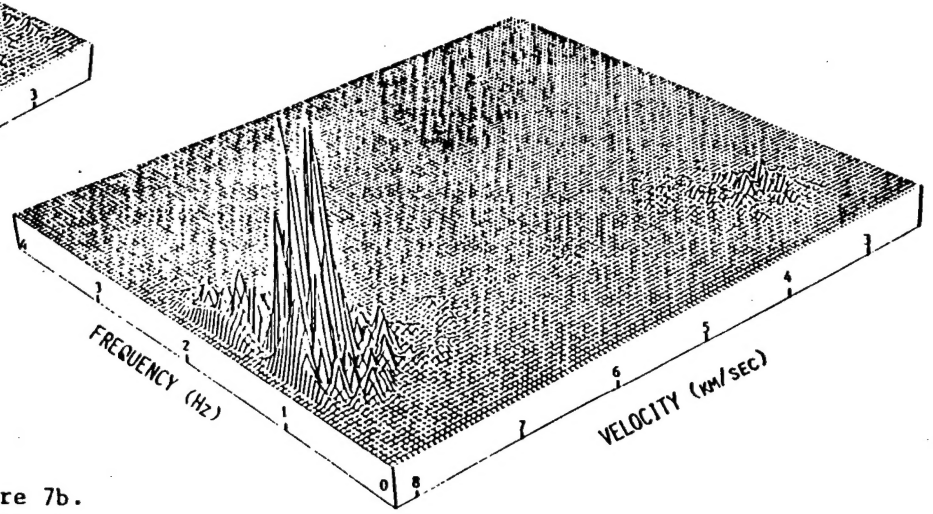

Event of 05/29/77, m_b 5.8, recorded at SRO station MAIO

Figure 7b.

Figure 5. Seismic images (frequency vs. velocity) for four events in the Degelen area of the Soviet Test Site recorded at the SRO station MAIO in Iran. Distance is approximately 2100 km.

enhancement of depth-phase delay times (Alexander and Yang, 1996; Yang (1996); Alexander and Yang, 1997). The reason for further enhancement is that other cepstral peaks ("noise") in individual-station, stacked cepstra that may result from receiver site effects such as P to S conversions at sharp layer boundaries beneath the station, discrete local scatterers, multipathing, or random noise generally are not in common among separated stations and consequently are suppressed after network stacking, compared to the depth-phase delay times common to all stations. As in the single-station case, product stacking is more effective than sum-stacking over an array or network; however, if some stations have a poor signal-to-noise ratio relative to others, sum-stacking may be more appropriate, because S/N weighting can be used.

As an example, Figure 6 compares several individual-station, product-stacked cepstra and the combined array-stacked cepstrum for a magnitude 4.6 earthquake in the Yellow Sea recorded regionally (distance of approximately 470 km) at the KS array in Korea. The combined stack has a single, sharp peak at about 2 seconds. Similarly, Figure 7 shows the individual-station, product-stacked cepstra and the combined stack for widely-separated regional stations in China for the same event; the combined, four-station stack has a single dominant peak at about 2.1 seconds, in close agreement with the KS array-stacked result. If this is the pP delay time, the source depth is approximately 5-6 km; the depth is approximately 4 km if the delay time is sP.

Comparable enhancements of depth phases for regional events have been found using MAIO and the ILPA array in Iran and the TXAR Alpha array in Texas (Yang, 1996).

Yang (1996) implemented and tested other modifications of the CSM that may be useful in enhancing the desired delay times. Effects of noise can be reduced by bandpass filtering the signal, keeping only frequencies where the S/N in the power spectrum is greater than some chosen level; the tradeoff is a reduction in the band-width of the remaining signal, which limits the time resolution of the depth-phase cepstral peak(s). Subtracting the noise power obtained from a noise window ahead of the first P arrival from the power spectrum of each sub-window before computing the sub-window cepstrum is another alternative for suppressing noise effects; this should be done when the S/N is low over the entire frequency band. An new envelope-normalization approach was implemented for reducing cepstral peaks from prominent crustal phase delay times relative to depth-phase cepstral peaks; it consists of computing the envelope of the input signal and dividing the input signal by the envelope before applying the CSM. An example comparing the CSM results using each of these procedures and the conventional approach where none of these special procedures is used is shown in Figure 8 for a single KS array station. Figure 9 shows the corresponding combined stacking results for the KS array. All appear to work, but none consistently outperforms the other for the events analyzed, all of which have relatively high S/N; however, results for other events and other areas suggest that the envelope normalization gives the most-consistent results.

Yang (1996) also carried out tests to determine the dependence of the CSM results on sub-window length and percent overlap of successive sub-windows. It was found that in terms of signal-to-noise ratio (SNR) of the cepstral peak the sum-stacked results are relatively insensitive to either sub-window length or percent overlap. In contrast the SNR of the product-stacked cepstral peak has a strong dependence on both; the SNR increases as the sub-window length

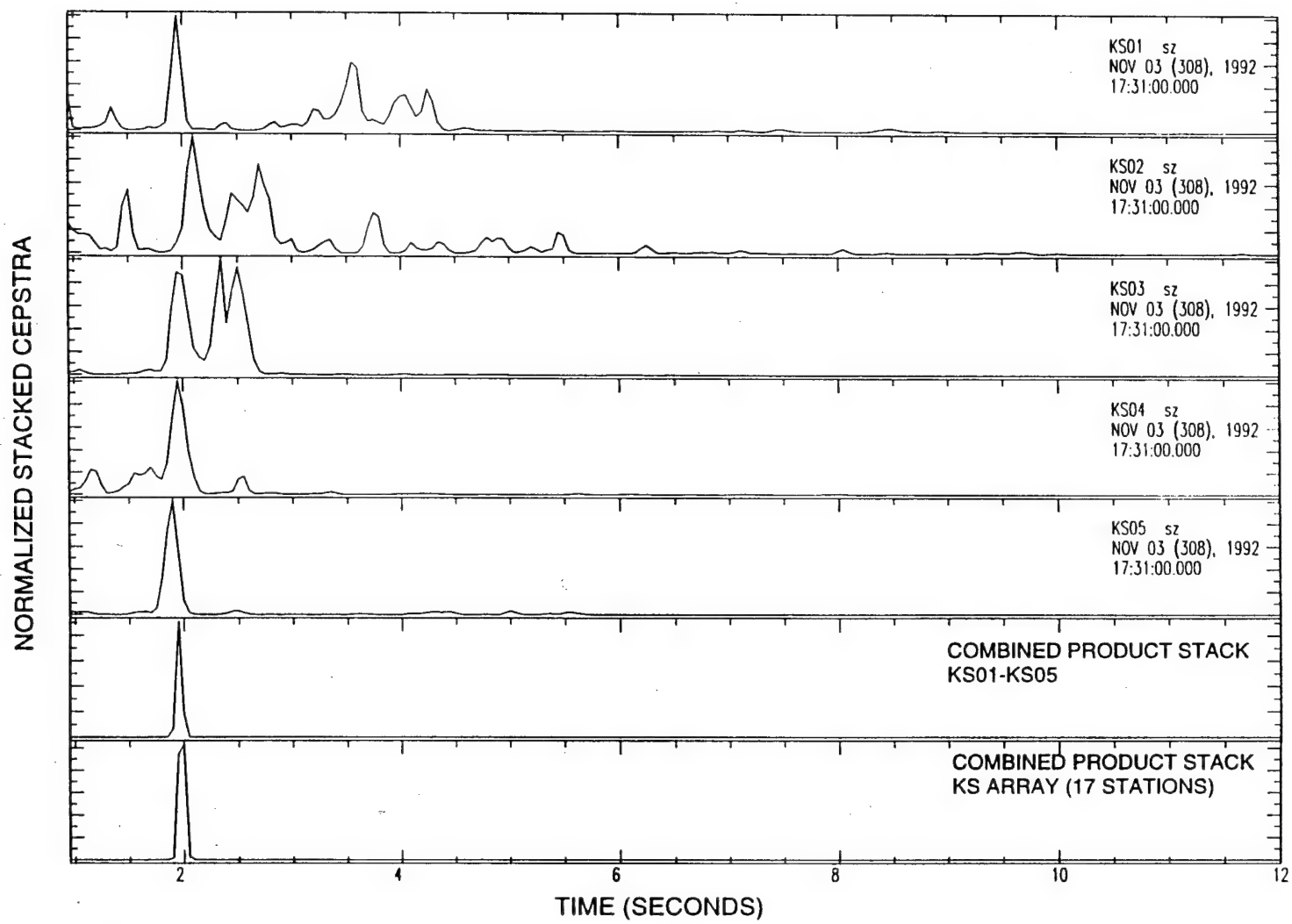

Figure 6. Individual station, product-stacked cepstra for a magnitude 4.6 regional earthquake in the Yellow Sea (istance approximately 470 km) recorded at the KS array in Korea (top 5 panels). Combined product-stacked cepstra for the five stations and for the entire KS array are shown (bottom two panels) showing a prominent depth-phase cepstral peak at about 2 sec.

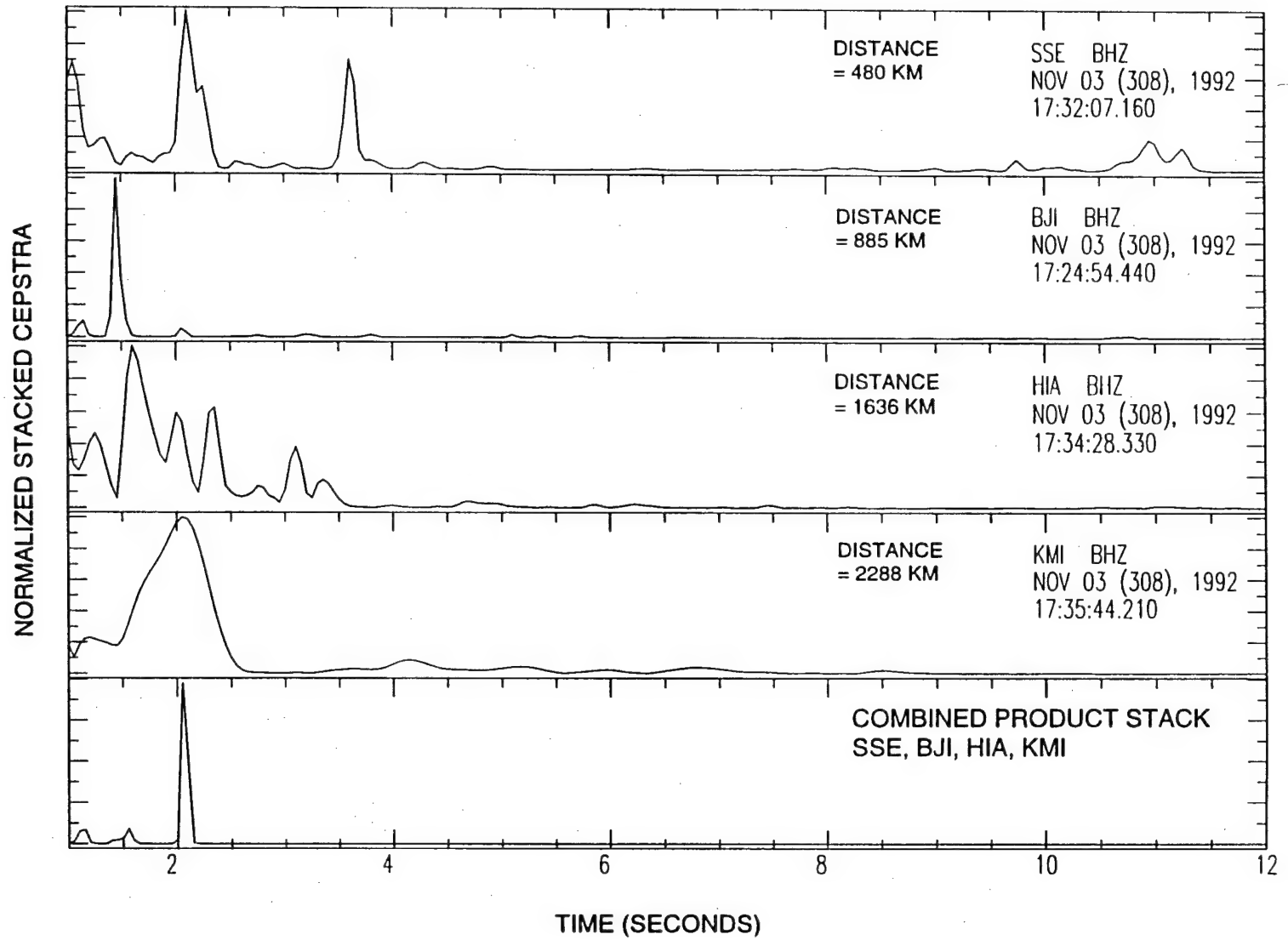

Figure 7. Individual-station, product-stacked cepstra for the magnitude 4.6 regional earthquake in the yellow Sea precorded at four widely-separated regional distances in China (top 4 panels). The combined product-stacked cepstra for the four reigonal stations (bottom panel) has a prominent depth-phase cepstral peak at about 2.1 seconds in close agreement with the results for the KS array (Figure 6).

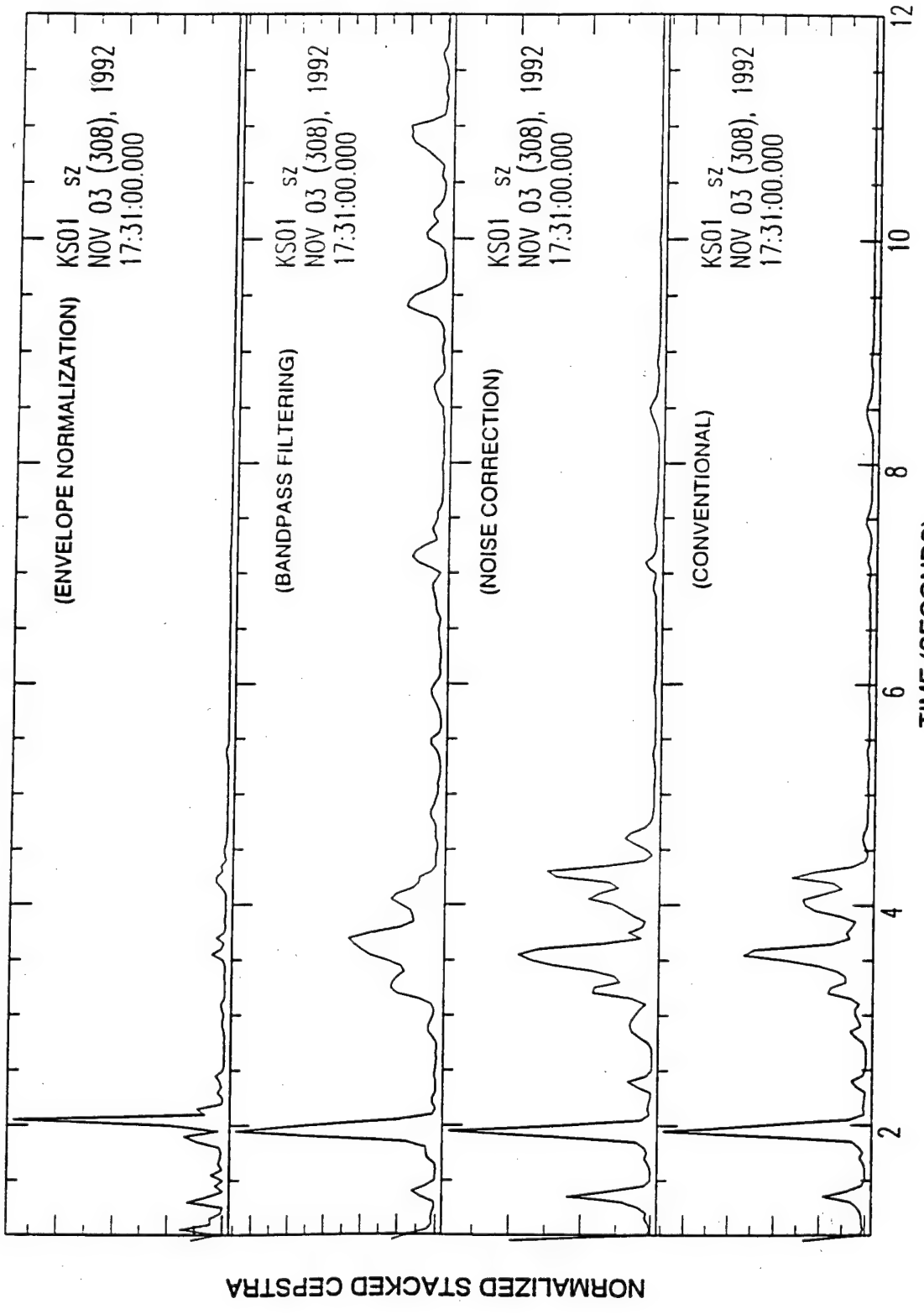

Figure 8. Comparison of the conventional and modified CSM approaches for KS array station KS01 for the 3 November 1992 Yellow Sea earthquake.

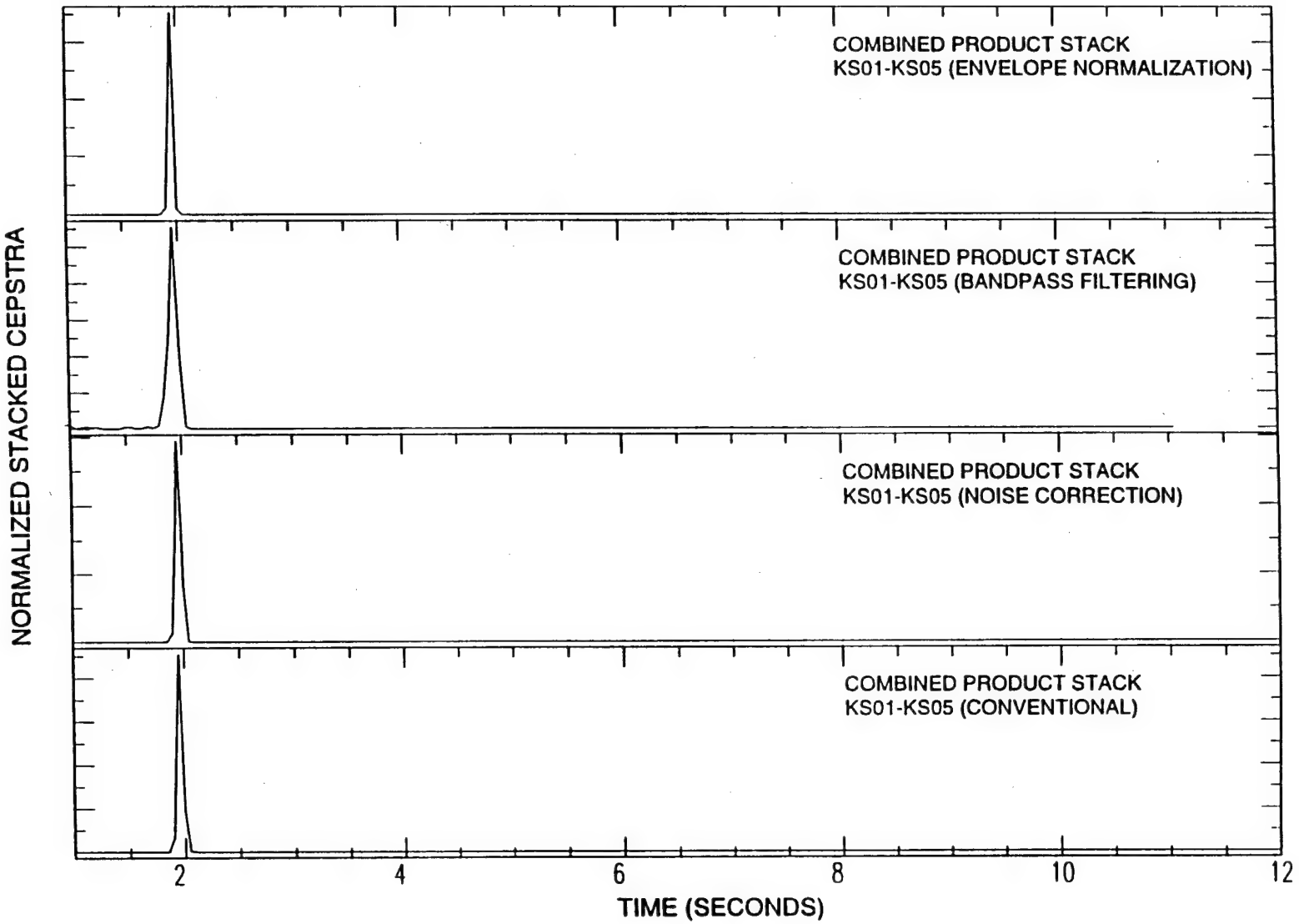

Figure 9. Comparison of the combined product-stacked cepstra for the conventional and modified CSM approaches using all stations in the KS array for the 3 November 1992 Yellow Sea earthquake.

decreases and as the percent overlap increases. Tables 1 and 2 for an Iranian regional earthquake illustrate these dependencies. Because product-stacking is more effective than sum-stacking, relatively short sub-windows and overlaps of over 50 percent should be used, based on the tests carried out thus far. However, the sub-window length must be greater than the (unknown) depth-phase delay time; using a sub-window length of 20 seconds or greater would allow the CSM method to work for events anywhere in the crust in most regions of interest.

It is important to note that the CSM can be automated and applied in near-real time for operational use. Once an event is detected and located, the P and P-coda time window before the S arrival can be determined for each regional station or array element and the cepstral stacking carried out for overlapping sub-windows spanning this interval; in turn these individual stacked cepstra can be stacked over all regional stations and array elements. If a single dominant peak is found, its delay time can be used to estimate source depth, assuming alternatively that it is pP or sP; if two prominent peaks are present with the appropriate relative times to be pP and sP, the event is likely to be an earthquake and its depth can be calculated. To calculate the depth from the depth-phase delay time(s) the crustal velocity structure at the source is needed; this can be extracted from a data base of crustal structure in the vicinity of the epicenter. However, the crustal velocities need to be known only approximately to obtain depths accurate to within 1 km for shallow events; for example, if the delay time is 2 seconds, the inferred depth would be about 6 km, if the average crustal velocity is 6 km/sec, and 5 km if the velocity is 5 km/sec. Except for source areas with thick, low-velocity sedimentary sections, depth-phase delay times greater than about 2-3 seconds will correspond to a source depth greater than 5 km and, therefore, indicate that the event is an earthquake.

Software implementing the CSM was developed and used for applications of the CSM. This software has been provided to AFTAC researchers for their further evaluation and possible use in monitoring.

Regional Event Identification

An event with a source depth greater than about 5 km is almost certainly an earthquake. When such an estimate is obtained using the CSM, several relatively straightforward other analyses can be carried out to verify that the event is an earthquake and that it is deeper than 5 km. These include the absence of 1-2 second Rg signals for source-station paths known to transmit Rg, radiation patterns in body and surface waves (e.g. dilatational first P motions at some azimuth(s) and azimuthally-varying Rayleigh wave amplitudes), characteristic Love to Rayleigh wave spectral ratios, and relatively-large, high-frequency Lg/P ratios.

An event with a CSM source depth less than about 5 km can be either an earthquake or an explosion (chemical or nuclear). Verification that the event is shallower than 5 km can come from the presence of 1-2 second Rg signals at the closer regional stations, the presence of a later-arriving acoustic wave associated with the seismic signal at a time consistent with air-wave propagation to the receiver, characteristic Love to Rayleigh spectral ratios and evidence of some surface disturbance associated with the event.

Table 1. Comparison of SNRs of product- and sum-stacked cepstral peaks for different sub-window lengths for the regional Iranian earthquake recorded at IR1 (Figure 2a).

	SNR (Product stack)	SNR (Sum stack)
Sub-window length=60sec.	41.0	4.3
Sub-window length=50sec.	101.9	3.8
Sub-window length=40sec.	178.0	3.4
Sub-window length=30sec.	287.5	2.7
Sub-window length=20sec.	537.9	2.1

Table 2. Comparison of SNRs of product- and sum-stacked cepstral peaks for different sub-window overlap percentages for the regional Iranian earthquake recorded at IR1 (Figure 2a).

	SNR (Product stack)	SNR (Sum stack)
Overlap percentage=60%	287.5	2.7
Overlap percentage=40%	125.4	3.1
Overlap percentage=20%	47.2	3.0
Overlap percentage=10%	42.8	2.9
Overlap percentage= 0%	38.3	2.9

However, the actual identification of very shallow events must be made using other regional discriminants such as high-frequency Lg/P ratios, Ms vs mb values typical of earthquake or explosive sources; radiation patterns of P and Rayleigh waves or lack thereof; relative excitation of other crustal phases; accurate event location (e.g. at or very near an active mining area or very close to an active fault); and the presence of spectral modulation throughout the signal (ripple-fired mining blasts or repeated events). Appendix A summarizes the application of these types of source discriminants for thirteen regional events in Iran, recorded at the station MAIO. In addition, Figure 10 shows two examples of shallow regional events in Iran. Small CSM depth-phase delay times and the presence of Rg indicate that both of these events are shallow, but the stacked cepstra (Figure 10e) show that the February 23, 1977 event is deeper (around 7 km) than the June 4, 1977 event (about 2.5 km); both are identified as earthquakes.

If an event is identified as an explosion using discriminants other than depth, then a very shallow depth estimate that is accurate to within about 1 km would help to corroborate the identification. Therefore, the CSM could be applied to obtain a depth estimate for any event suspected to be an explosion to verify that the event is very shallow. For example, the Soviet Test Site (Degelen) event of 20 March 1978 could be classified as an explosion, based on the similarity of its frequency-velocity seismic image at the regional SRO station MAIO to those of other, larger underground nuclear explosions at Degelen, as shown in Figure 5. The CSM results for this event, shown in Figure 4, confirm that it is very shallow.

In earlier work in this study by Hsu and Alexander (1994) on the use of pattern recognition for regional event identification it was shown that transformation of regional signals into seismic images (frequency-velocity or frequency-slowness) permits direct comparison among events located at different distances of the partitioning of signal energy in the earlier, P-wave portion of the signal to that in the later, S and Lg portion. Normalization by the maximum for each frequency approximately removes effects of frequency-dependent attenuation and source spectral shape differences for events of different magnitude. These normalized seismic images can then be used for visual pattern recognition to identify events, as in Figure 5, and they can be used in more-sophisticated, formal pattern recognition identification schemes, including trained artificial neural networks (ANNs) (e.g. Hsu (1995), Hsu and Alexander (1994)). These images were used both for layered perceptron and image reconstruction ANNs and shown to correctly identify regional earthquakes and mining explosions in western Scandanavia, recorded at the NORESS array. Hsu (1995) also applied the same approach to a set of widely-distributed regional earthquakes and nuclear explosions at Semipalatinsk and Lop Nor, all recorded at the station WMQ. Interestingly, when the Lop Nor explosion was excluded from the training, such that all the underground explosions used in the ANN training were located at Semipalatinsk, both the layered perceptron and image reconstruction ANN analyses correctly identified the Lop Nor explosion located in a completely different geographic region as seen in Figure 11; this indicates that for this large region underground nuclear explosions located quite far from known testing sites can still be correctly identified as explosions.

The noise-corrected, frequency vs. velocity seismic images can be generated very rapidly and routinely for each individual station or array element once an event has been detected and located Hsu, 1995; Hsu and Alexander, 1994); it was also shown that stacking of the individual noise-

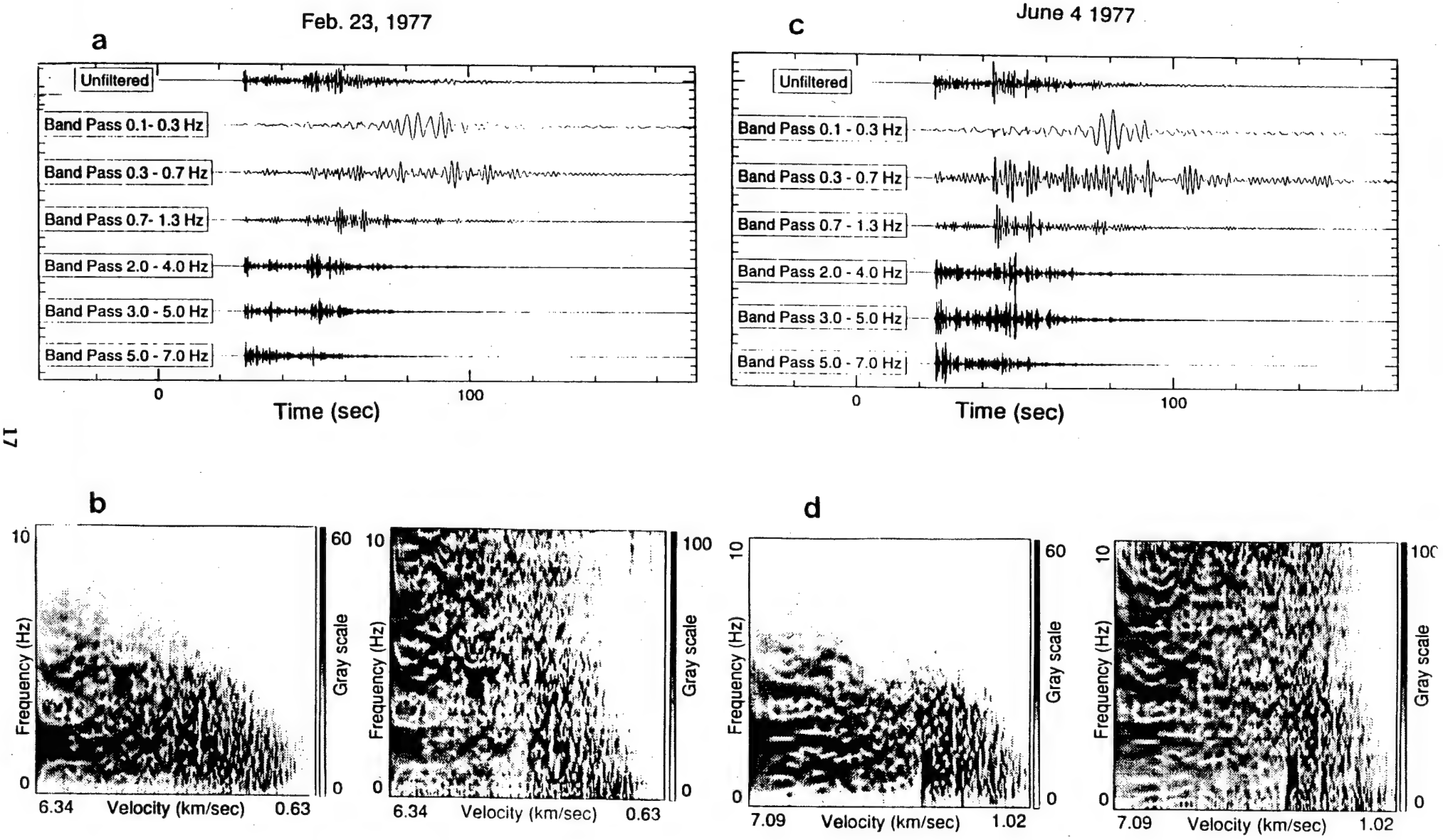

Figure 10 (a). Raw and bandpass-filtered seismograms for event of 2/23/77; (b) Un-normalized frequency vs velocity image of 2/23/77 event (left and the corresponding image normalized at each frequency (right); (c) Raw and bandpass-filtered seismograms for event of 6/4/77; (d) Un-normalized frequency vs velocity image of 6/4/77 event (left) and the corresponding image normalized at each frequency (right).

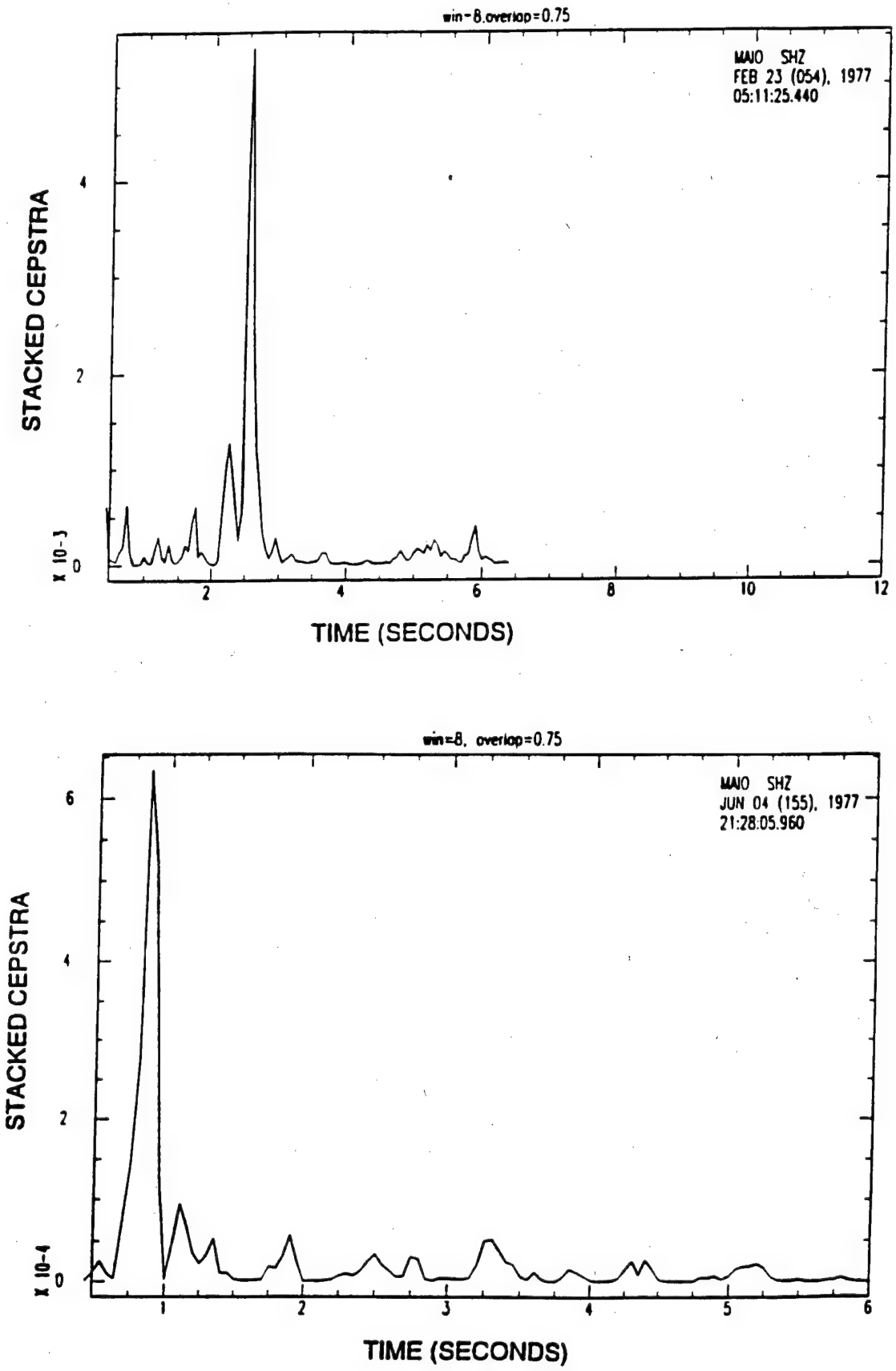

Figure 10e. CSM cepstsral stack for the 2/23/77 and 6/4/77 event at MAIO shown in 10 (a) and 10 (c) respectively.

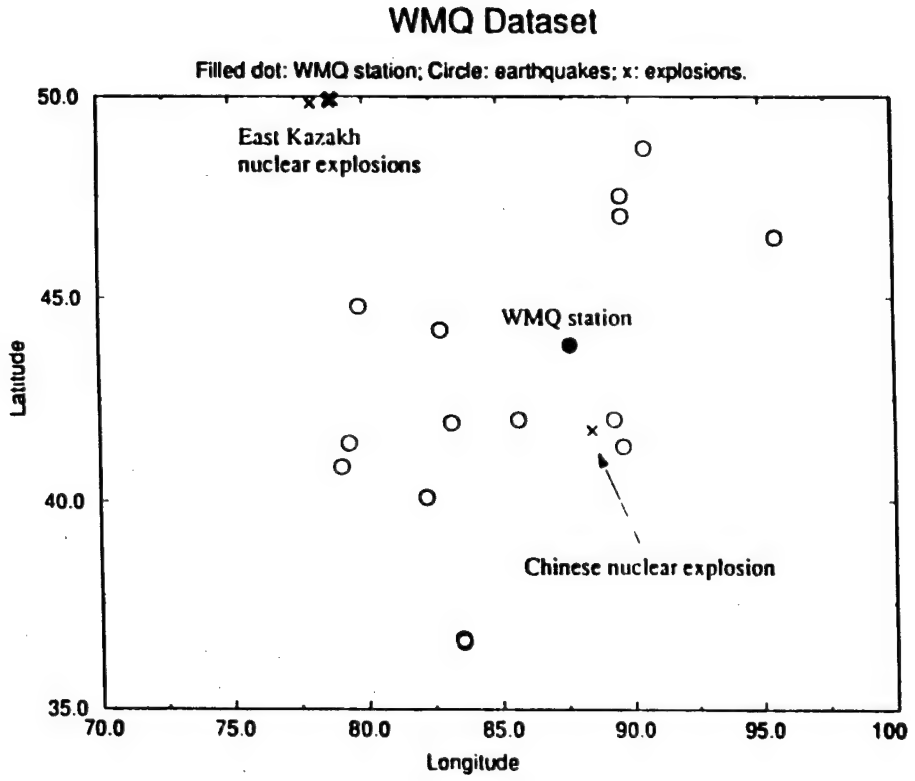

CLASSIFICATION OF EVENTS

"Unknown" Events	NMSE* (Earthquake NN Reconstruction)	NMSE* (Explosion NN Reconstruction)	Correct Iden.?
EQ1	0.1292	0.1791	Yes
EQ2	0.1217	0.6168	Yes
EQ3	0.1430	0.6020	Yes
EQ4	0.1549	0.2644	Yes
EQ5	0.1577	0.8475	Yes
EQ6	0.0986	0.3851	Yes
EQ7	0.0640	0.3842	Yes
EQ8	0.2419	0.5023	Yes
EQ9	0.6020	0.7185	Yes
EQ10	0.1940	0.2355	Yes
EQ11	0.2107	0.3446	Yes
EQ12	0.0741	0.2509	Yes
EQ13	0.1060	0.3018	Yes
EQ14	0.0704	0.1881	Yes
EQ15	0.1086	0.1349	Yes
EXP1	0.3410	0.1262	Yes
EXP2	0.2128	0.1312	Yes
EXP3	0.1212	0.0796	Yes
EXP4	0.3899	0.0879	Yes
EXP5	0.1203	0.1910	No
EXP6	0.2378	0.0969	Yes
EXP7	0.1900	0.0783	Yes
EXP8	0.4205	0.1315	Yes
EXP9	0.5857	0.2025	Yes
EXP10	0.1966	0.0778	Yes
▶ EXP11	0.6418	0.2921	Yes
EXP12	0.1971	0.0833	Yes
EXP13	0.2430	0.0840	Yes
EXP14	0.2333	0.0687	Yes
EXP15	0.4282	0.1005	Yes

* NMSE: Normalized Mean Square Error

Figure 11. The map shows locations of the underground nuclear explosions at East Kazakh and the natural earthquakes in the neighboring area of the WMQ station. The Table shows recognition results for WMQ events using an image compression neural network where each event is treated as an "unknown" and omitted from the neural net training. Exp 11, the LopNor nuclear explosion, is clearly recognized as an explosion.

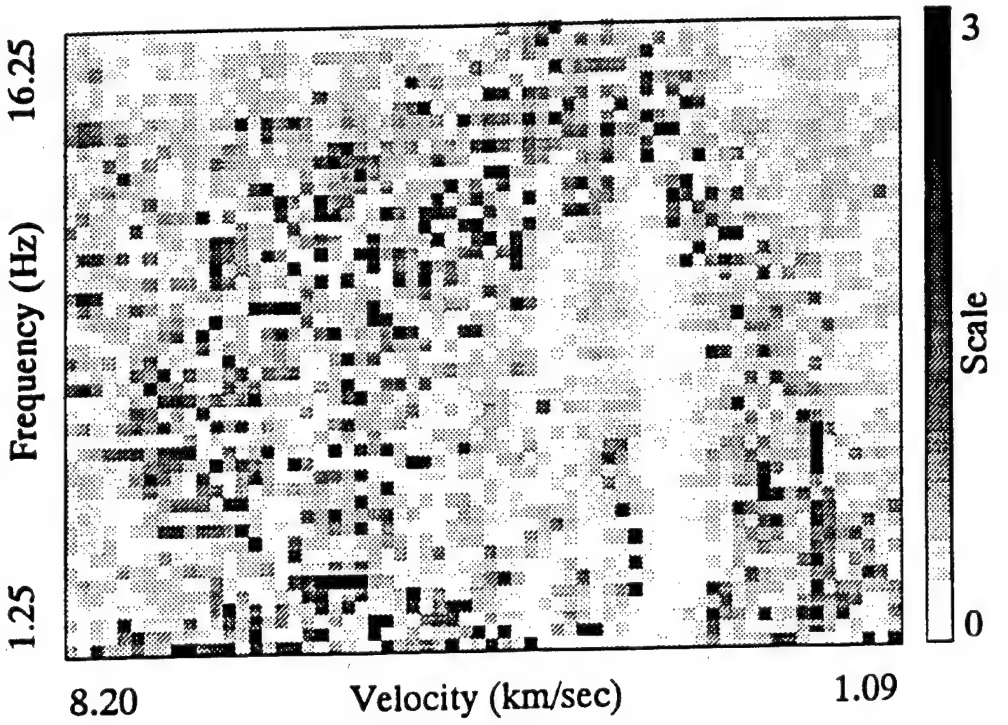

(a)

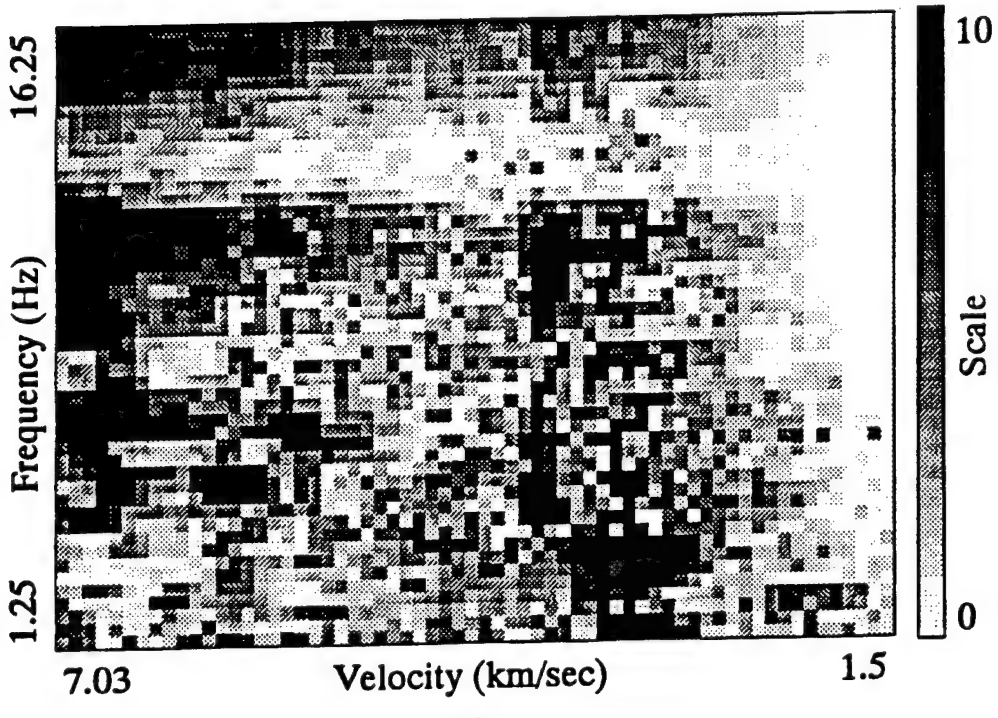

(b)

Figure 12. (a). Residual image of the reconstructed earthquake obtained from an earthquake-trained neural network. (b) The residual image of a reconstructed explosion obtained from the same earthquake-trained neural network; large residual values indicate which parts of the seismic image are diagnostically different between explosions and earthquakes in this source region. In this case the greatest differences are high-frequency P and Lg at all frequencies.

corrected seismic images over the elements of a local array like NORESS or an Alpha array significantly improves the composite image's signal to noise ratio and hence lowers the identification threshold for small events.

The image reconstruction ANN provides a very important capability in addition to event identification. By calculating the residual image obtained by subtracting the reconstructed image using the explosion-trained ANN from the original image, pixel by pixel, and separately the residual image using the earthquake-trained ANN, it is possible not only to identify the unknown event correctly, but also determine the particular parts of the entire seismic signature that controls the ANN identification. Figure 12 shows an example where the unknown event is an explosion. The relatively small values in the residual image obtained from the explosion-trained ANN (top panel) compared to the residual image from the earthquake-trained ANN (bottom panel) clearly identifies the unknown event as an explosion. The largest residual values in the bottom image represent those portions of the frequency-velocity image that are most different between earthquakes and explosions and that explain the success of the ANN for identification. Thus, we see that the greatest diagnostic differences are in the high-frequency P and Lg portions of the image, consistent with a lot of other work on regional discriminants. This approach provides a practical means of determining what parts of the entire event signature are diagnostically different between earthquakes and explosions from a given area of interest, giving physical insight into what otherwise is essentially a "blackbox" identification method. Carrying out this type of analysis for sets of known explosions and earthquakes in various regions of interest will determine the most diagnostic portions of the entire seismic signatures observed at regional distances. As noted earlier, this approach was used successfully by Hsu (1995) to distinguish between earthquakes and nuclear explosions recorded at the WMQ station in western China; again, the high-frequency P and Lg portions of the seismic image were the most diagnostic. Initial training of the layered perceptron or image reconstruction ANNs using a set of known earthquakes and known explosions takes considerable time computationally, but once trained, unknown events can be analyzed and identified in near-real time. Therefore, this approach lends itself to largely-automated processing that would be important for operational use. Software developed in this study can be used for near-real-time regional event identification using individual stations or IMS (or other) arrays.

The research carried out on this grant provides several important new methods for monitoring a Comprehensive Test Ban Treaty.

REFERENCES (Publications Based on Research Results of This Study)

Hsu, R. C. and S. S. Alexander, 1993, Recognition of Earthquakes and Explosions Using a Data Compression Neural Network, Proc. IEEE-SP Workshop on Neural Networks for Signal Processing III, 421-430.

Hsu, R. C. and S. S. Alexander, 1993, Seismic Signal Recognition Using Layered Perceptron and Data Compression Neural Networks, Proc. Intl. Symposium on Artificial Neural Networks, Hsin Chu, Taiwan, 35-44.

Alexander, S. S., R. C. Hsu, I. N. Gupta, and D. H. Salzberg, 1994, Development of Discriminants and Improved Locations for Regional Events in Iran, Proc. 16th Annual Seismic Research Symposium, Thornwood, New York, Sept. 7-9, 12-19.

Hsu, R. C. and S. S. Alexander, 1994, A Neural Network Approach to Seismic Event Identification Using Reference Seismic Images, Proc. IEEE Intl. Conference on Systems, Man and Cybernetics, San Antonio, October 2-5, 2108-2113.

Alexander, S. S., R. C. Hsu, S. L. Karl, I. N. Gupta, and D. H. Salzberg, 1995, New Techniques for Estimating Source Depth and Other Diagnostic Source Characteristics of Shallow Events From Regional Observations of P. Lg and Rg signals, Proc. 17th Seis. Res. Symposium on Monitoring a Comprehensive Test Ban Treaty, PL-TR-95-2108, Env. Res. Paper, No. 1173, 821-830.

Hsu, C. 1995, Seismic Signal Pattern Recognition, Ph.D. Thesis, EE, The Pennsylvania State University, 185 pp. (See Appendix B for a summary.)

Karl, S. L., 1995, Magnitude and Source Depth Estimates for Earthquakes and Explosions in Iran--Regional Observations, B.S. Thesis in Geosciences, The Pennsylvania State University, 185 pp. (See Appendix C for a summary.)

Alexander, S. S., 1996, A New Method for Determining Source Depth From a Single Regional Station, Seis. Res. Ltrs., Vol. 67, No. 1, p. 63.

Alexander, S. S., 1996, Use of the Cepstral Stacking Method (CSM) for Improved Source Depth Determinations from Combined Single-Station and Array or Network Observations at Regional Distances, Proc. of the 18th Annual Seismic Research Symposium on Monitoring a Comprehensive Test Ban Treaty, 4-6 Sept. 1996, PL-TR-96-2153, Env. Res. Papers, No. 1195, 647-656.

Yang, C. C., 1996, Investigation of Cepstral Stacking Methods for Time Delay Extraction, M.S. Thesis (EE), The Pennsylvania State University, 113 pp. (See Appendix D for a summary.)

Alexander, S. S. and C-C. Yang, 1997, Accurate Depth Determinations and Other Diagnostic Event Characteristics in Near-Real Time from Regional Signals, Proc. of 19th Annual Seismic Research Symposium on Monitoring a Comprehensive Test Ban Treaty, 23-25 Sept. 1997, 181-190. (See Appendix E for details.)

Alexander, S. S., 1998, A Reliable New Method for Accurate Event Depth Determinations (invited paper submitted to Geophysical J. International).

Appendix A

Source Discrimination of Seismic Events in Iran *

Indra N. Gupta and Tianrun Zhang
Multimax Inc.
1441 McCormick Drive
Landover, Maryland 20785

Introduction

In our earlier work (Alexander *et al.*, 1994, Gupta *et al.*, 1994), regional distance records of seismic events from regions of both known mine activity and an aftershock sequence in Iran were examined on records of the digital SRO station, Mashhad (MAIO). This set of data consisted of 13 events at epicentral distances varying from about 100 to 300 km. The raw waveforms are shown in Figure 1; four events are clipped and could not be used for spectral analysis. Spectral characteristics of the observed phases Pn, Lg, and Rg were examined by bandpass filtering, spectral ratios, and waveform modeling.

Figures 2 through 10 show raw (unfiltered) and 7 bandpass-filtered seismograms for the nine events, as indicated. Bandpass-filtered seismograms and energy envelopes, each for the frequency range of 6.0- 9.0 Hz, for these nine events are shown in Figures 11 and 12, respectively. Three events (Nos. 4, 9, and 10), located within an area of known mining activity and low seismicity, are inferred to be mine blasts. They have small Lg/P ratios at high frequencies and prominant Rg, indicating shallow depth. The low-frequency codas from Events 4 and 9 show rapid decay, suggesting near-surface sources such as quarry blasts (Su *et al.*, 1991). Such is not the case for Event No. 10 which, however, shows evidence of scalloping in both P and Lg spectra, an indication of ripple firing. Two

* This is a report of work by Co-Investigator Dr. Indra Gupta and co-workers as part of a sub-contract to Multimax Inc.

events (Nos. 3 and 5), presumably aftershocks of an earlier larger (magnitude 5.6) earthquake, have large Lg/P ratios at high frequencies, and long durations of low-frequency coda. Most other events show characteristics of earthquake sources: large high-frequency Lg/P and longer duration of low-frequency coda, except for Event No. 8 which has small high-frequency Lg/Pn. This event does not lie within a region of mine activity and may, therefore, be just a shallow earthquake. Additional information is needed to identify this event with some confidence.

Synthetic seismograms based on published crustal structure for Iran were computed by using wavenumber integration codes for regional seismograms. In order to understand the observed differences in the excitation of various regional phases, synthetics for various sources (including earthquake, explosion, and CLVD) at different depths were computed. Remarkable similarity of explosion and earthquake synthetics to several observed seismograms provided strong support to the source discrimination process.

Lg/Rg Amplitude Ratios Derived from Narrow Bandpass Filtering

Short-period Rg consists of fundamental-mode Rayleigh wave with amplitudes decreasing exponentially with depth, whereas Lg includes higher-modes so that its amplitudes do not decrease as rapidly with source depth. As mentioned earlier, several records (Figures 2 through 10) indicate prominent low-frequency Rg so that the Lg/Rg ratio could be a useful source discriminant. Additional support for this possibility comes from the theoretical and observational results of Hanka (1982) and Langston (1987) who found the ratio Rg/Lg or Rg/S to be an indicator of source depth and therefore a possible source discriminant if explosions are assumed to occur at much shallower depths than

earthquakes. Hanka (1982) suggested that amplitude ratio of Lg and Rg, measured within certain period-velocity windows, may be a useful discriminant. Langston (1987) derived synthetic seismograms for the four fundamental terms needed to construct a general moment tensor point source and found that for distances of about 100 km, Rg/S ratio is an effective indicator of source depth; Rg/S ratios of 10 or more implied shallow source depths of less than 2 km.

We examine the time-varying spectral characteristics of the observed seismic arrivals, including Lg and Rg, by narrow bandpass filtering (NBF) which provides amplitudes for various values of wave period and group velocity. The NBF technique, described in detail by Seneff (1978), has been employed by several investigators (*e.g.* Kafka, 1990) to study Rg from shallow sources. The group velocity curves are computed by using a moving zero-phase Gaussian filter. The period axis represents the central period of the filter and the velocity axis is simply epicentral distance/travel-time. The filter is applied at each period, the energy envelope computed, and the energy envelope curves are represented in the form of a two-dimensional matrix which is contoured.

The SRO instrument at MAIO is peaked at about 1 sec. For NBF to be useful, it is desirable to have broadband data. The SRO instrument response was therefore removed and replaced by response of the broadband instrument used by the Lawrence Livermore National Lab. On all seismograms, the beginning of Lg was clearly identifiable but, on the basis of their available location (Table 1, Alexander *et al.*, 1994), its group velocity was considerably different from 3.5 km/sec for several events, implying errors in location because the beginning of Lg is known to always have a velocity of approximately

3.5 km/sec. The Lg-P times were measured and the start times on each record were adjusted so that the beginning of Lg had a velocity of 3.5 km/sec. NBF of the resulting seismograms of nine (9) events are shown in Figures 13 through 21 in which the amplitudes of energy are on log scale. On all NBF plots, both Lg and Rg are strong (much above the background noise) phases over fairly wide range of periods.

Short-period Lg from explosions is probably mainly due to the near-source scattering of explosion-generated Rg into S (Gupta *et al.*, 1992; Patton and Taylor, 1995). We therefore used relatively longer-period (larger than 1 sec) Lg and Rg to examine their discrimination capability. An examination of the NBF plots indicates that, for periods greater than about 2 sec, low-velocity (about 2 km/sec) Rg is the dominant phase for the presumably explosion events 4 and 9 (Figures 15 and 19), whereas both Lg and Rg are fairly strong for the earthquake events 3 and 5 (Figures 14 and 16). We obtained averages of energy in several period-velocity windows for both Lg and Rg and a few results of Lg/Rg ratios are shown in Figures 22 through 24. The ratios are plotted versus Lg-P time, a measure of the source-receiver distance, so that any systematic dpendence with distance due to different attenuation rates of Lg and Rg could be observed. Due to the limited data in Figures 22 through 24, no such dependence is obvious and so no distance correction could be applied. The period-velocity windows used in Figures 22 and 23, with the lowest Lg/Rg ratios for Events 4 and 9 and therefore perhaps the best for source discrimination, suggest that although Event 10 may be an explosion, the remaining 6 events, including Event 8, are likely to be earthquakes. Note that the high-frequency discriminant, Lg/P was not very effective in identifying Event 8 as an earthquake.

However, the low-frequency discriminant, Lg/Rg leaves no doubt regarding the identity of this event as an earthquake. It appears therefore that a combination of high and low-frequency discriminants, such as the high-frequency Lg/P and the low-frequency Lg/Rg used in this study, can provide improved discrimination capability, perhaps not possible to accomplish by a single band-limited method.

Conclusion

Low-frequency Lg/Rg ratio, based on the use of suitable period-velocity windows on NBF plots, appears to be a good source discriminant for regional data. However, the data used in this study are very limited and the methodology needs to be tried on considerably more data from known events in several regions of the world.

References

Alexander, S. S., R. C. Hsu, I. N. Gupta, and D. H. Salzberg (1994). Development of discriminants and improved locations for regional events in Iran, Proc. of the 16th Annual Seismic Research Symposium, 7-9 September, 1994, PL-TR-94-2217, Phillips Laboratory, Hanscom Air Force Base, Massachusetts, pp. 13-19.

Gupta, I. N., W. W. Chan, and R. A. Wagner (1992). A comparison of regional phases from underground nuclear explosions at East Kazakh and Nevada test sites, *Bull. Seism. Soc. Am.* 82, 352-382.

Gupta, I. N., D. H. Salzberg, and S. S. Alexander (1994). A study of regional discriminants for seismic events in Iran, EOS 75, no. 44, 428 (abstract).

Hanka, W. (1982). Analysis of broad-band Rayleigh waves: a possibility for seismic discrimination, J. Geophys. 51, 165-179.

Kafka, A. L. (1990). Rg as a depth discriminant for earthquakes and explosions: a case study in New England, Bull. Seism. Soc. Am. 80, 373-394.

Langston, C. A. (1987). Depth of faulting during the 1968 Meckering, Australia, earthquake sequence determined from waveform analysis of local seismograms, Jour. Geophys. Res. 92, 11,561-11,574.

Patton, H. J. and S. R. Taylor (1995). Analysis of Lg spectral ratios from NTS explosions: implications for the source mechanisms of spall and the generation of Lg waves, *Bull. Seism. Soc. Am.* 85, 220-236

Seneff, S. (1978). A fast new method for frequency-filter analysis of surface waves: application in the west Pacific, Bull. Seism. Soc. Am. 68, 1031-1048.

Su, F., K. Aki, and N. N. Biswas (1991). Discriminating quarry blasts from earthquakes using coda waves, Bull. Seism. Soc. Am. 81, 162-178.

LIST OF FIGURES

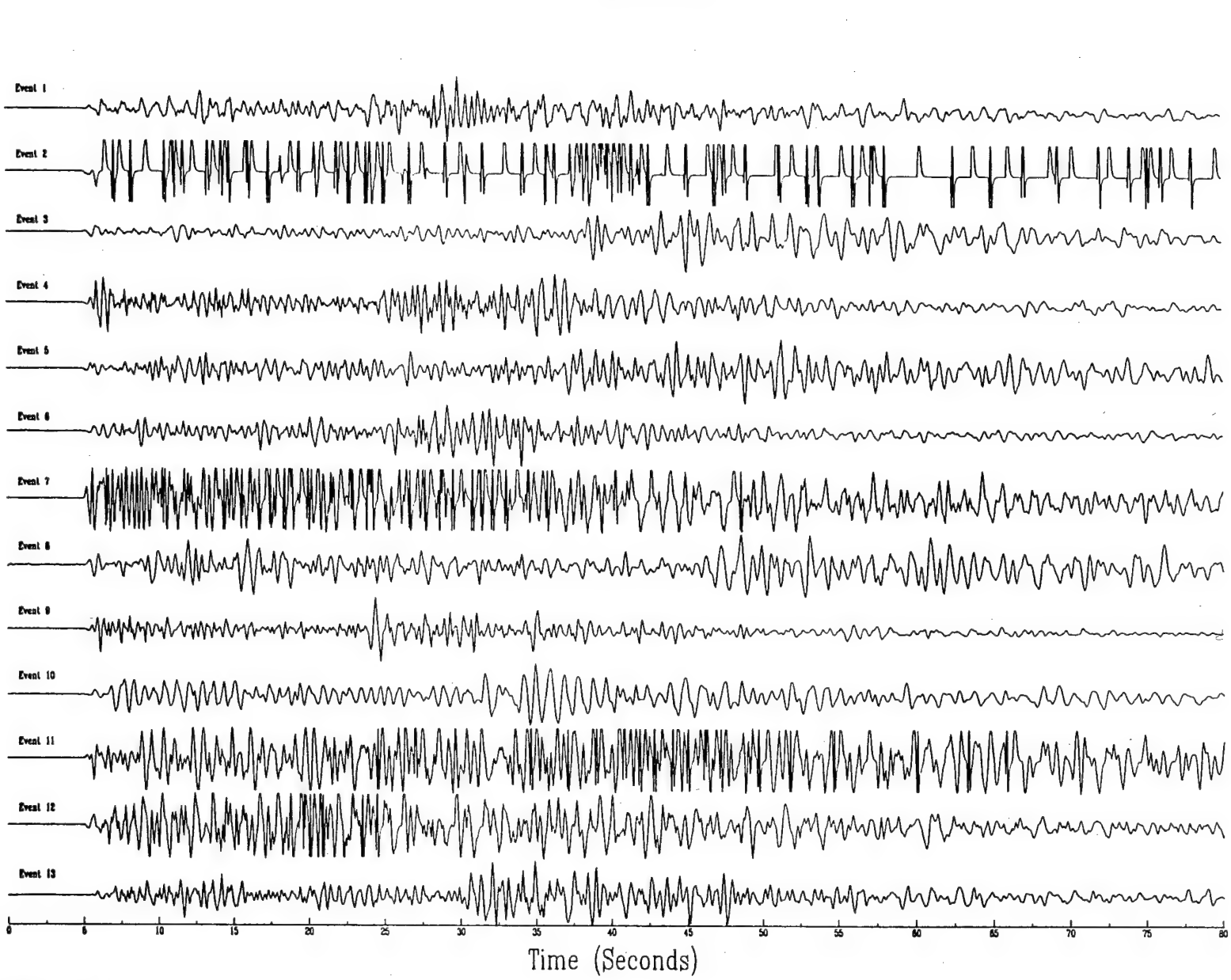
All 13 Waveforms
Event 1
Event 2
Event 3
Event 4
Event 5
Event 6
Event 7
Event 8
Event 9
Event 10
Event 11
Event 12
Event 13
0
5
10
15
20
25
30
35
40
45
50
55
60
65
70
75
80
Time (Seconds)

Figure 1

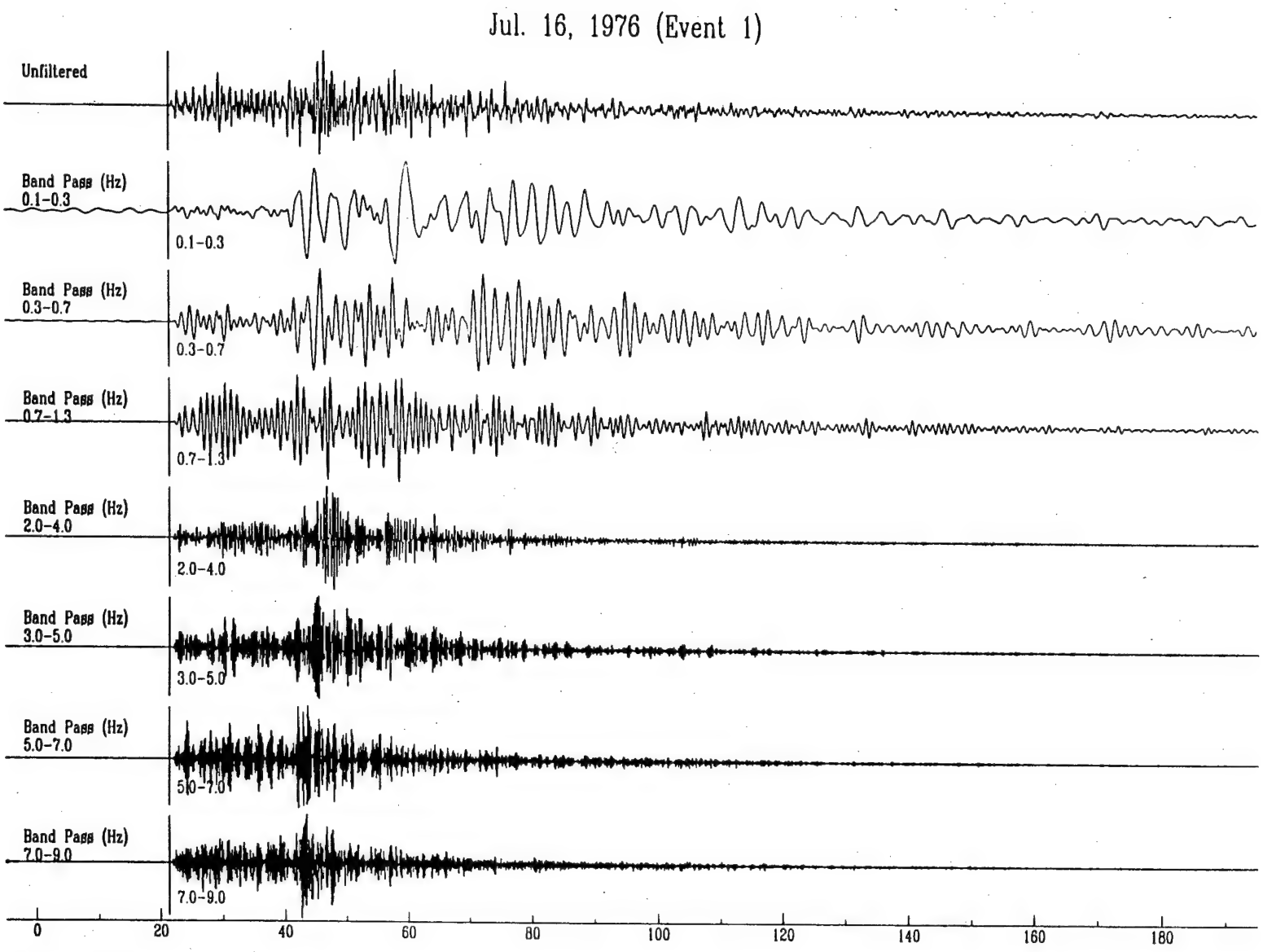
Jul. 16, 1976 (Event 1)
Unfiltered
Band Pass (Hz)
0.1-0.3
0.1-0.3
Band Pass (Hz)
0.3-0.7
0.3-0.7
Band Pass (Hz)
0.7-1.3
0.7-1.3
Band Pass (Hz)
2.0-4.0
2.0-4.0
Band Pass (Hz)
3.0-5.0
3.0-5.0
Band Pass (Hz)
5.0-7.0
5.0-7.0
Band Pass (Hz)
7.0-9.0
7.0-9.0
0
20
40
60
80
100
120
140
160
180

Figure 2

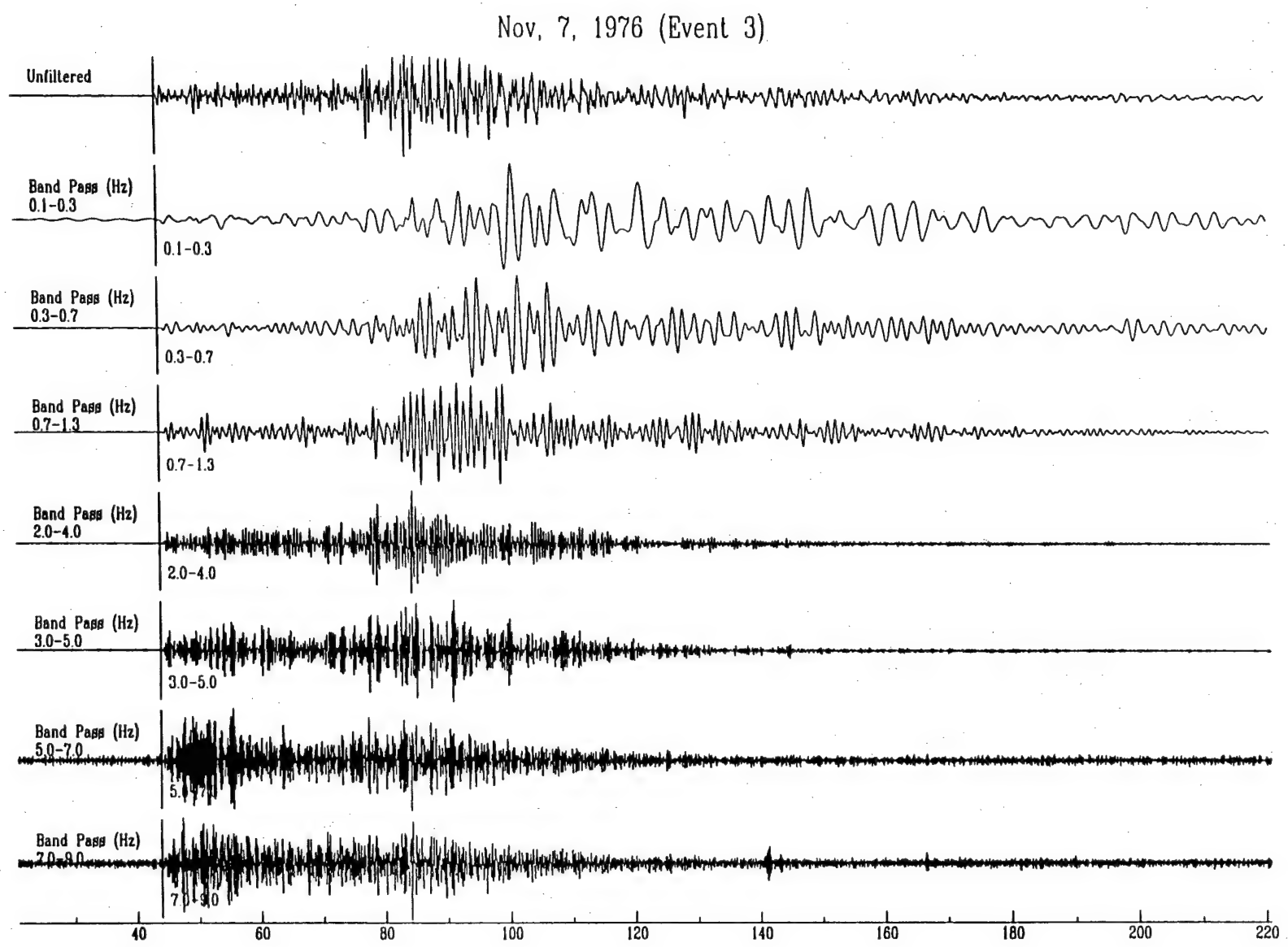
Nov, 7, 1976 (Event 3)
Unfiltered
Band Pass (Hz)
0.1-0.3
0.1-0.3
Band Pass (Hz)
0.3-0.7
0.3-0.7
Band Pass (Hz)
0.7-1.3
0.7-1.3
Band Pass (Hz)
2.0-4.0
2.0-4.0
Band Pass (Hz)
3.0-5.0
3.0-5.0
Band Pass (Hz)
5.0-7.0
Band Pass (Hz)
7.0-9.0
40
60
80
100
120
140
160
180
200
220

Figure 3

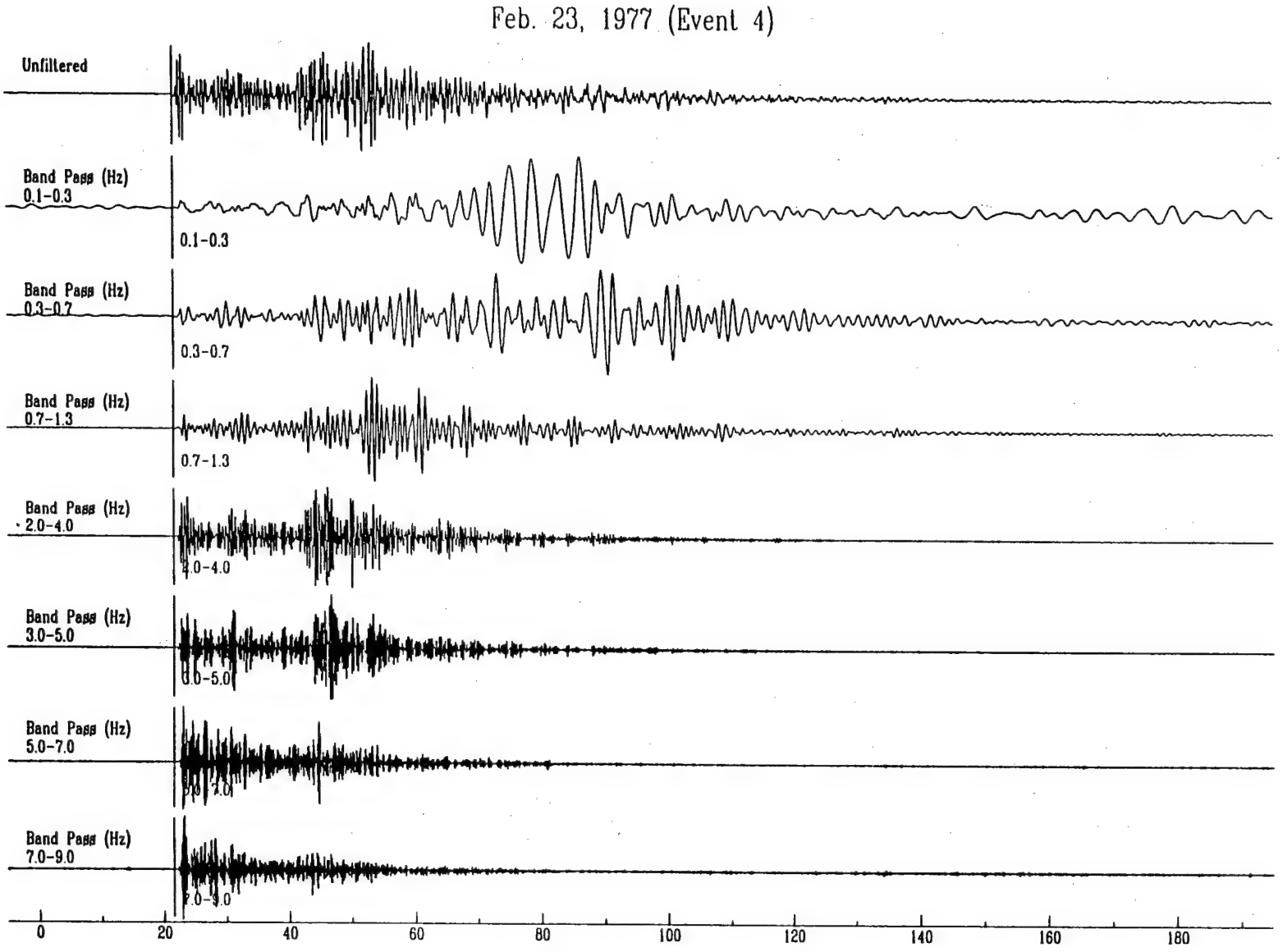
Feb. 23, 1977 (Event 4)
Unfiltered
Band Pass (Hz)
0.1-0.3
0.1-0.3
Band Pass (Hz)
0.3-0.7
0.3-0.7
Band Pass (Hz)
0.7-1.3
0.7-1.3
Band Pass (Hz)
2.0-4.0
2.0-4.0
Band Pass (Hz)
3.0-5.0
3.0-5.0
Band Pass (Hz)
5.0-7.0
Band Pass (Hz)
7.0-9.0
7.0-9.0
0
20
40
60
80
100
120
140
160
180

Figure 4

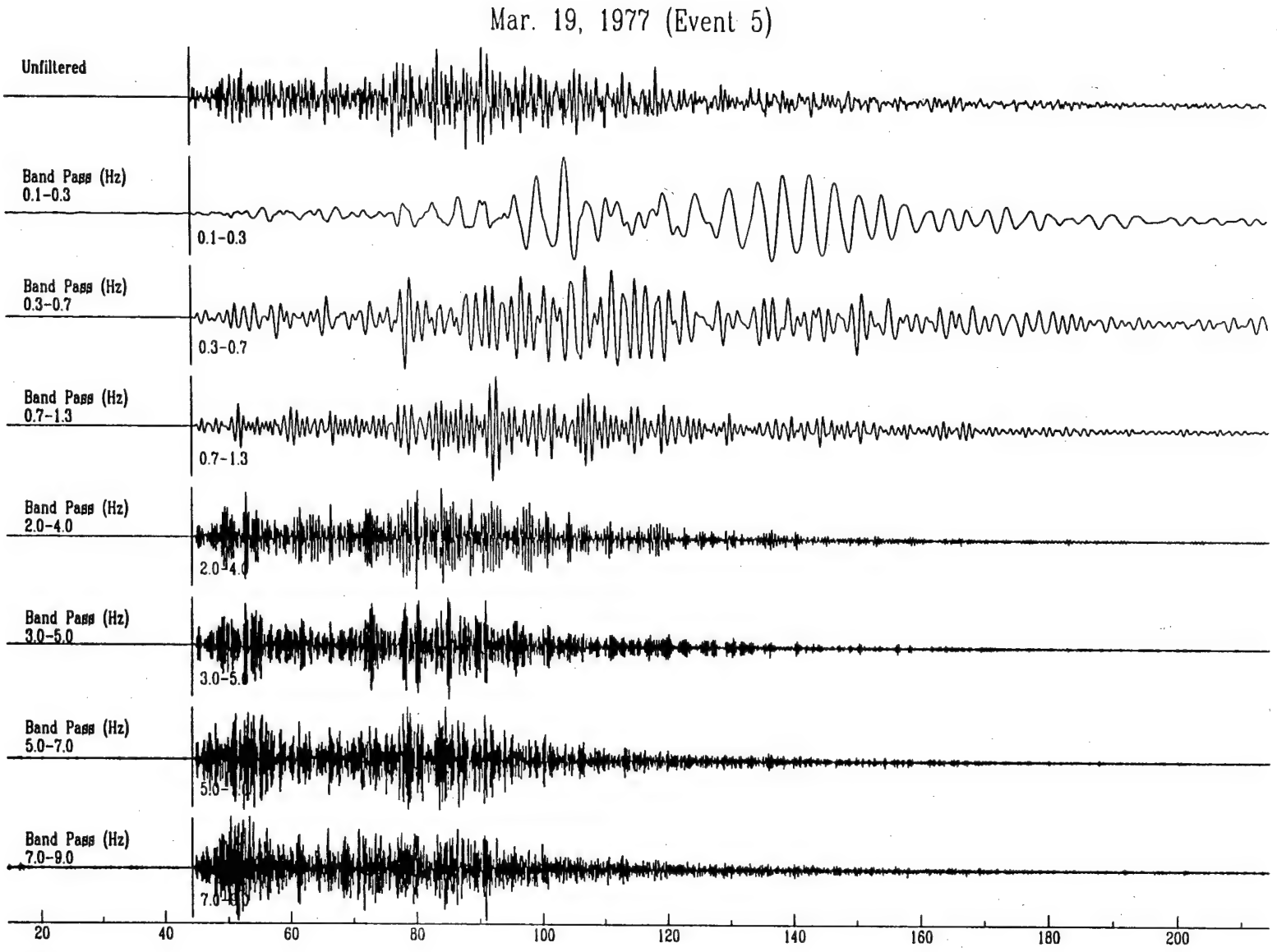
Mar. 19, 1977 (Event 5)
Unfiltered
Band Pass (Hz)
0.1-0.3
0.1-0.3
Band Pass (Hz)
0.3-0.7
0.3-0.7
Band Pass (Hz)
0.7-1.3
0.7-1.3
Band Pass (Hz)
2.0-4.0
Band Pass (Hz)
3.0-5.0
Band Pass (Hz)
5.0-7.0
Band Pass (Hz)
7.0-9.0
20
40
60
80
100
120
140
160
180
200

Figure 5

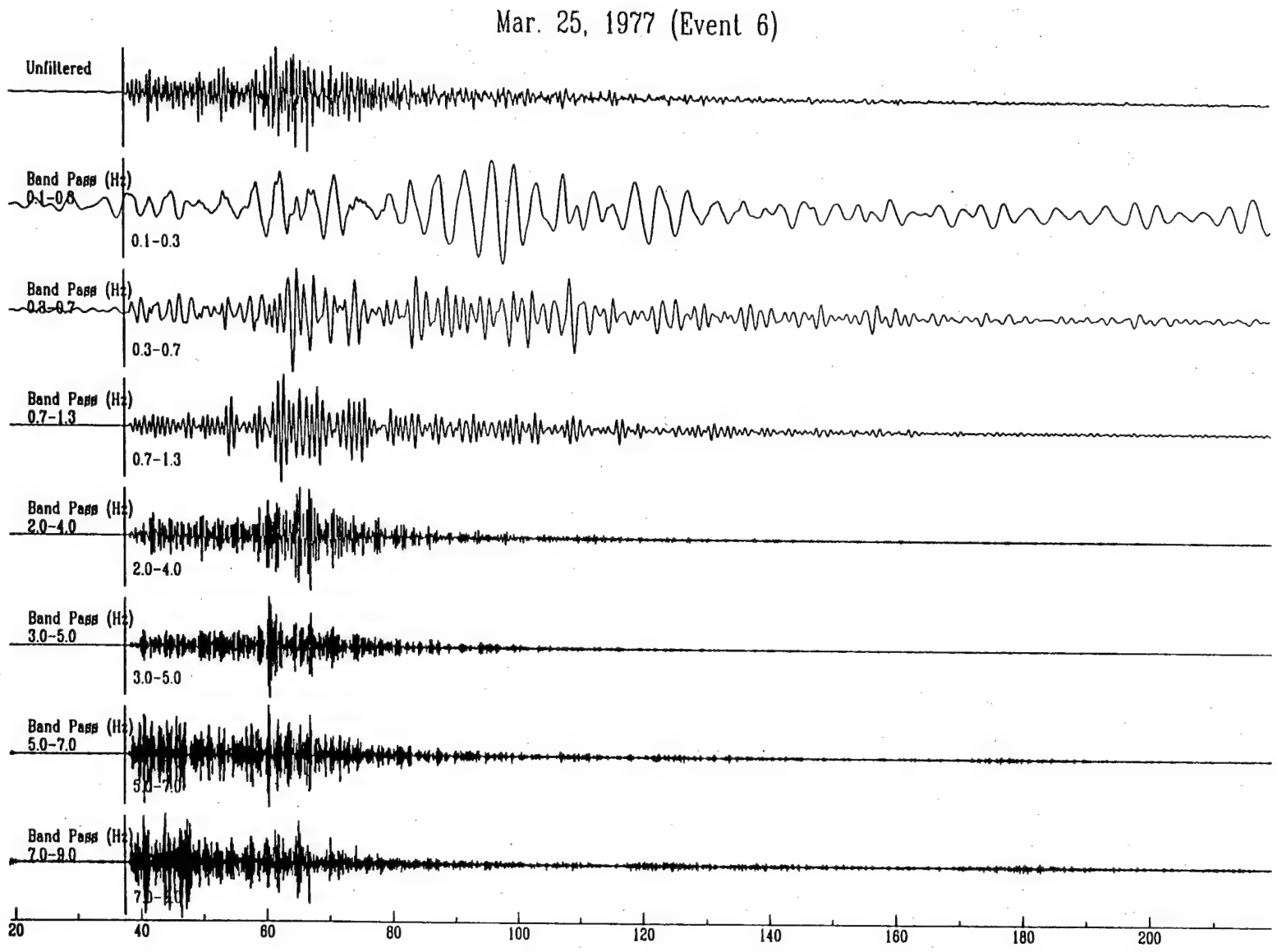
Mar. 25, 1977 (Event 6)
Unfiltered
Band Pass (Hz)
0.1-0.8
0.1-0.3
Band Pass (Hz)
0.3-0.7
0.3-0.7
Band Pass (Hz)
0.7-1.3
0.7-1.3
Band Pass (Hz)
2.0-4.0
2.0-4.0
Band Pass (Hz)
3.0-5.0
3.0-5.0
Band Pass (Hz)
5.0-7.0
Band Pass (Hz)
7.0-9.0
20
40
60
80
100
120
140
160
180
200

Figure 6

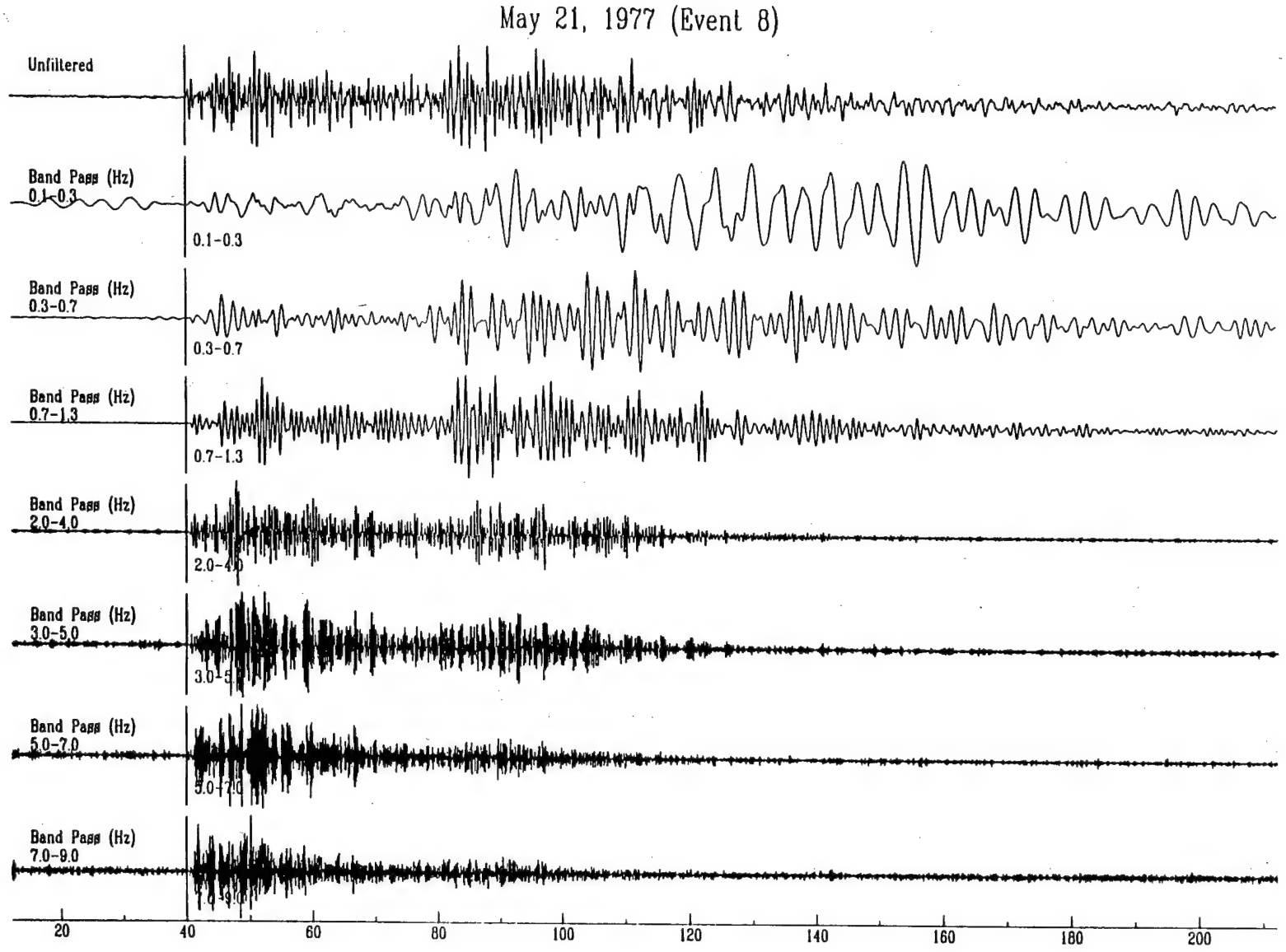
May 21, 1977 (Event 8)
Unfiltered
Band Pass (Hz)
0.1-0.3
0.1-0.3
Band Pass (Hz)
0.3-0.7
0.3-0.7
Band Pass (Hz)
0.7-1.3
0.7-1.3
Band Pass (Hz)
2.0-4.0
Band Pass (Hz)
3.0-5.0
Band Pass (Hz)
5.0-7.0
Band Pass (Hz)
7.0-9.0
20
40
60
80
100
120
140
160
180
200

Figure 7

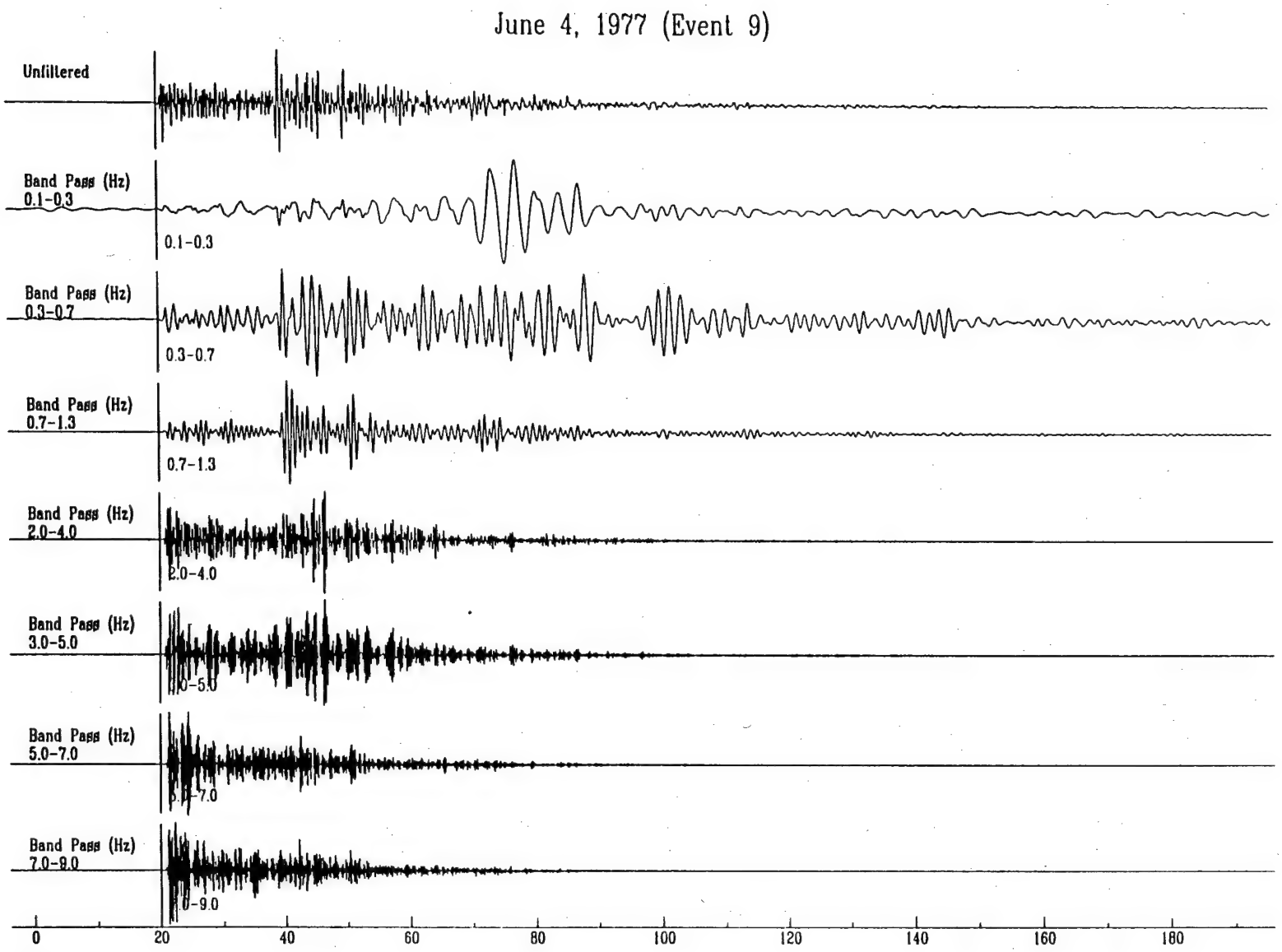
June 4, 1977 (Event 9)
Unfiltered
Band Pass (Hz)
0.1-0.3
0.1-0.3
Band Pass (Hz)
0.3-0.7
0.3-0.7
Band Pass (Hz)
0.7-1.3
0.7-1.3
Band Pass (Hz)
2.0-4.0
2.0-4.0
Band Pass (Hz)
3.0-5.0
Band Pass (Hz)
5.0-7.0
Band Pass (Hz)
7.0-9.0
0
20
40
60
80
100
120
140
160
180

Figure 8

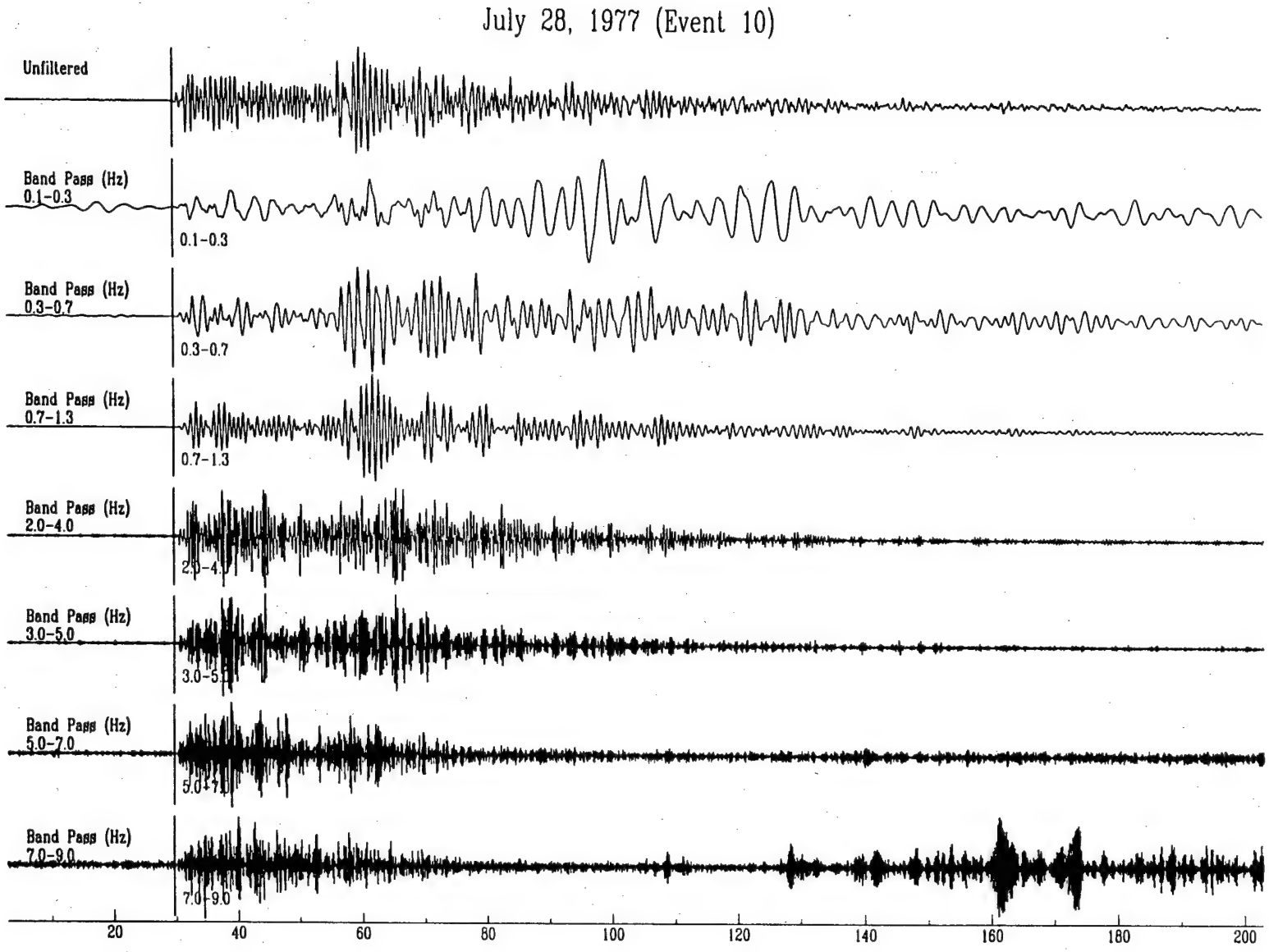
July 28, 1977 (Event 10)
Unfiltered
Band Pass (Hz)
0.1-0.3
0.1-0.3
Band Pass (Hz)
0.3-0.7
0.3-0.7
Band Pass (Hz)
0.7-1.3
0.7-1.3
Band Pass (Hz)
2.0-4.0
Band Pass (Hz)
3.0-5.0
Band Pass (Hz)
5.0-7.0
Band Pass (Hz)
7.0-9.0
20
40
60
80
100
120
140
160
180
200

Figure 9

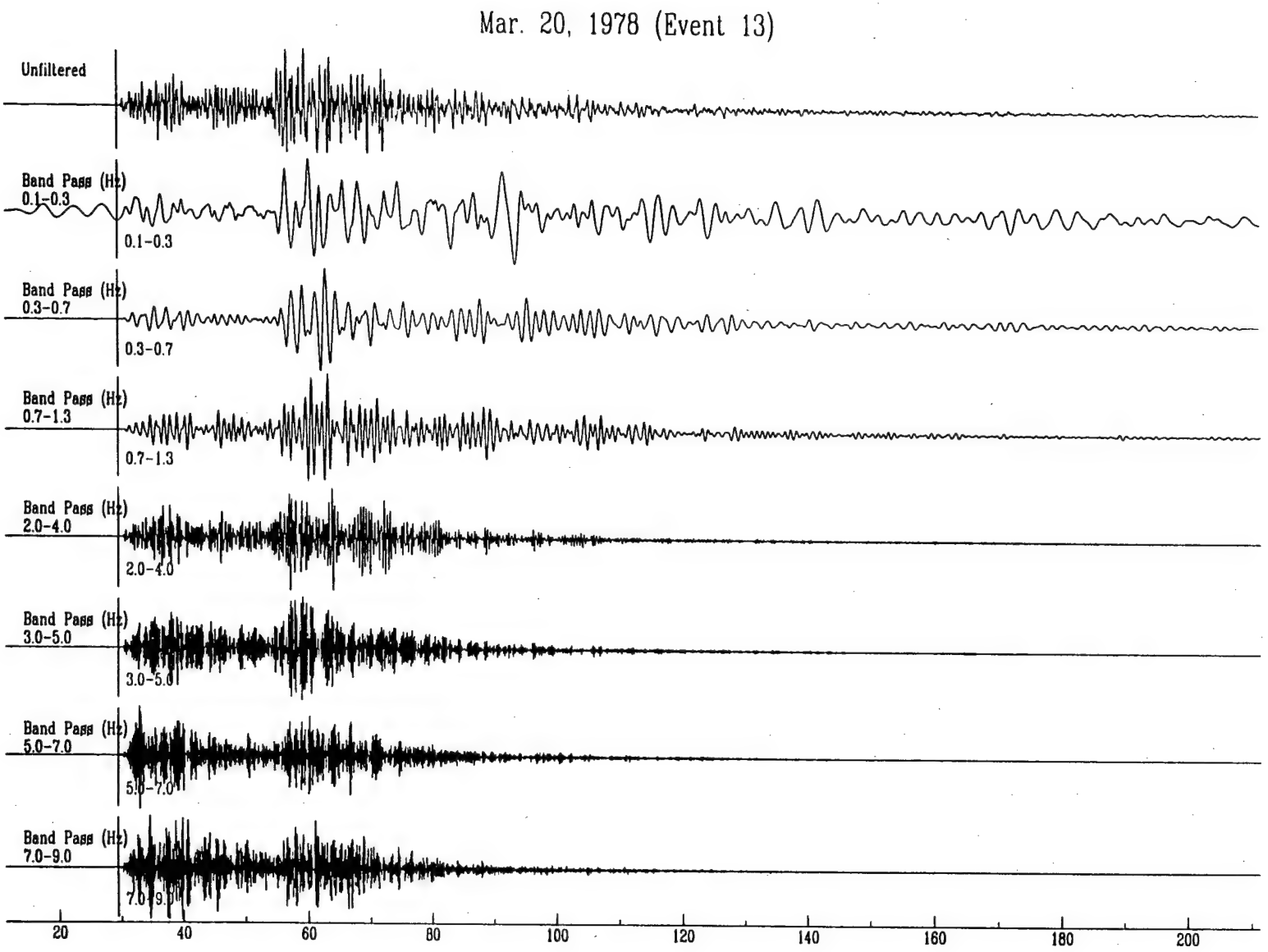
Mar. 20, 1978 (Event 13)
Unfiltered
Band Pass (Hz)
0.1-0.3
0.1-0.3
Band Pass (Hz)
0.3-0.7
0.3-0.7
Band Pass (Hz)
0.7-1.3
0.7-1.3
Band Pass (Hz)
2.0-4.0
2.0-4.0
Band Pass (Hz)
3.0-5.0
3.0-5.0
Band Pass (Hz)
5.0-7.0
5.0-7.0
Band Pass (Hz)
7.0-9.0
7.0-9.0
20
40
60
80
100
120
140
160
180
200

Figure 10

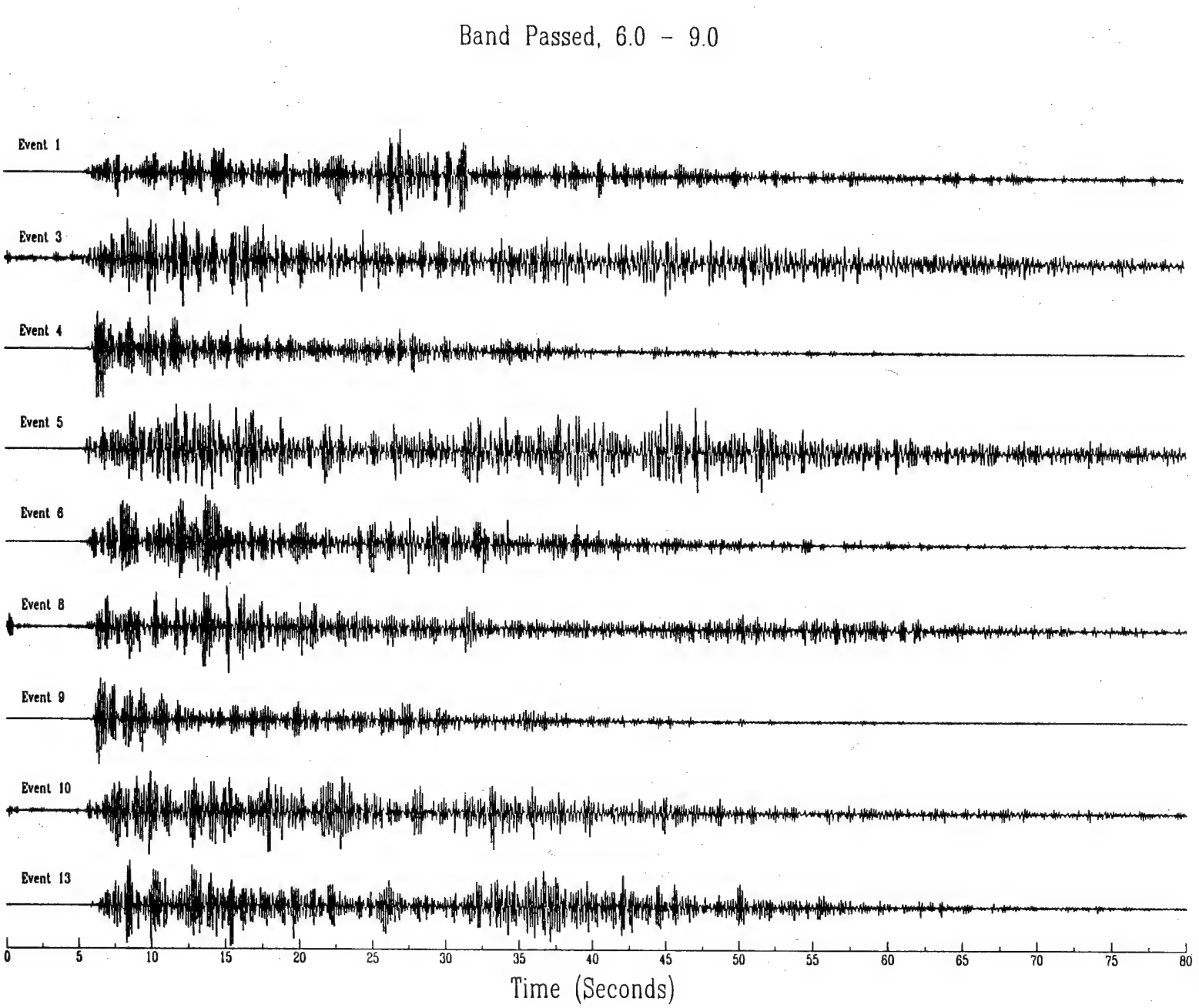
Band Passed, 6.0 - 9.0
Event 1
Event 3
Event 4
Event 5
Event 6
Event 8
Event 9
Event 10
Event 13
0
5
10
15
20
25
30
35
40
45
50
55
60
65
70
75
80
Time (Seconds)

Figure 11

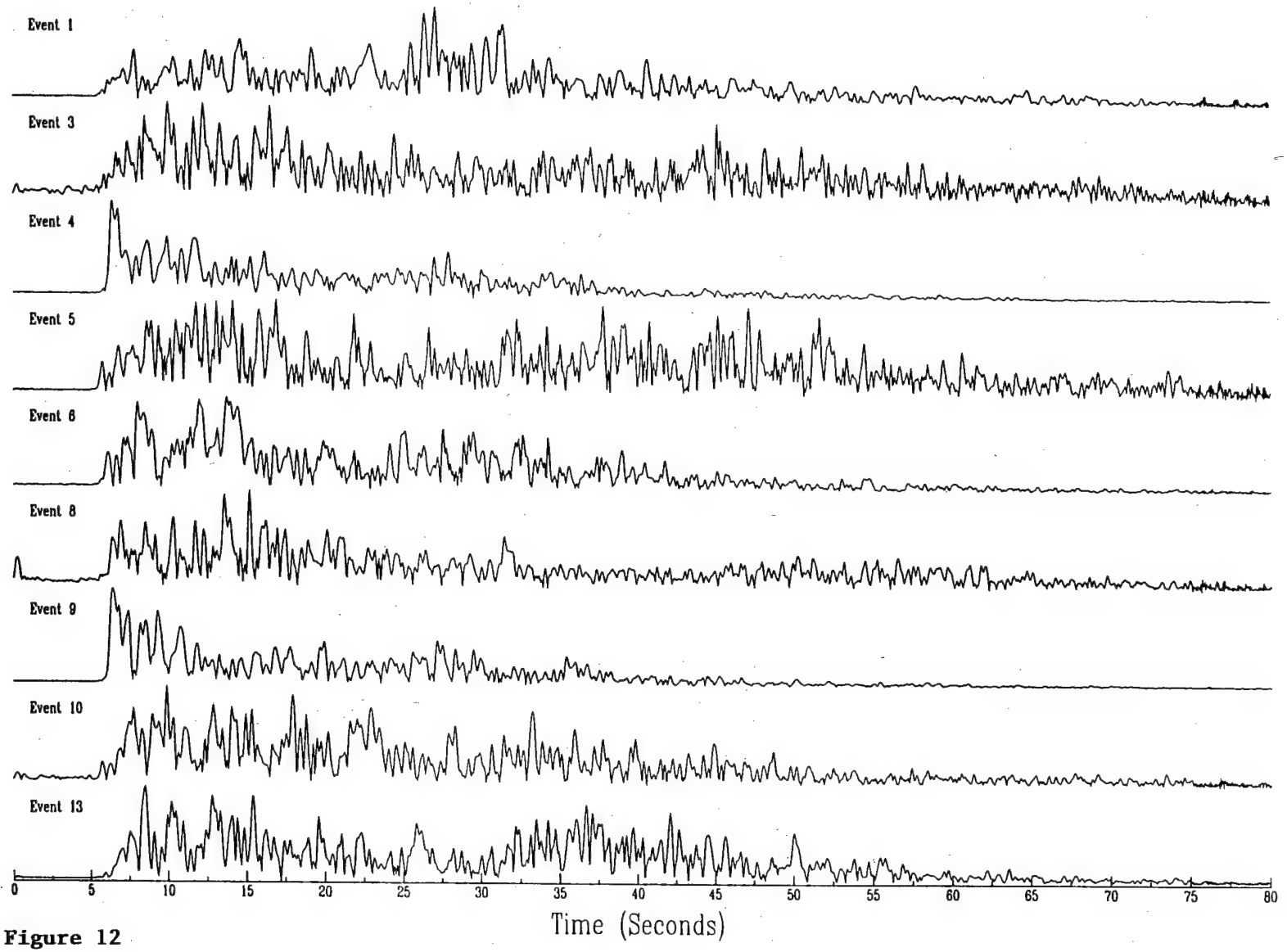
Energy Envelope: Band Passed, 6.0 - 9.0
Event 1
Event 3
Event 4
Event 5
Event 6
Event 8
Event 9
Event 10
Event 13
0
5
10
15
20
25
30
35
40
45
50
55
60
65
70
75
80
Time (Seconds)

Figure 12

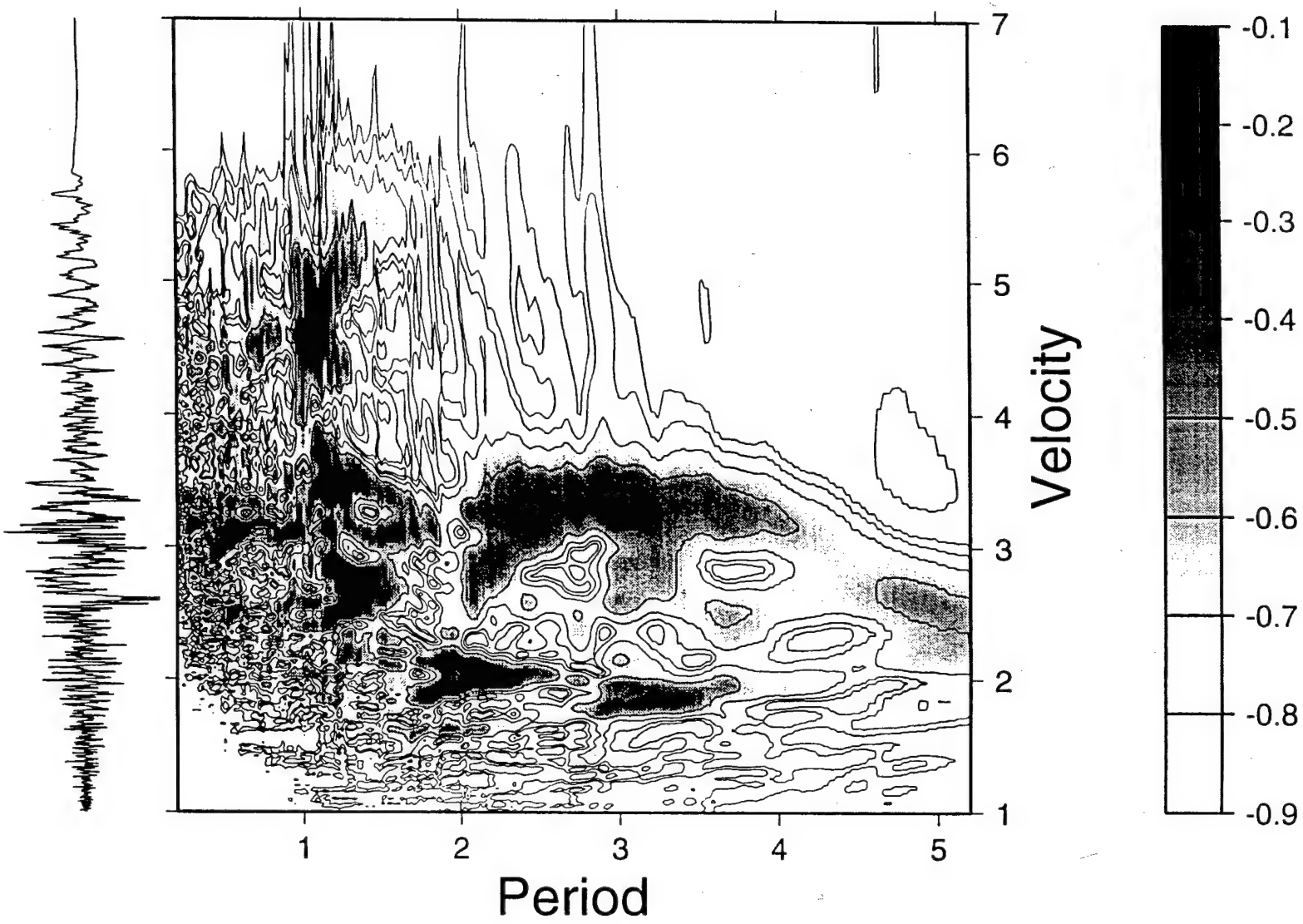
MAIO.1.SZ.BB log
Velocity
Period
1
2
3
4
5
6
7
-0.1
-0.2
-0.3
-0.4
-0.5
-0.6
-0.7
-0.8
-0.9

Figure 13

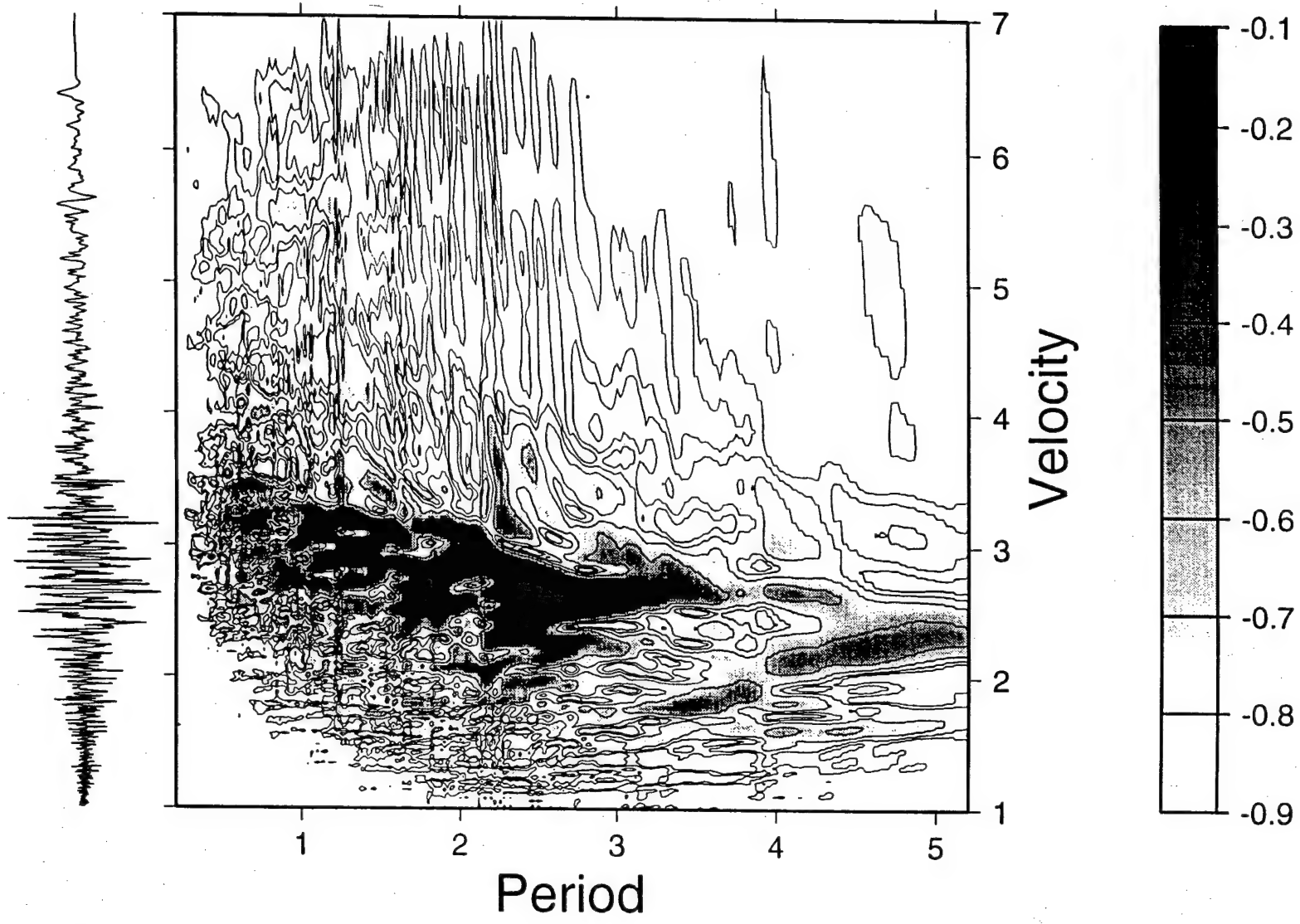
MAIO.3.SZ.BB log
Velocity
Period
1
2
3
4
5
6
7
-0.1
-0.2
-0.3
-0.4
-0.5
-0.6
-0.7
-0.8
-0.9

Figure 14

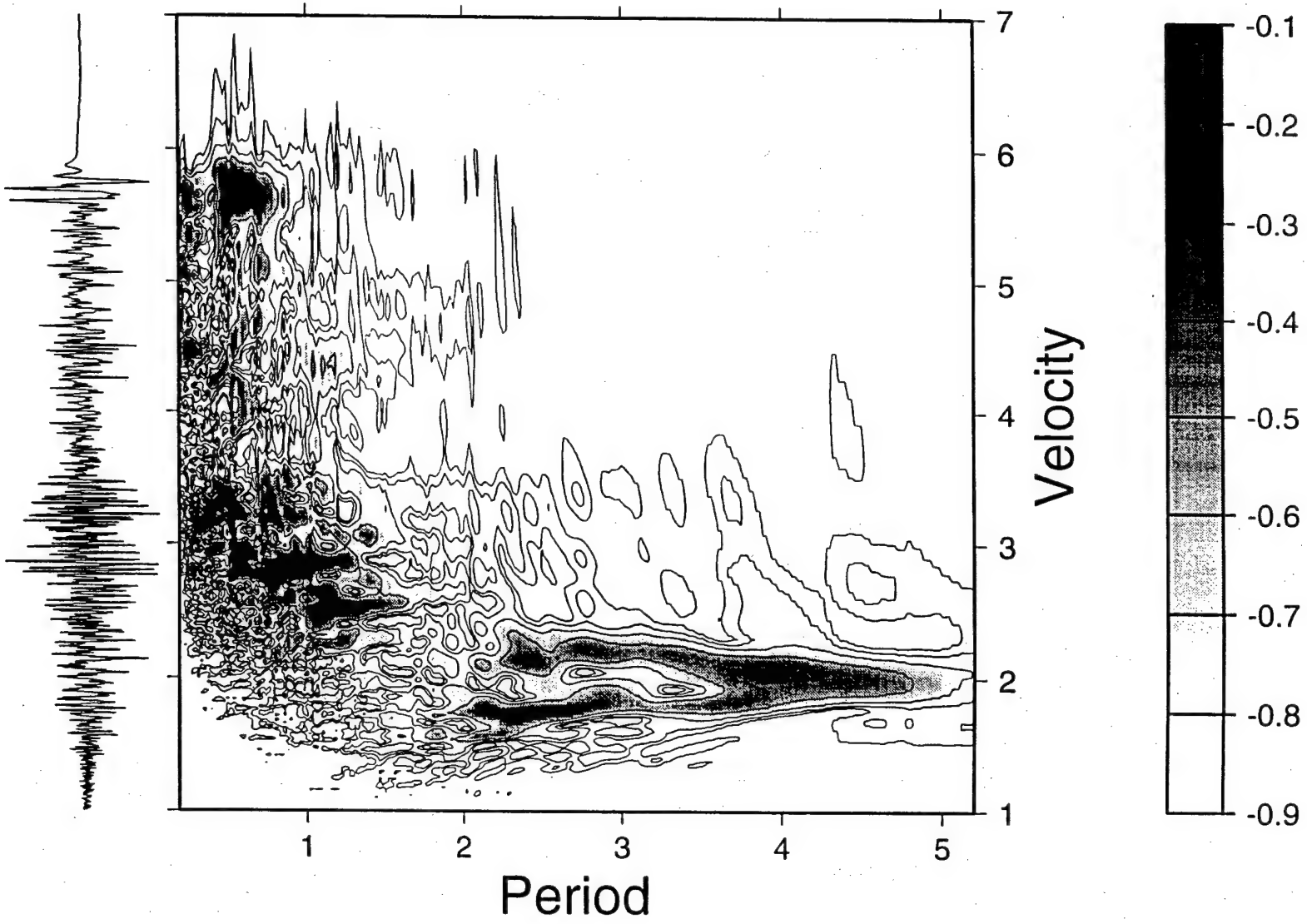
MAIO.4.SZ.BB log
Velocity
Period
1
2
3
4
5
6
7
-0.1
-0.2
-0.3
-0.4
-0.5
-0.6
-0.7
-0.8
-0.9

Figure 15

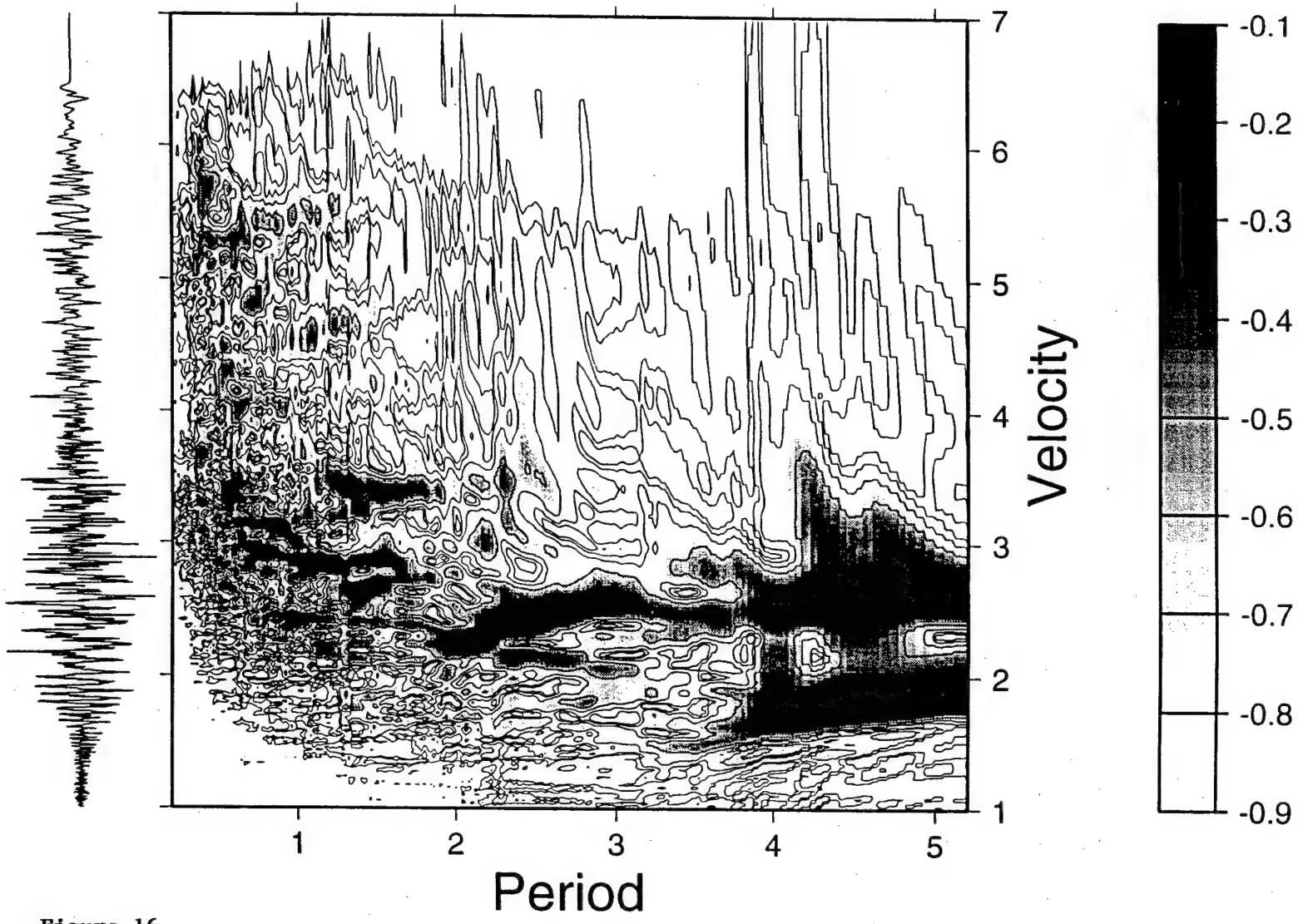
MAIO.5.SZ.BB log
Velocity
Period
1
2
3
4
5
6
7
-0.1
-0.2
-0.3
-0.4
-0.5
-0.6
-0.7
-0.8
-0.9

Figure 16

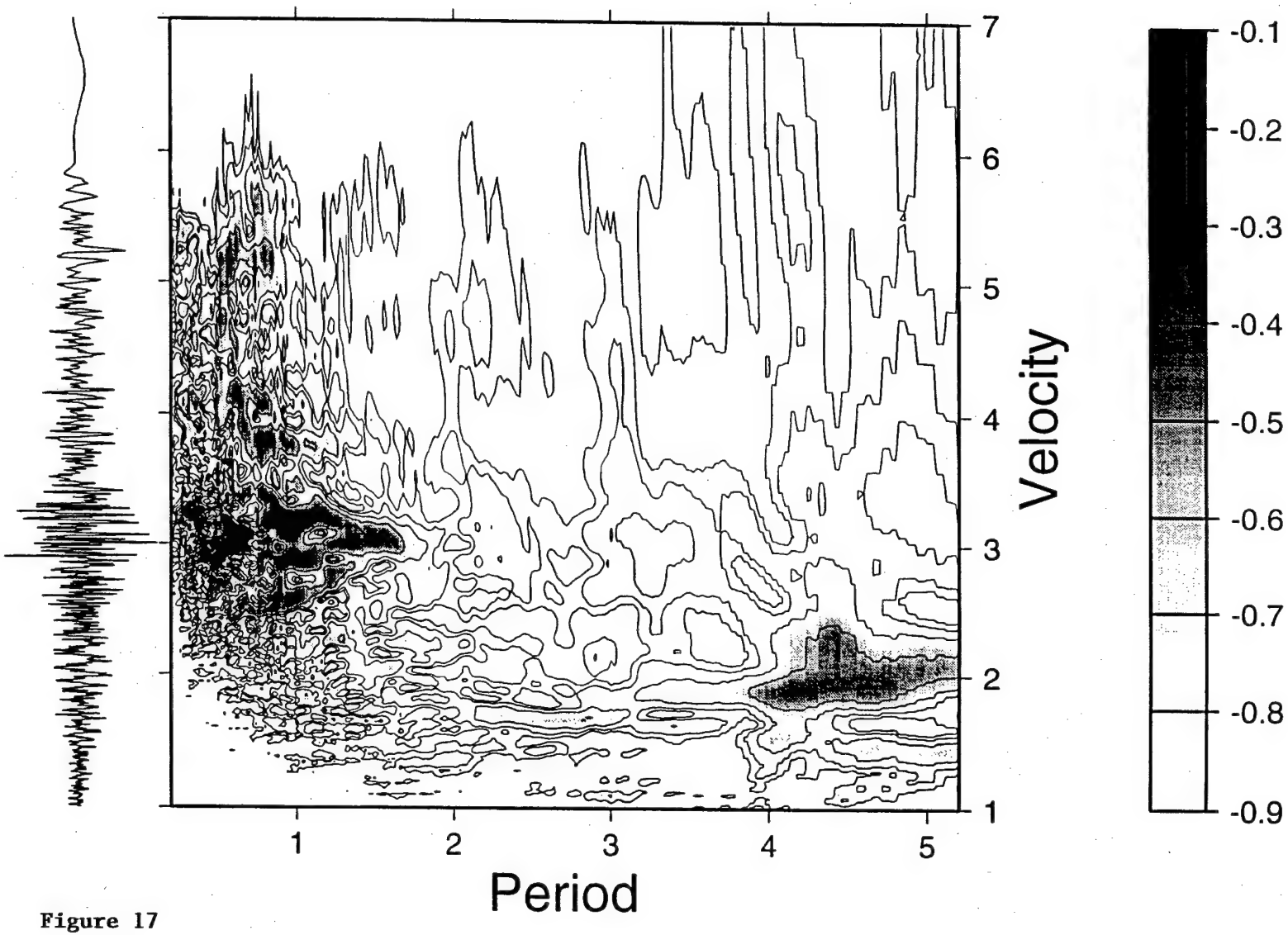
MAIO.6.SZ.BB log
Velocity
Period
1
2
3
4
5
6
7
-0.1
-0.2
-0.3
-0.4
-0.5
-0.6
-0.7
-0.8
-0.9

Figure 17

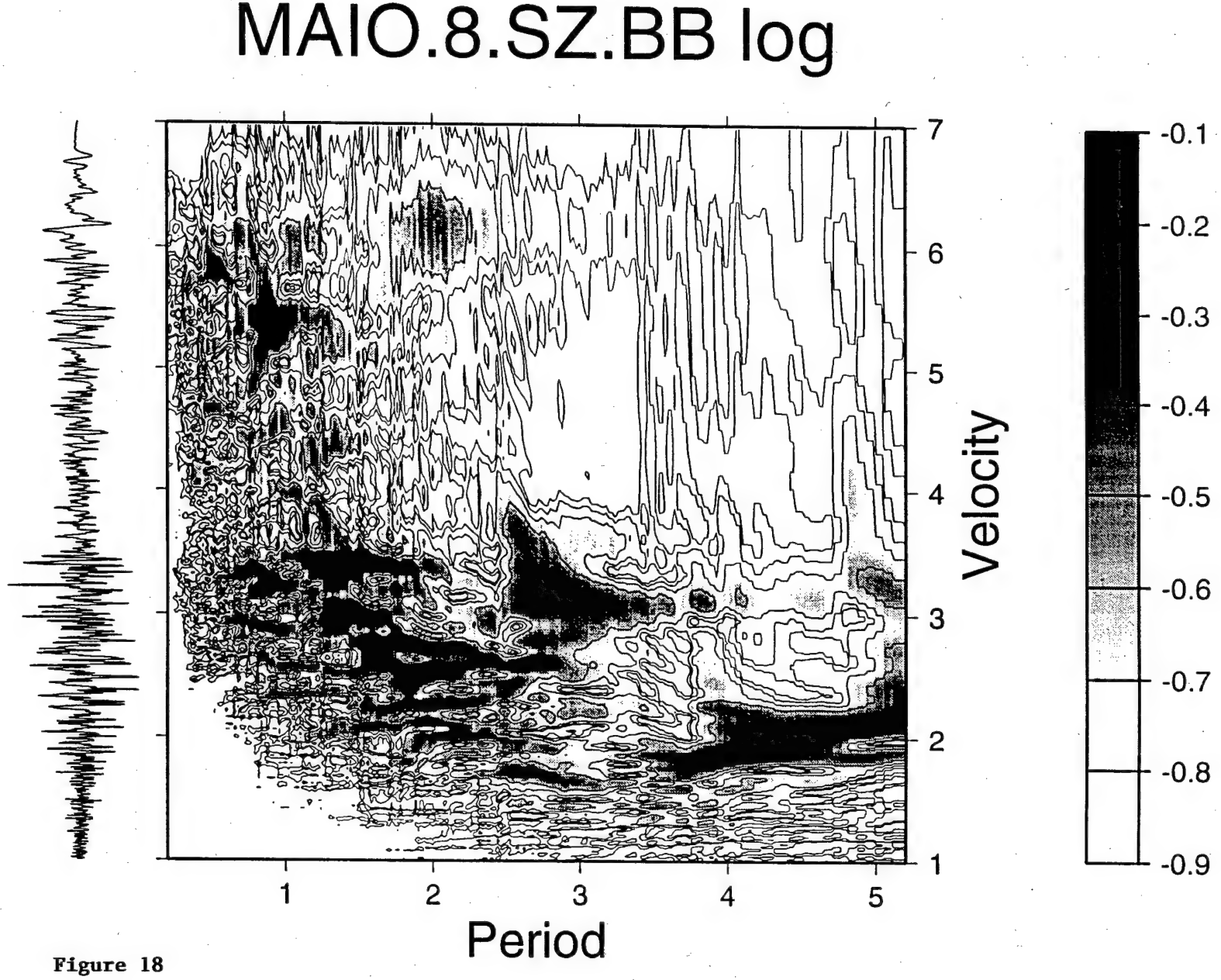
MAIO.8.SZ.BB log
7
6
5
4
3
2
1
Velocity
-0.1
-0.2
-0.3
-0.4
-0.5
-0.6
-0.7
-0.8
-0.9
1
2
3
4
5
Period

Figure 18

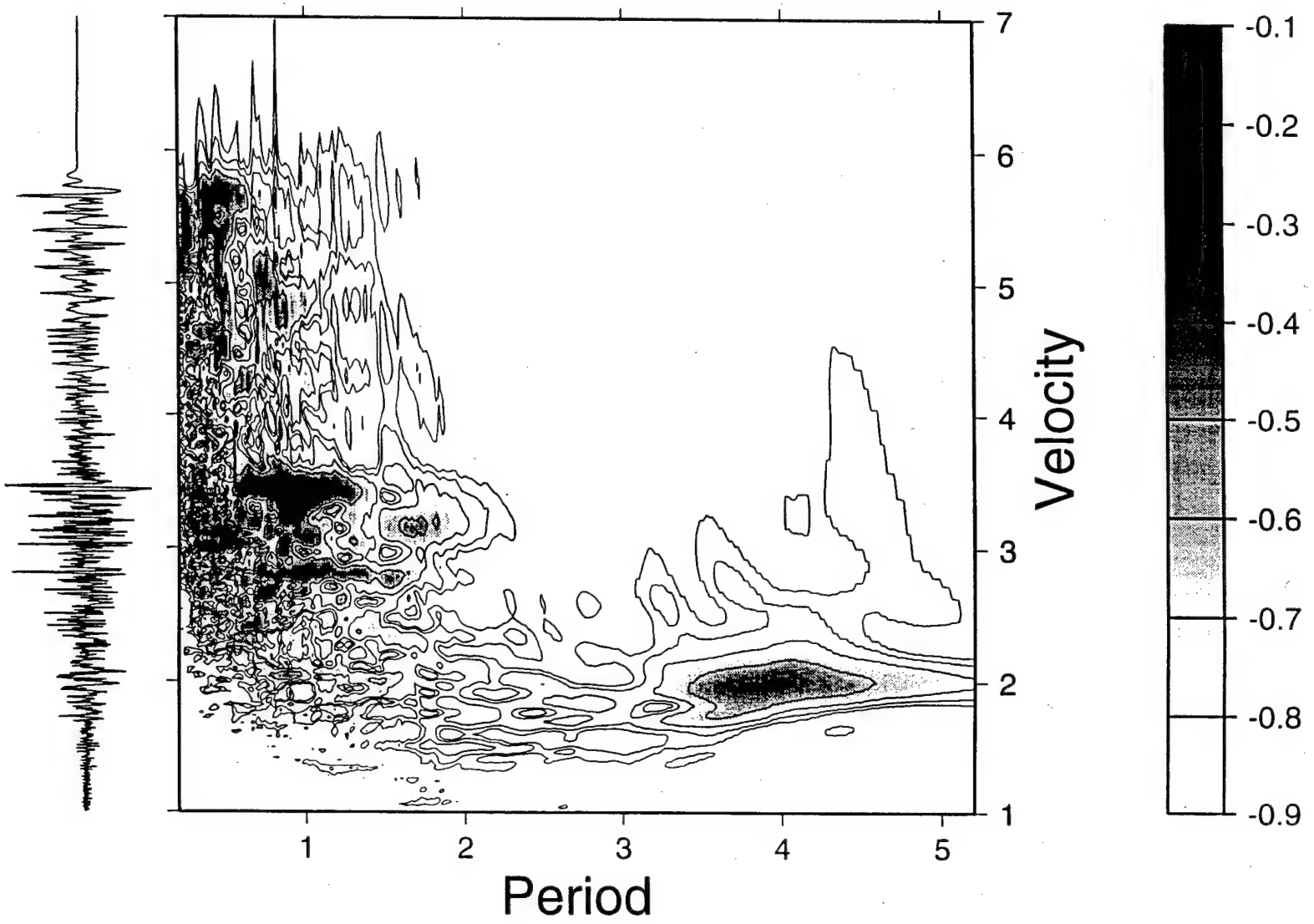
MAIO.9.SZ.BB log
Velocity
Period
1
2
3
4
5
6
7
-0.1
-0.2
-0.3
-0.4
-0.5
-0.6
-0.7
-0.8
-0.9

Figure 19

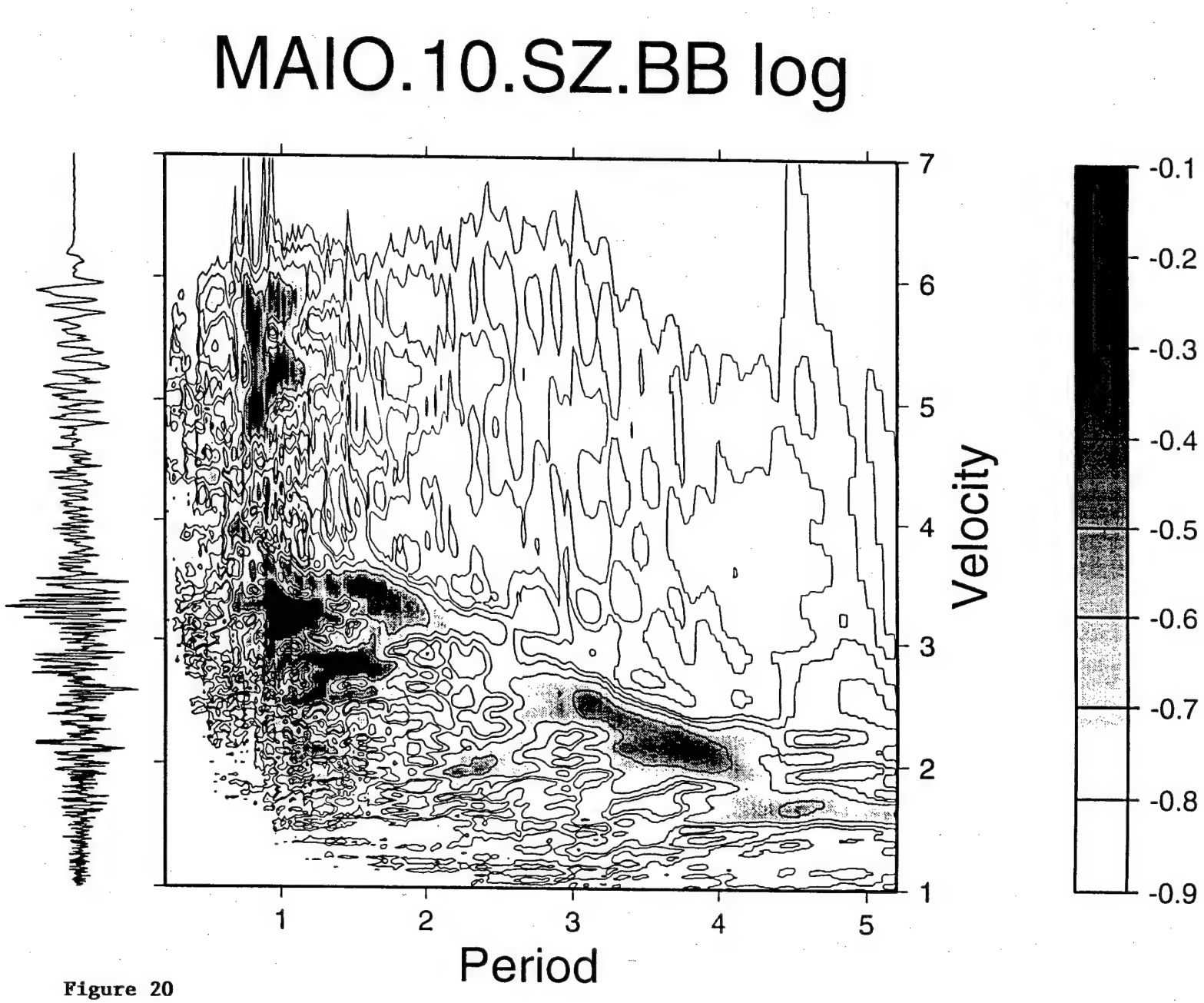
MAIO.10.SZ.BB log
Velocity
Period
1
2
3
4
5
6
7
-0.1
-0.2
-0.3
-0.4
-0.5
-0.6
-0.7
-0.8
-0.9

Figure 20

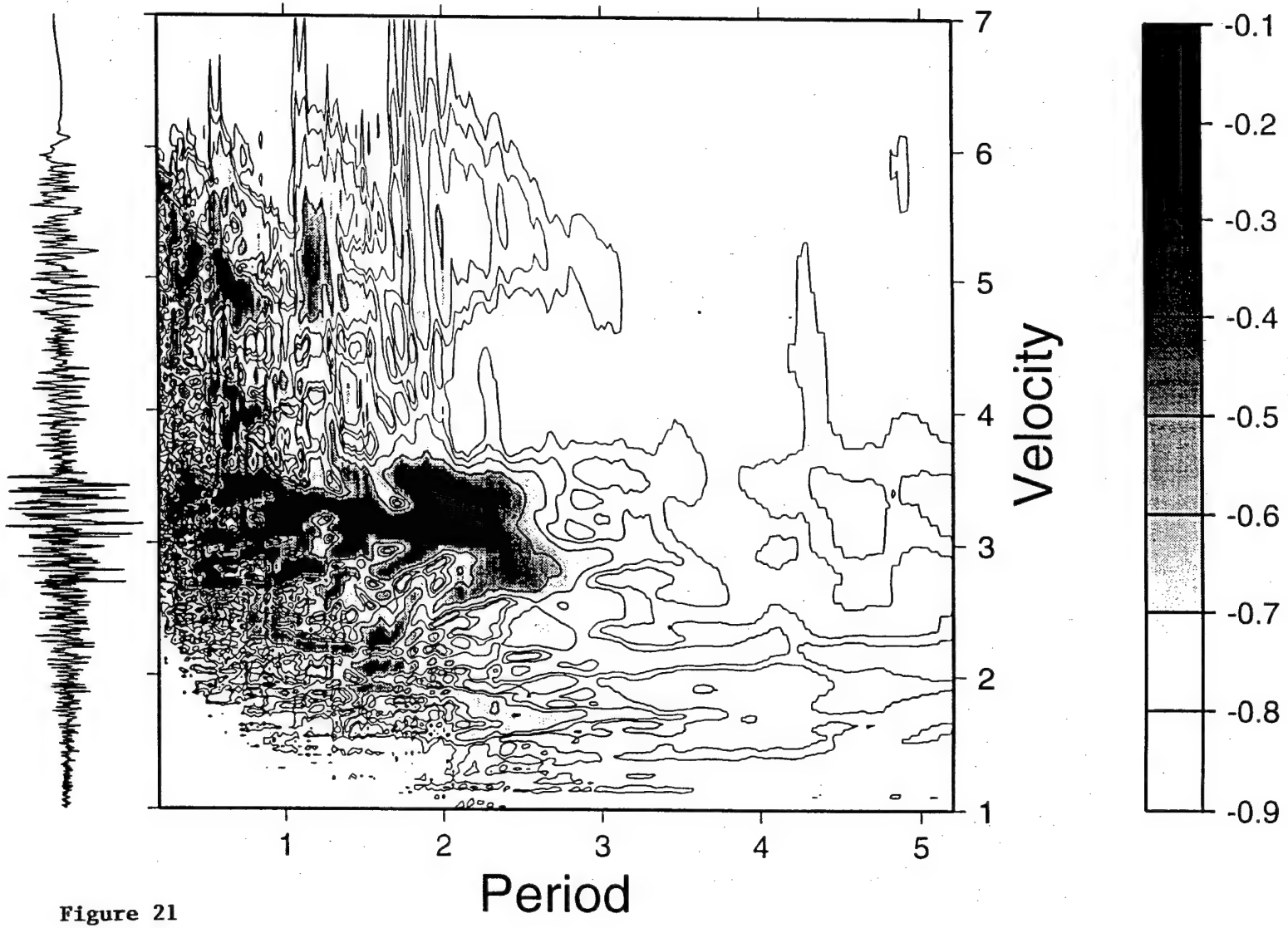
MAIO.13.SZ.BB log
7
6
5
4
3
2
1
Velocity
-0.1
-0.2
-0.3
-0.4
-0.5
-0.6
-0.7
-0.8
-0.9
1
2
3
4
5
Period

Figure 21

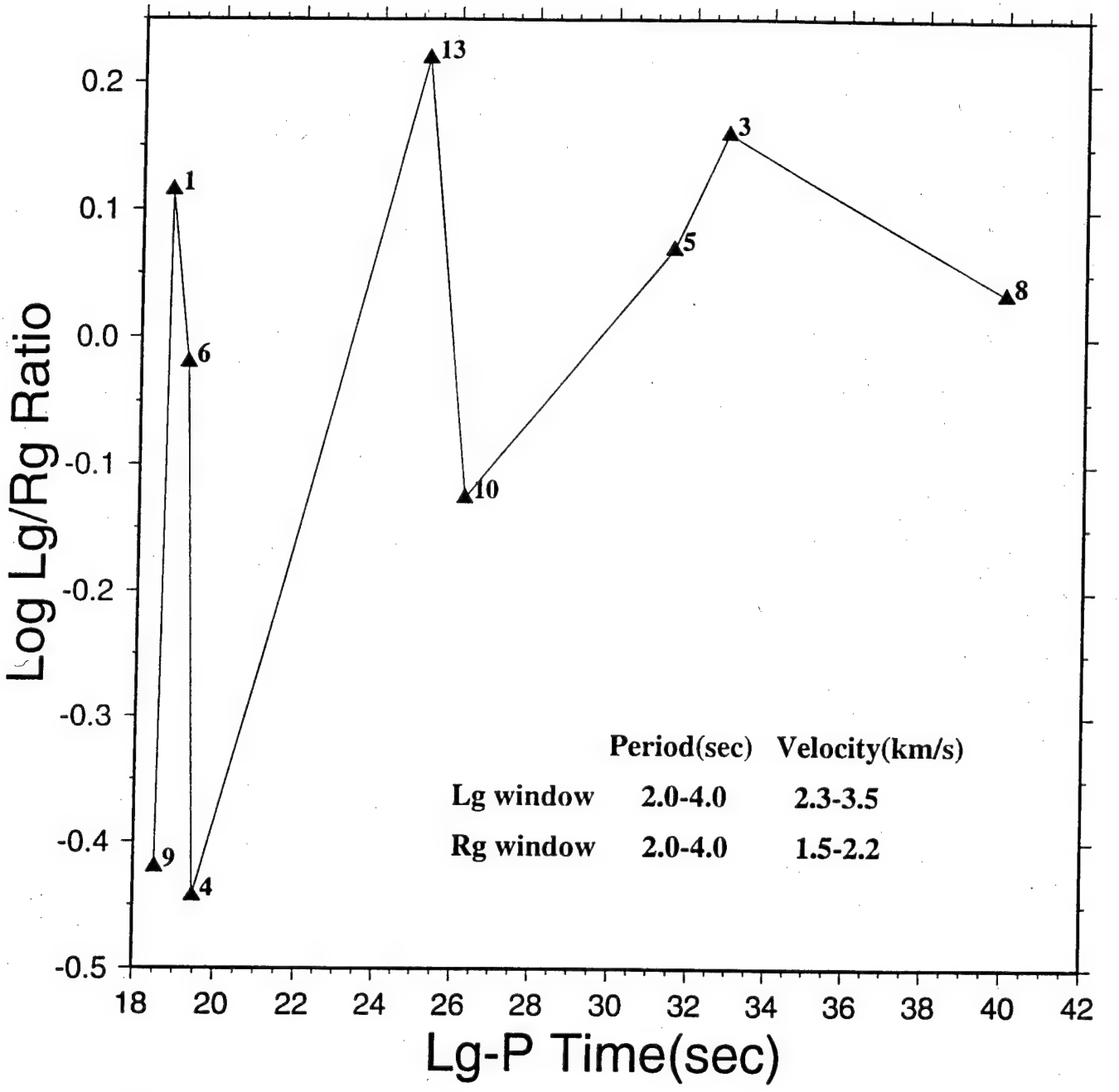
Log Lg/Rg Ratio
Lg-P Time(sec)
0.2
0.1
0.0
-0.1
-0.2
-0.3
-0.4
-0.5
18
20
22
24
26
28
30
32
34
36
38
40
42
1
3
4
5
6
8
9
10
13
Period(sec) Velocity(km/s)
Lg window 2.0-4.0 2.3-3.5
Rg window 2.0-4.0 1.5-2.2

Figure 22

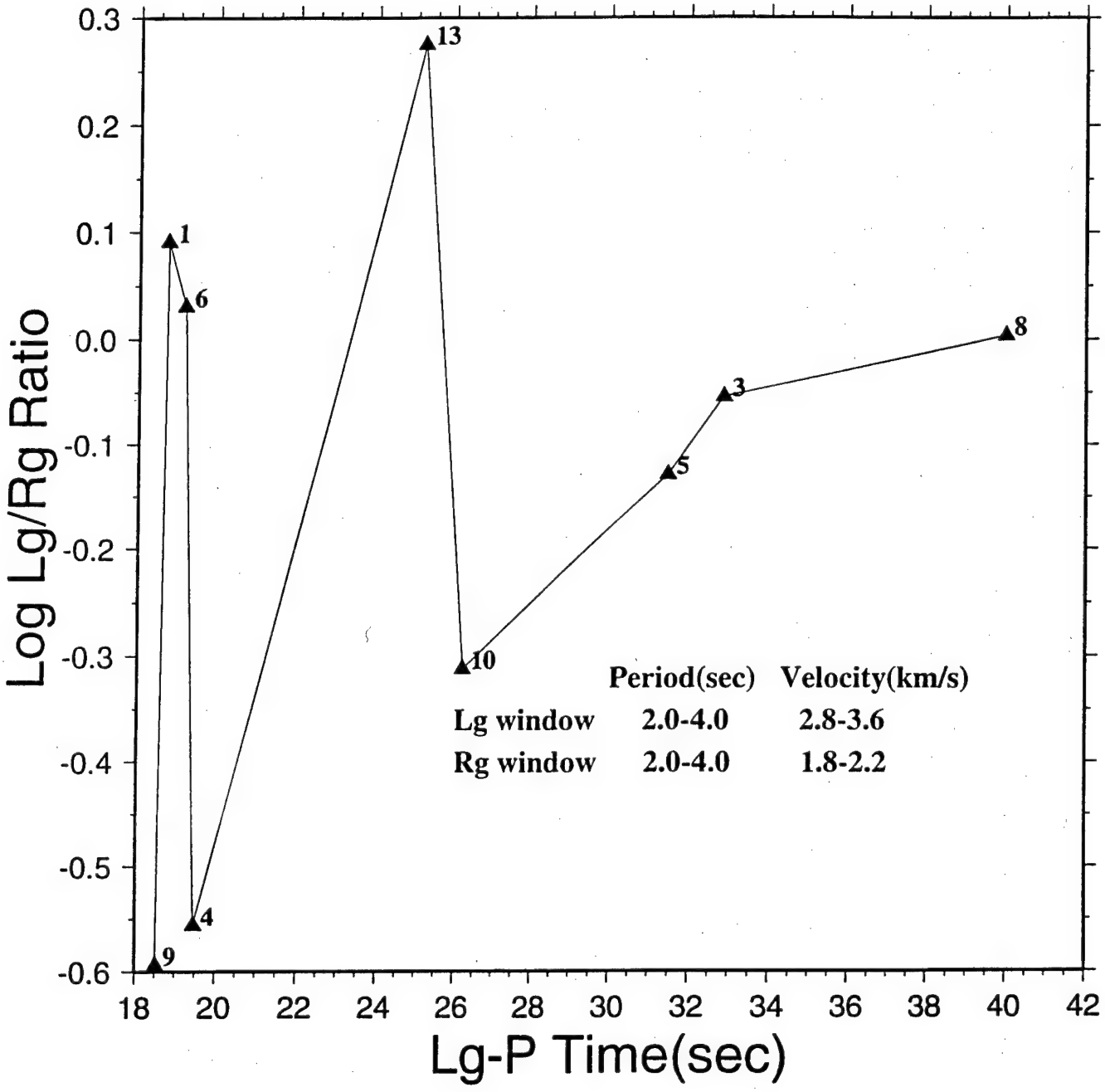
Log Lg/Rg Ratio
Lg-P Time(sec)
0.3
0.2
0.1
0.0
-0.1
-0.2
-0.3
-0.4
-0.5
-0.6
18
20
22
24
26
28
30
32
34
36
38
40
42
1
3
4
5
6
8
9
10
13
Period(sec) Velocity(km/s)
Lg window 2.0-4.0 2.8-3.6
Rg window 2.0-4.0 1.8-2.2

Figure 23

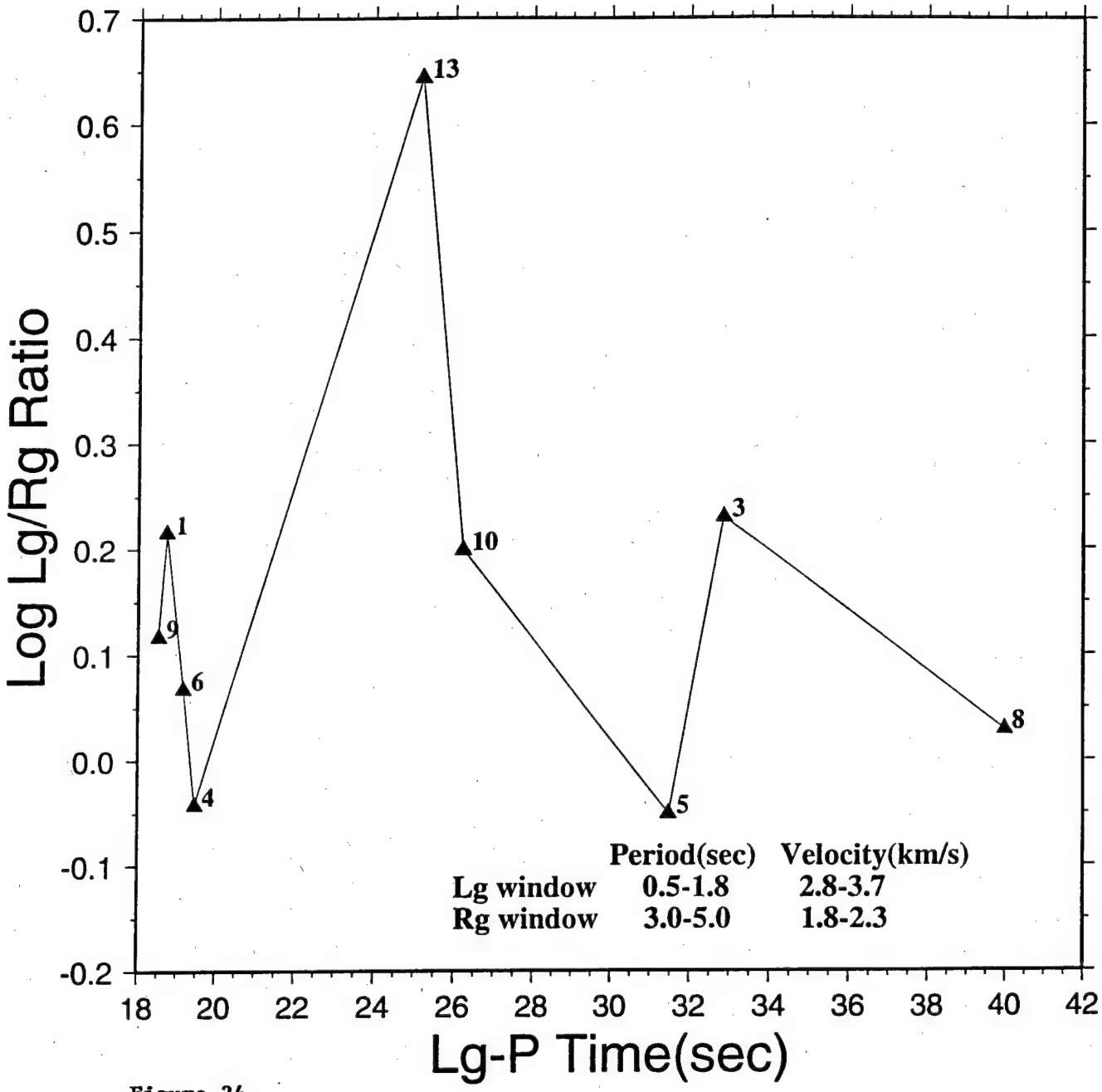
0.7
0.6
0.5
0.4
0.3
0.2
0.1
0.0
-0.1
-0.2
Log Lg/Rg Ratio
18
20
22
24
26
28
30
32
34
36
38
40
42
Lg-P Time(sec)
13
1
10
3
9
6
8
4
5
Period(sec) Velocity(km/s)
Lg window 0.5-1.8 2.8-3.7
Rg window 3.0-5.0 1.8-2.3

Figure 24

Appendix B

The Pennsylvania State University

The Graduate School

Department of Electrical Engineering

SEISMIC SIGNAL PATTERN RECOGNITION

A Thesis in

Electrical Enginering

by

Chaoming Hsu

Submitted in Partial Fulfillment
of the Requirements
for the Degree of

Doctor of Philosophy

May 1995

ABSTRACT

In this study several artificial neural network pattern recognition techniques have been developed and implemented to discriminate between natural earthquakes and underground explosions using entire seismic signatures recorded at regional distances. Seismic events collected from the regional array (NORESS) in Norway and the single station (WMQ) in China are used for the purpose of testing various seismic signal discrimination methods. To compare on a common basis seismic signals that have travelled different distances and hence have different durations, signals are transformed from time to velocity or slowness. It is also desirable to compare the spectral distribution of signal energy present at common propagation velocities or slownesses. Thus, the starting point of this study is the transformation of observed time-domain seismic signals into spectrum-normalized and noise-corrected frequency-velocity or frequency-slowness spectral images. Artificial neural network (ANN) pattern recognition models are then designed and applied to these noise-corrected composite seismic images.

Recent developments indicate that artificial neural networks are appropriate for solving difficult problems in signal discrimination and classification. An ANN learns to solve a problem by training on examples of real or simulated data; thus, with ANNs it is not necessary to specify classification rules or algorithms explicitly. To test the ANN models, the entire composite seismic images or feature images are used as input to the ANN models. Thus, the geophysical information content of the entire seismic image can be fully utilized. Several design strategies using neural network

pattern recognition methods for seismic event identification are investigated and applied to actual data from several geographical regions. These include multilayer perceptron, image compression neural network and reference image identification. The ANN techniques for seismic event identification are the principal focus in this study.

For data sets of 11 natural earthquakes and 11 mining (chemical) explosions recorded by the NORESS array in Norway and 15 natural earthquakes and 15 nuclear explosions recorded by the single station WMQ in China, each event group (earthquake or explosion) is found to be separable by the ANNs in the feature space chosen. The recognition results of three different neural network methods to seismic event identification show that these neural network approaches are all very effective and suitable for near-real-time, automatic event recognition. They have the advantages that entire seismic signatures rather than small subsets of observations are used in the recognition and once trained, the ANNs can be applied automatically, eliminating or minimizing the need for human intervention in the identification process.

TABLE OF CONTENTS

The results described in detail in this thesis appear in the following publications:

Hsu, R. C. and S. S. Alexander, 1993, Recognition of Earthquakes and Explosions Using a Data Compression Neural Network, Proc. IEEE-SP Workshop on Neural Networks for Signal Processing III, 421-430.

Hsu, R. C. and S. S. Alexander, 1993, Seismic Signal Recognition Using Layered Perceptron and Data Compression Neural Networks, Proc. Intl. Symposium on Artificial Neural Networks, Hsin Chu, Taiwan, 35-44.

Alexander, S. S., R. C. Hsu, I. N. Gupta, and D. H. Salzberg, 1994, Development of Discriminants and Improved Locations for Regional Events in Iran, Proc. 16th Annual Seismic Research Symposium, Thornwood, New York, Sept. 7-9, 12-19.

Hsu, R. C. and S. S. Alexander, 1994, A Neural Network Approach to Seismic Event Identification Using Reference Seismic Images, Proc. IEEE Intl. Conference on Systems, Man and Cybernetics, San Antonio, October 2-5, 2108-2113.

Alexander, S. S., R. C. Hsu, S. L. Karl, I. N. Gupta, and D. H. Salzberg, 1995, New Techniques for Estimating Source Depth and Other Diagnostic Source Characteristics of Shallow Events From Regional Observations of P. Lg and Rg signals, Proc. 17th Seis. Res. Symposium on Monitoring a Comprehensive Test Ban Treaty, PL-TR-95-2108, Env. Res. Paper, No. 1173, 821-830.

Appendix C

The Pennsylvania State University

College of Earth and Mineral Sciences

Department of Geosciences

MAGNITUDE AND SOURCE DEPTH ESTIMATES OF EARTHQUAKES IN IRAN FROM REGIONAL OBSERVATIONS

A Thesis in

Geosciences

by

Sheri Lynn Karl

Submitted in Partial Fulfillment
of the Requirements
for the degree of

Bachelor of Science in Geosciences

May 1995

We approve this thesis. Date of Signature

Shelton S. Alexander, Professor of Geophysics
Thesis Advisor — May 8, 1995

Albert L. Guber, Professor of Geology
Chair of the Undergraduate Program — 5/8/95

MAGNITUDE AND SOURCE DEPTH ESTIMATES FOR EARTHQUAKES AND EXPLOSIONS IN IRAN FROM REGIONAL OBSERVATIONS

Abstract

Short-period signals recorded digitally at the station MAIO and the ILPA array in Iran have been analyzed for a number of Iranian earthquakes and explosions. The events are in the distance range of approximately 300 to 1000 km.

Estimation of the relative excitation of the various regional phases is facilitated by multiple narrow-band filtering. Empirical regional magnitude estimation formulas using coda-length and Lg amplitude respectively have been developed. These formulas are derived by measuring durations, Lg amplitudes, and distances for a set of calibration events that have well-determined teleseismic magnitudes. Regression fits to these data establish the magnitude relationships that can be used to estimate magnitudes of regional events too small to be recorded teleseismically.

Focal depth determination using regional recordings can be achieved from cepstral analysis of the P and P-coda time window which contains the persistent delay-time pattern of pP-P and sP-P arrivals. The cepstra for several different time windows within the S - P window are stacked, resulting in a prominent peak above the noise that indicates the pP-P and/or sP-P two-way travel times. Thus, it is possible to make depth estimates based on regional data at only one receiver. Examples for events whose depths are independently known from teleseismic pP-P observations or from Rg phases demonstrate the effectiveness of this cepstral stacking method for depth estimation.

Table of Contents

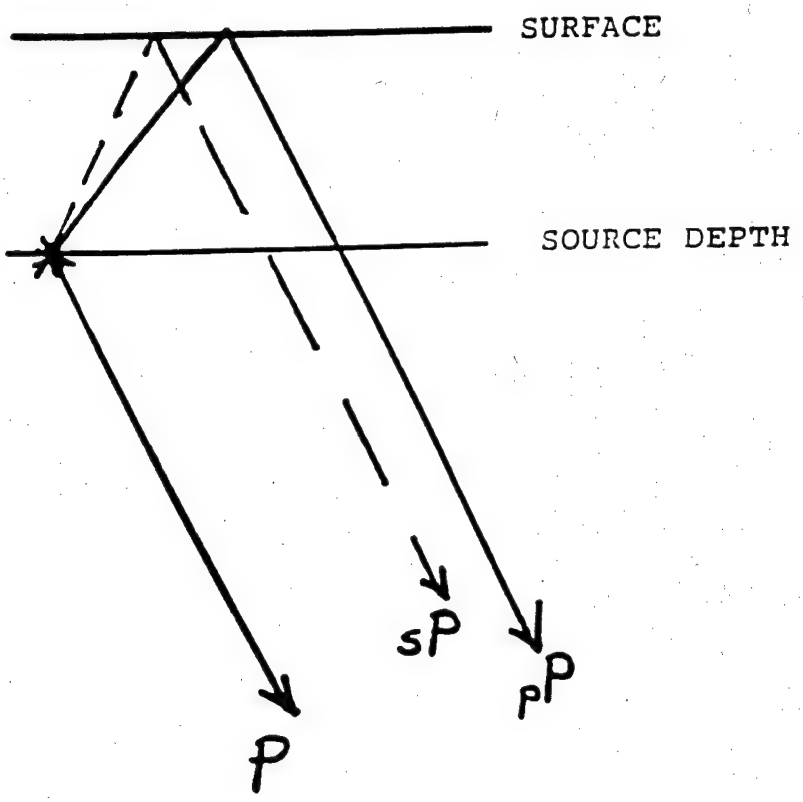

* - INDICATES EVENT

Figure 13. A sketch of the ray paths for P, pP and sP.

5.0 Discussion

5.1 Coda-Magnitude Method

Coda-magnitude relationships allow for magnitude estimates to be made for small events recorded at only one or a small number of stations. The coda-magnitude formula also does not exhibit a strong distance dependence which means that accurate epicenter locations are not necessary to determine an event's magnitude. It will be important to know the magnitudes of the smallest events in Iran in order to assess the practical threshold where various regional discriminants begin to fail. If a new regional station or dense array becomes operational, a coda magnitude formula for that receiver site can be derived following the same approach used in this study.

5.2 Lg Magnitude Method

The Lg-magnitude formula developed by Nuttli (1973) has proven successful for estimating magnitudes of seismic events in eastern North America. His formula was established using regional observations of Lg amplitude for earthquakes whose teleseismic magnitudes were available. His equation for the NE United States is:

$$m_{b_{Lg}} = \log(A/T) + 0.90\log(\Delta) + 3.75$$

$$0.5^\circ \leq \Delta \leq 4^\circ$$

$$m_{b_{Lg}} = \log(A/T) + 1.66\log(\Delta) + 3.30$$
$$4° \leq \Delta \leq 30°$$

where A is the maximum sustained Lg amplitude in microns, T is the period in seconds and, Δ is the epicentral distance in degrees.

An analogous relationship was developed by Nuttli (1980) for Iran using analog WWSSN stations. His results for Iran have been discussed in a previous section, but the formula he found was: $m_{b_{Lg}} = \log10(A) + 3.62\log10(\Delta) - 4.80$. The present study made use of digital data from the ILPA array in Iran to develop an Lg magnitude formula. A comparable procedure to the one used by Nuttli (1973) was used to develop an empirical Lg magnitude relationship that agrees reasonably well with Nuttli's formula for Iran; it is: $m_{b_{Lg}} = \log10(A) + 4.047\log10(A) - 0.7722$. Hence, this relationship would be appropriate to apply to other regional events in Iran recorded by in the ILPA array. Note that instrument gain at ILPA has not been considered in this study; this is reflected in the constant term in the regression fit which is different from the constant term in Nuttli's formula.

An important point with regard to Lg-based magnitudes is that Lg is the high frequency equivalent of M_S, the long-period surface wave magnitude. M_S vs m_b is one of the most powerful

discriminants, such that for a given m_b, M_s for an underground nuclear explosion is typically .6 to .8 or more magnitude units smaller than the M of an earthquake with the same m_b. The physical reason for this difference is that an explosion source theoretically generates only P-waves whereas an earthquake source generates strong S-waves (as well as P-wave) which contribute significantly to the observed Rayleigh wave signals. The vertical-component Lg used for the m_{bLg} determination is composed of higher-mode Rayleigh waves whose excitation is significantly larger for earthquakes than explosions (i.e. the Lg/P discriminant). Therefore, an explosion of the same teleseismic m_b as an earthquake will have a m_{bLg} that is significantly smaller, whereas, by construction in developing the m_{bLg} formula the teleseismic m_b and m_{bLg} are the same for earthquakes. This leads to the interesting possibility that coda magnitude vs. m_{bLg} may serve as a regional discriminant that is the direct analog of m_b vs. M_s. The two empirical magnitude formulas for m_c and m_{bLg} developed in this study could be used in this way.

5.3 Cepstral Stacking Method

The new depth determination method using cepstral stacking is based on the same principles as the cepstral method developed by Stockar (1986), where stacking cepstra for the S - P time-windows from a regional network proved successful for enhancing depth phases for regional seismic events.

Both cepstral methods work because the entire S - P window contains common depth-phase delay times for pP-P and sP-P. The S - P window, at different stations, contains differing delay times (with respect to the initial P-arrival) for various regional phases Pn, Pg, etc. That is, from receiver to receiver, crustal phases show up with different relative delay times. When the cepstra of these individual windows are stacked the common delay times of pP-P and sP-P are enhanced, while the crustal arrivals with differing delay times become muted. The new cepstral stacking method developed and implemented in this study uses a similar rationale that by stacking cepstra for sub-windows in the S - P window the depth phases common to all the sub-windows will then be enhanced while different crustal phases appear in different sub-windows such that their delay times are not common to all the sub-window cepstra. Thus taking the sub-window stacks, the common delay times of the depth phases are preserved while delay times associated with different crustal arrivals not common to all are dampened. Stacking using both arithmetic and geometrical means was performed. They both produce enhanced depth phase delay times; however, the geometrical mean (product of all individual cepstra yields more dramatic enhancement of the depth phases.

The new method was tested by analyzing Iranian earthquakes with several pP-P teleseismic depth phases reported in the ISC bulletin or with prominent Rg phases. As discussed earlier, there is close agreement between the teleseismic and regional

pP-P times (hence depth) for the magnitude 4.7 Iranian earthquak that occurred on 6 December 1978. This example illustrated the ability of the new cepstral stacking technique to determine pP-P delay times that are remarkably consistent with those observed teleseismically and, therefore, to obtain a reliable depth estimate from a single regional station. Similarly, shallow cepstral depths were found for events with prominent Rg phases, and a Kazakhstan underground nuclear explosion recorded at MAIO gave a very shallow cepstral depth.

It is important to emphasize that while teleseismic and regional depth-phase delays (hence depths) of Iranian events were found to be in close agreement, the published ISC hypocente determinations of their depth are systematically biased too deep by 10-20 km compared to depths from pP-P and or sP-P alone. This bias was noted earlier by Asudeh (1983), and in this study it was evident from examining the ISC pP-P residuals for standar hypocenter determinations that used mostly P-arrivals at many teleseismic stations. The inference is that the upper mantle beneath Iran has a higher velocity than that corresponding to the standard travel-time curves used for hypocenter determinations. This is the opposite of what one might expect in a region of active tectonism and low Pn velocities that imply higher-than-normal temperatures at the Moho. In any case, this bias, if not accounted for, could lead to misidentification of explosions as earthquakes based on teleseismic observations alone, because they would appear to be too deep to be explosions

5.4 Advantages: Cepstral Stacking Method

(1) The new cepstral stacking approach to depth determination requires only one regional station's data whereas other depth estimation techniques require a network of regional stations.

(2) The calculation can be performed routinely and rapidly; thus it may be largely automated for near real-time depth determinations.

(3) The approach may remain reliable for very small magnitude events where the signal to noise ratio is marginal. The presence of random noise in each sub-window should not introduce systematic cepstral peaks, whereas the depth phases would continue to be enhanced.

6.0 Conclusions

An empirical coda-magnitude formula has been developed for regional use in Iran. The equation is calibrated using data from teleseismic events. It allows the magnitude to be estimated for small events not recorded well teleseismically.

An empirical Lg magnitude formula for Iran was developed using regional earthquake data recorded at the ILPA array. It agrees reasonably well with the $m_{b_{Lg}}$ formula developed by Nuttli (1980) for Iran using analog data at WWSSN stations. It is suggested that the coda magnitude vs. $m_{b_{Lg}}$ for small events may serve as the approximate equivalent of the m_b vs. M_S discriminant.

A new method for depth estimation has been developed and tested in this study. It consists of cepstral stacking for different sub-windows in the S - P window of events recorded at a single regional station. Based on test cases it appears to provide depth-phase delays (pP-P and sP-P) which agree closely with depth-phase delays observed teleseismically or with other depth constraints. The observed delays are then used with an average crustal velocity to obtain the depth in Iran. Individual station cepstral stacks can also be extended to network stacks which further enhance depth-phase delay times.

Appendix D

The Pennsylvania State University

The Graduate School

Department of Electrical Engineering

INVESTIGATION OF CEPSTRAL STACKING METHODS FOR TIME DELAY EXTRACTION

A Thesis in

Electrical Engineering

by

Chih-Chieh Yang

Submitted in Partial Fulfillment

of the Requirements

for the Degree of

Master of Science

August 1997

ABSTRACT

Cepstral theory is appropriate for analyzing data that contain echoes or reverberations of a composite wavelet (signature) whose shape need not be known. In this study, several time delay extraction techniques have been developed and implemented to determine the focal depth of earthquakes and explosions using cepstral stacking. The cepstral stacking method investigated consists of computing the cepstra of sub-windows of recorded signals and taking their product or sum. Several modified procedures using cepstral stacking are developed and applied to actual seismic data from several geographical regions. These include envelope normalization, noise power subtraction, bandpass filtering and array stacking. Seismic events recorded at three regional arrays (ILPA, TXAR, KS) are used for the purpose of testing these modified cepstral stacking methods.

Experimental results show that depth-phase delay time cepstral peaks are significantly enhanced through cepstral stacking, allowing accurate and reliable source depths to be determined from complicated regional recordings. Combined individual station and multiple-station cepstral stacking is shown to further enhance the depth-phase delay time cepstral peaks compared to individual station results. Depths accurate to within approximately 1 km can be determined using these methods.

TABLE OF CONTENTS

Page

Chapter 8

SUMMARY AND CONCLUSIONS

The principal objective of this thesis was to study time delay extraction by using cepstral stacking techniques to estimate the focal depth of seismic events. It was shown that cepstral stacking methods can improve the desired time delay extraction by enhancing the depth-phase cepstral peaks and suppressing other unwanted time delays that are present in only a few of the sub-windows.

This thesis has presented the relevant cepstral theory; applications of cepstral stacking approaches to extract depth-phase time delay for source depth determination; and the dependence of cepstral stacking results on three effective parameters (sub-window length, percent overlap and types of stacking). The cepstral method will fail if the signal bandwidth is so small that several cycles of the spectral modulation are not available.(See Cohen (1970) for using spectral stacking over multiple stations to get the first null when the delay time is small.) Several modified cepstral stacking approaches to improve the time delay extraction were developed and tested. A specific signal-to-noise ratio test and a signal detection method were developed to determine the likelihood that a cepstral peak is significant (not noise).

According to the empirical test cases analyzed, a shorter sub-window is better for a real seismic signal, while theoretically a longer sub-window is more appropriate for an ideal, noise-free signal. The ideal overlap percentage depends on the sub-window length and the depth-phase time delay of each individual signal. Each sub-window must be longer than that depth-phase delay time; since this delay time is not known in advance, a sub-window length that would capture the pP and P for any crustal source depth (about 15 seconds or greater) should be used. The overlap should be at least equal to the (unknown) pP-P delay time to assure that all the pP-P delay times present are included at least once in the stacking. From the empirical tests done it appears that a 60-75% overlap gives the best results. All of the experimental cepstral stacking results show that product stacking is better than sum stacking, so product stacking is suggested.

Four modified cepstral stacking approaches were investigated in this study: envelope normalization, noise power subtraction, bandpass filtering and combined individual receiver and array stacking. The primary objective of envelope normalization is to reduce contributions from unwanted crustal arrivals; it achieves this goal in the experiments carried out for two different arrays. Bandpass filtering is a straightforward way to improve the cepstral results; application of bandwidth selection procedures developed in this study enhanced the depth-phase cepstral peaks. For the regional seismic signals analyzed for the TXAR array, the signal bandwidth is 0.2-10 HZ; the optimal bandwidth is 0.5-8 HZ for a Yellow Sea earthquake observed at the KS array in Korea. Array stacking was employed for three experimental arrays; the improved cepstral results

indicate that array stacking should be carried out when a seismic array or network is available.

The depth phase time delay for the 6 December 1978 Iranian event, obtained from cepstral stacking of the ILPA array, is about 7.1 seconds which agrees within 0.1 seconds with the independent determinations from observations of the teleseismic pP and P; using the depth formula with an assumed crustal velocity of 6 km/sec for Iran, the source depth for this event is approximately 21 km. Thus this event can be reliably recognized to be an earthquake. The depth-phase time delay for the 23 December 1995 northern California event recorded by the TXAR array is about 1.8 seconds corresponding to a source depth of about 4.5-5 km; this result agrees well with depth determinations from a dense local network in California. The depth-phase time delay for a Yellow Sea earthquake on 3 November 1992 recorded at the KS array in Korea is about 2.0 seconds. Therefore, the source depth for this event is approximately 5-6 km if the delay time represents pP, and approximately 4 km if it represents sP.

This thesis has demonstrated the effectiveness and feasibility of using cepstral stacking, or modified cepstral stacking, to extract the depth-phase time delay from regional seismic signals. All of the modified cepstral methods investigated in this study could be applied whether or not cepstral stacking is done, as they are, in effect, pre-processors in the time or frequency domain prior to computing the cepstrum. Based on cepstral stacking results for events whose depths are independently known, it appears that depths accurate to within about 1 km can be estimated solely from regional seismic

recordings. Such a capability will allow source depth to be used as a discriminant to distinguish earthquakes from underground nuclear explosions when the events are too small to be well recorded teleseismically.

Appendix E

Proceedings of the 19th Annual Seismic Research Symposium on Monitoring a Comprehensive Test Ban Treaty

23-25 September 1997

Editors:
Michael J. Shore
Rong Song Jih
Anton Dainty
Joan Erwin

5 September 1997

APPROVED FOR PUBLIC RELEASE; DISTRIBUTION UNLIMITED.

Defense Special Weapons Agency/Special Programs
6801 Telegraph Road
Alexandria, VA 22310

HQ Air Force Technical Applications Center
Nuclear Treaty Monitoring Directorate
Patrick Air Force Base, FL 32925-3002

Department of Energy
Office of Nonproliferation & National Security
Washington, DC 20585

ACCURATE DEPTH DETERMINATIONS AND OTHER DIAGNOSTIC EVENT CHARACTERISTICS IN NEAR-REAL TIME FROM REGIONAL SIGNALS

Shelton S. Alexander and Chih-Chieh Yang
The Pennsylvania State University

Sponsored by the Air Force Office of Scientific Research
Grant No. F49620-94-1-0179

ABSTRACT

Further tests of the Cepstral Stacking Method (CSM) developed in earlier phases of this study have been conducted for crustal events in different geologic settings recorded at regional distances. CSM can be used to obtain accurate focal depth from only one regional station as well as from arrays and combinations of arrays and individual stations when they are available. The procedure is to stack the cepstra of a set of overlapping sub-windows in the (S - P) signal window for each station or array element; for the multi-station or array case the individual stacked cepstra for each station/array element are stacked. Depth-phase delay times are enhanced by this process while delay times between various crustal arrivals are suppressed. Product stacking is shown to be superior to sum stacking.

Software developed to implement the CSM allows depth determinations to be made in near-real time. Various pre-processing options to enhance the effectiveness of the method are also available; they include band-pass filtering, envelope normalization, spectral smoothing, and noise power subtraction.

Based on results for events with independently-known focal depths, accuracies of about 1 km or better can be achieved when signal bandwidths are greater than approximately 5 Hz.

Other diagnostic event characteristics can also be derived from the same data sets in near-real time. For example, band-pass filtering can be used to look for Rg. The presence of Rg indicates that the event is shallow and can be used to confirm a shallow depth obtained by the CSM. When an event is shallower than about 5 km, other information must be used to distinguish earthquakes from explosions; pattern recognition or artificial neural network techniques, among others, can be used to identify regional events in near-real time.

Examples are given to illustrate these methods for different types of regional events.

OBJECTIVE

The overall objective of this research is to develop regional discriminants that can be obtained in near-real time to facilitate automated or mostly-automated regional event identification. Recent efforts have been focused on obtaining accurate focal depths from regional observations in different source regions using the Cepstral Stacking Method developed in this project; investigating improvements in the effectiveness of the CSM; and configuring software for near-real-time depth determinations. Pattern recognition and artificial neural network (ANN) methods developed earlier in this work also can be used in conjunction with the CSM for automated or mostly-automated event discrimination. The relevance of this research to a CTBT is that the CSM provides accurate focal depths from regional observations, unlike other methods which commonly give biased depth estimates; near-real-time CSM depths can then be used to reduce the number of events that require detailed analysis by culling out events that are deeper than 5 km (earthquakes). The pattern recognition and ANN methods developed earlier provide additional capability for rapid regional event identification.

RESEARCH ACCOMPLISHED

The research reported here is an extension of earlier work under this Grant to develop and test the CSM for accurate depth determinations for regional events from single stations and from arrays or networks of regional stations. The CSM and previous results are described in Alexander et al. (1995), Karl (1995), Alexander (1996), and Alexander and Yang (1996). Yang (1996) and subsequent recent work have developed modifications to the basic CSM to ehance its effectiveness; in addition CSM analyses of events from Iran, Korea, western Turkey, and the western United States have been carried out. The CSM software has also been reconfigured to facilitate near-real-time analysis of regional events.

Results to date on crustal events (earthquakes and explosions) with independently-known source depths, indicate that, with signal band-widths of approximately 5 Hz or greater and reasonable signal-to-noise levels, accuracies in source depth of about 1 km or better can be achieved using the CSM.

Figures 1 and 2 show examples of single-station CSM results for two, small regional events in Iran recorded at the SRO station MAIO. Also shown are narrow-band-filtered signals for these events; it is clear that there is a good signal to noise ratio in the frequency band from 0.5 to 7 Hz in the S - P window for both events. The 2/23/77 event (Figure 1) has a strong cepstral peak at a delay time of 2.6 seconds, whereas the 6/04/77 event (Figure 2) has a strong cepstral peak at 0.8 seconds, indicating it is very shallow and significantly shallower than the 2/23/77 event. If the observed cepstral peaks correspond to pP - P delays, the depth of the 2/23/77 event is approximately 7.8 km and the 6/04/77 event is approximately 2.4 km deep, assuming an average crustal P-velocity of 6 km/sec; the depths would be 5.85 and 1.8 km respectively, assuming an average crustal P-velocity of 4.5 km/sec. If the peaks correspond to sP - P, the depths would be 5.85 and 1.8 km, respectively, for a 6 km/sec crustal P- velocity compared to 4.3 and 1.3 km, respectively, for a 4.5 km/sec crustal P-velocity. Therefore, the 2/23/77 event would be identified as an earthquake, whereas the 6/04/77 event cannot be identified based on focal depth alone (if the average shallow crustal

velocity is higher than 4.5 km/sec). The 0.1-0.3 band-pass-filtered signals for both events show the presence of a prominent Rg arrival, indicating that both events are relatively shallow but not indicating which one is shallower. However, the presence of Rg helps corroborate the CSM results that give relatively shallow source depths for both events.

In an operational mode the CSM would cull out the 2/23/77 event and keep the 6/04/77 event for further evaluation using other discriminants. The relatively large Lg/P ratios for the higher frequencies in the band-pass-filtered signals suggest that the 6/04/77 event is also an earthquake..

Other examples of single-station CSM depths are shown in Figures 3 for a magnitude 5 mainshock and two large aftershocks located in western Turkey (Figure 4) that were recorded at the broad-band station DPC at a distance of approximately 1515 km. These events were widely recorded globally, so both the absolute and relative locations are very well-constrained and a normal-fault focal mechanism of the main shock has been determined (Figure 4). If the focal depths of the three events, which occured only a few hours apart, can be determined accurately, the actual fault plane and its projection to the surface can be found. The table included in Figure 6 compares the focal depths for these three events determined from the ISC stations, the ISC using pP - P, and the CSM for DPC. The ISC (pP - P) and CSM depths agree within 1 km for the mainshock but disagree for the aftershocks. The standard ISC depths are very different, even though a large number of stations were used in the hypocenter determinations. Only a few pP observations were available for ISC's pP - P depth determinations for the two aftershocks and they are not all consistent, whereas the station, propagation path, and processing were identical for the CSM analysis. Therefore, the CSM depths are inferred to be the most accurate. From the manshock's focal mechanism and the CSM depths (Figure 4), one can infer that the actual fault plane is the one dipping to the southwest; it projects to the surface as shown in Figure 4. The relevance of this example to CTBT monitoring is that similar analyses can be done for areas of interest that are seismically active, such as Iran, to define active faults spatially in three dimensions. This would provide a valuable addition to the knowledge base needed to distinguish earthquakes from explosions in active seismic areas.

An example of combined array and individual station CSM depth determination is shown in Figure 5 for a regional event in north-central Iran recorded at the ILPA array and the SRO station MAIO. In this case the cepstrum for each sub-window was product stacked across the ILPA array and then a final product stack of these composite sub-window stacks and the MAIO cepstral stack was generated (bottom trace). The single, large peak in the final product cepstrum is at 1.5 seconds, corresponding to a source depth of approximately 4.5 km if the peak is pP - P, or 3.3 km if it is sP - P (assuming an average crustal P-velocity of 6 km/sec). If the average crustal P-velocity is less, say 4.5 km/sec, then these estimated depths would be less by a factor of 4.5/6. If this event were encountered during CTBT monitoring, it would be kept for further analysis, because its depth is less than 5 km.

The CSM method has also been applied to regional events recorded at Alpha arrays (e.g. TXAR, the KS Korean array, and NORESS) and to combined KS and individual stations in mainland China. Array stacking and combined array and individual station stacking generally

enhance the depth phase cepstral peak(s) compared to individual station or array-element cepstral peaks and should be used when such data are available.

Further analyses on the same data sets can also be carried out using the pattern recognition and artificial neural network approaches developed earlier in this project (e.g. Hsu, 1995), as well as other discriminant measures, to identify regional events. These CSM and pattern recognition or ANN methods can be applied in near-real-time in automated or mostly-automated operational systems.

CONCLUSIONS AND RECOMMENDATIONS

1. It has been demonstrated that the CSM gives accurate estimates of depth phase delay times using only single regional stations, individual arrays, or combined arrays and distributed regional stations. Tests on calibration events in different source regions indicate that CSM focal depth estimates typically are accurate to 1 km or better.

2. The CSM, as now implemented, allows accurate source depths to be determined in near-real time. In CTBT monitoring, this will permit events deeper than 5 km to be immediately identified as earthquakes requiring no further analysis, thereby significantly reducing the number of events that require more-extensive evaluation.

3. CSM can be used in conjunction with algorithms that give very accurate epicenters and focal mechanisms to determine the 3-dimensional geometry of active faults in source regions of interest for CTBT monitoring (e.g. Iran). Incorporating this information in the ground-truth data base will help identify unknown events located in such active regions.

4. Certain preprocessing steps, such as band-pass filtering, spectral smoothing, and envelope normalization can enhance the effectiveness of the CSM, and product stacking gives significantly better results than sum-stacking.

It is recommended that the CSM be routinely applied to a large number of regional events in different settings to gain further experience with the method and gain confidence in the accuracy of the source depth estimates obtained. In particular the CSM should be applied at all the new Alpha arrays and Beta stations that will be used for CTBT monitoring, to verify that CSM works as expected.

REFERENCES

Alexander, S. S. and C-C Yang, 1996, Use of the Cepstral Stacking Method (CSM) for Improved Source Depth Determinations from Combined Single-Station and Array or Network Observations at Regional Distances, Proc. of the 18th Annual Seismic Research Symposium on Monitoring a Comprehensive Test Ban Treaty, 4-6 Sept. 1996, PL-TR-96-2153, Env. Res. Papers, No. 1195, 647-656.

Alexander, S. S., 1996, A New Method for Determining Source Depth From a Single Regional Station, Seis. Res. Ltrs., Vol. 67, No. 1, p. 63.

Alexander, S. S., R. C. Hsu, S. L. Karl, I. N. Gupta, and D. H. Salzberg, 1995, New Techniques for Estimating Source Depth and Other Diagnostic Source Characteristics of Shallow Events From Regional Observations of P. Lg and Rg signals, Proc. 17th Seis. Res. Symposium on Monitoring a Comprehensive Test Ban Treaty, PL-TR-95-2108, Env. Res. Paper, No. 1173, 821-830.

Hsu, C. 1995, Seismic Signal Pattern Recognition, Ph.D. Thesis, EE, The Pennsylvania State University, 185 pp.

Karl, S. L., 1995, Magnitude and Source Depth Estimates for Earthquakes and Explosions in Iran--Regional Observations, B.S. Thesis in Geosciences, The Pennsylvania State University, 185 pp.

Yang, C. C., 1996, Investigation of Cepstral Stacking Methods for Time Delay Extraction, M.S. Thesis (EE), The Pennsylvania State University, 113 pp.

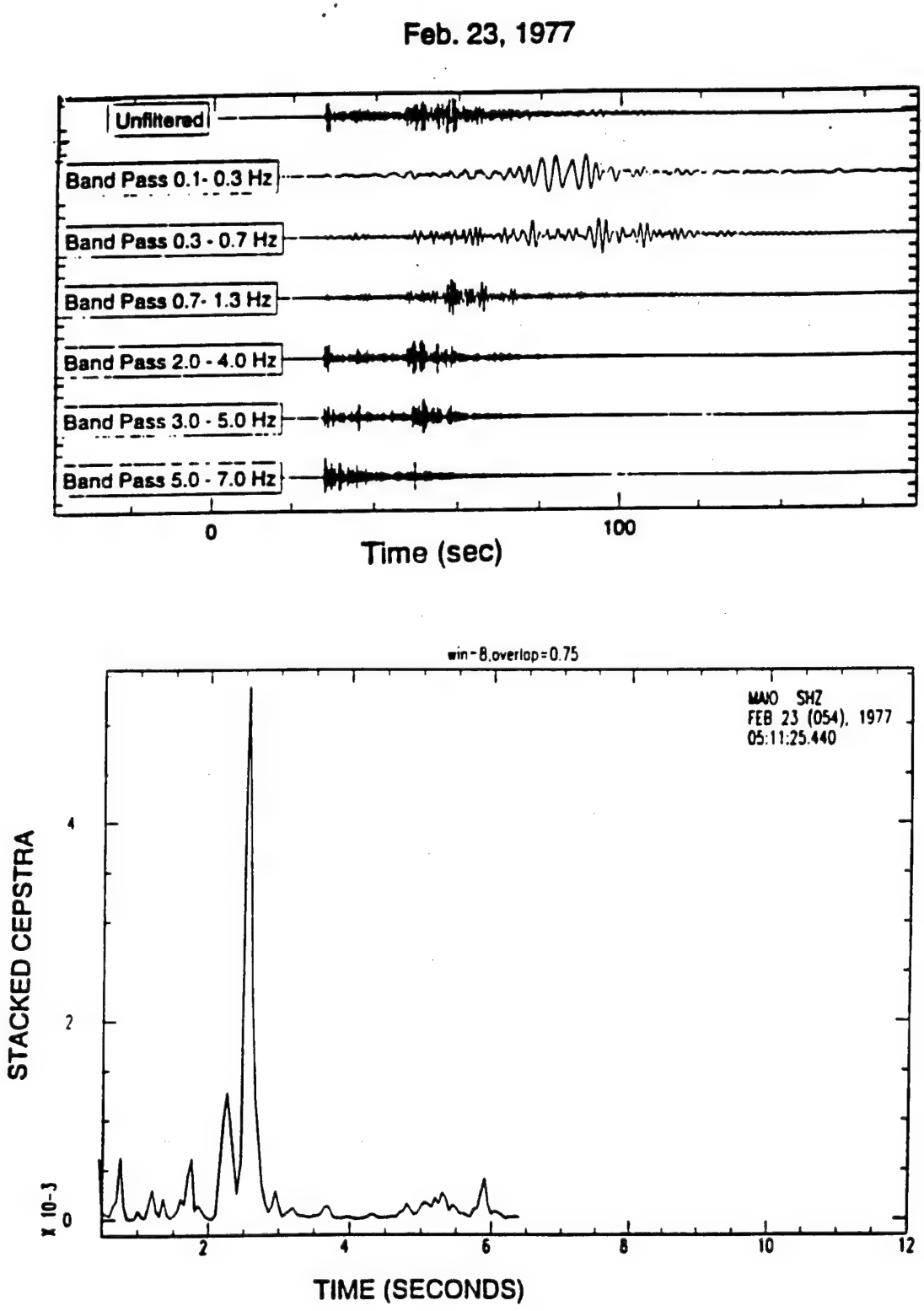

Figure 1. Original and band-pass filtered signals for a regional event on 2/23/77 in Iran recorded at station MAIO (top panel); product-stacked cepstra of sub-windows (bottom).

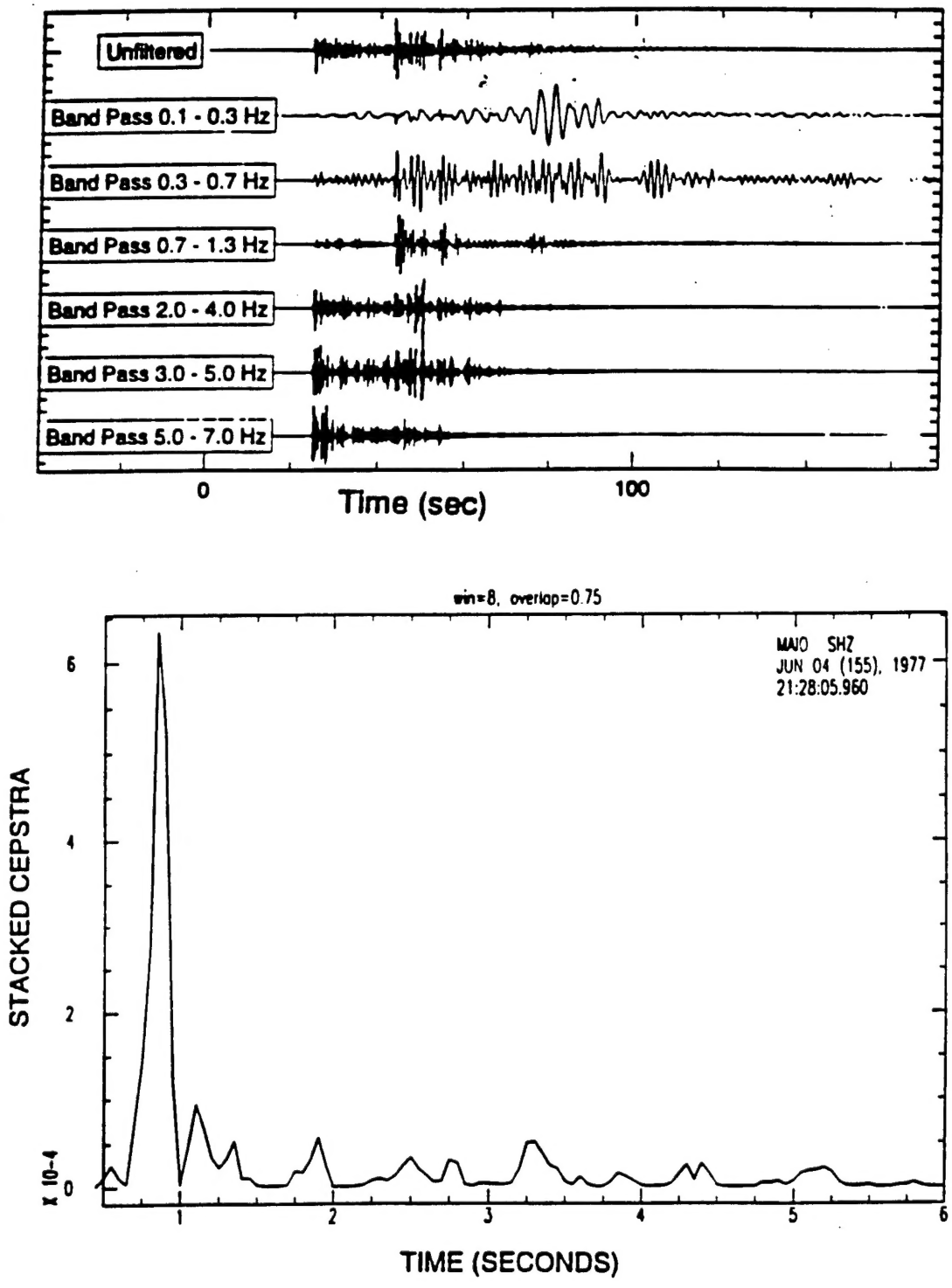

Figure 2. Original and band-pass filtered signals for a regional event on 6/04/77 in Iran recorded at station MAIO (top panel); product-stacked cepstra of sub-windows (bottom).

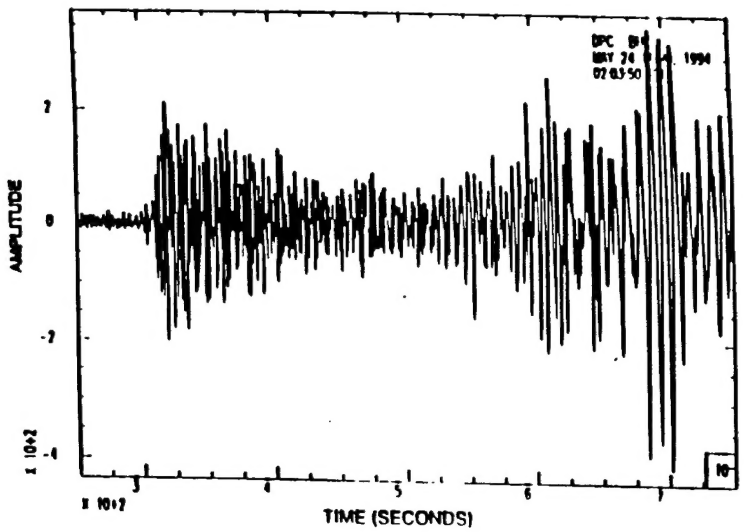

24 May 1994 event signal recorded by DPC station
Bandpass filtering 0.5 Hz - 5 Hz, origin time: 02:05:34.4

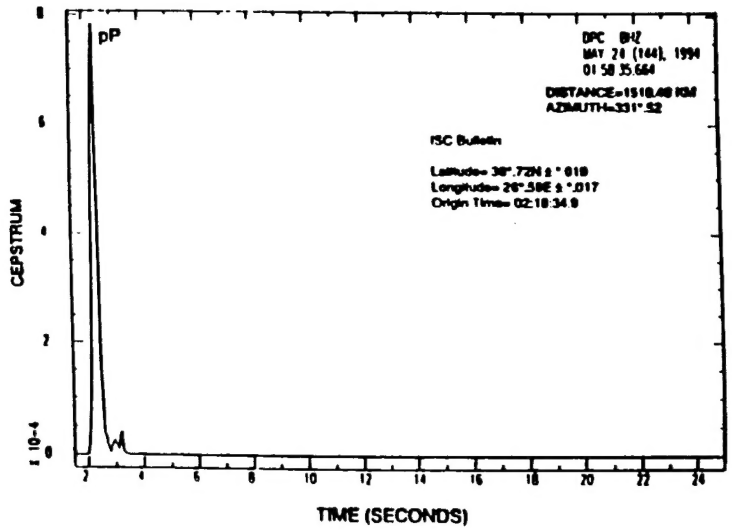

Product cepstrum of 24 May 1994 event recorded by DPC station
window length=40 sec., overlap=80% through envelope normalization

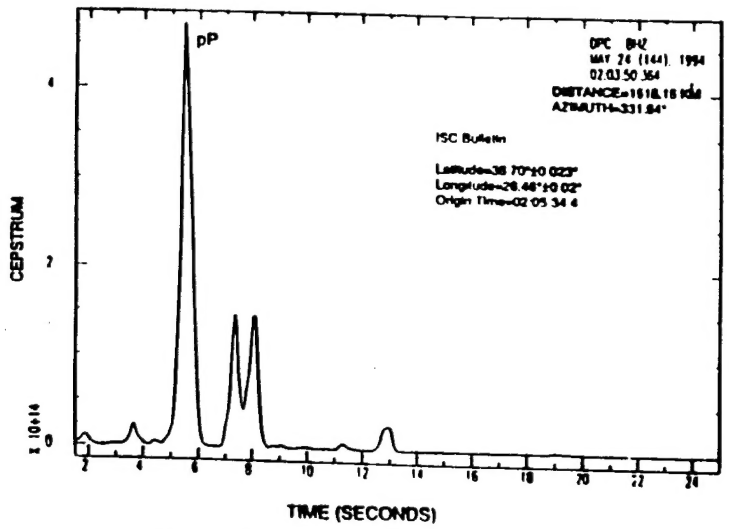

Product cepstrum of 24 May 1994 event recorded by DPC station
window length= 40 sec, overlap=80%

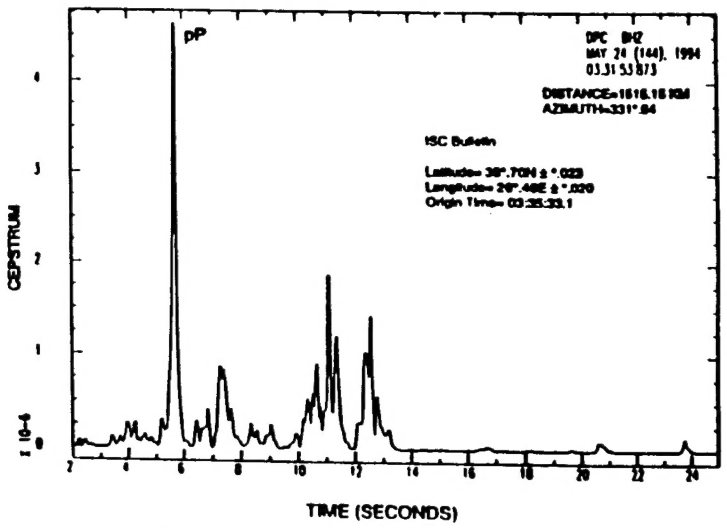

Product cepstrum of 24 May 1994 event recorded by DPC station
window length=40 sec., overlap=80% through envelope normalization

Figure 3. Mainshock signal and product-stacked cepstra for the mainshock and two aftershocks in western Turkey (Figure 4) recorded at regional station DPC.

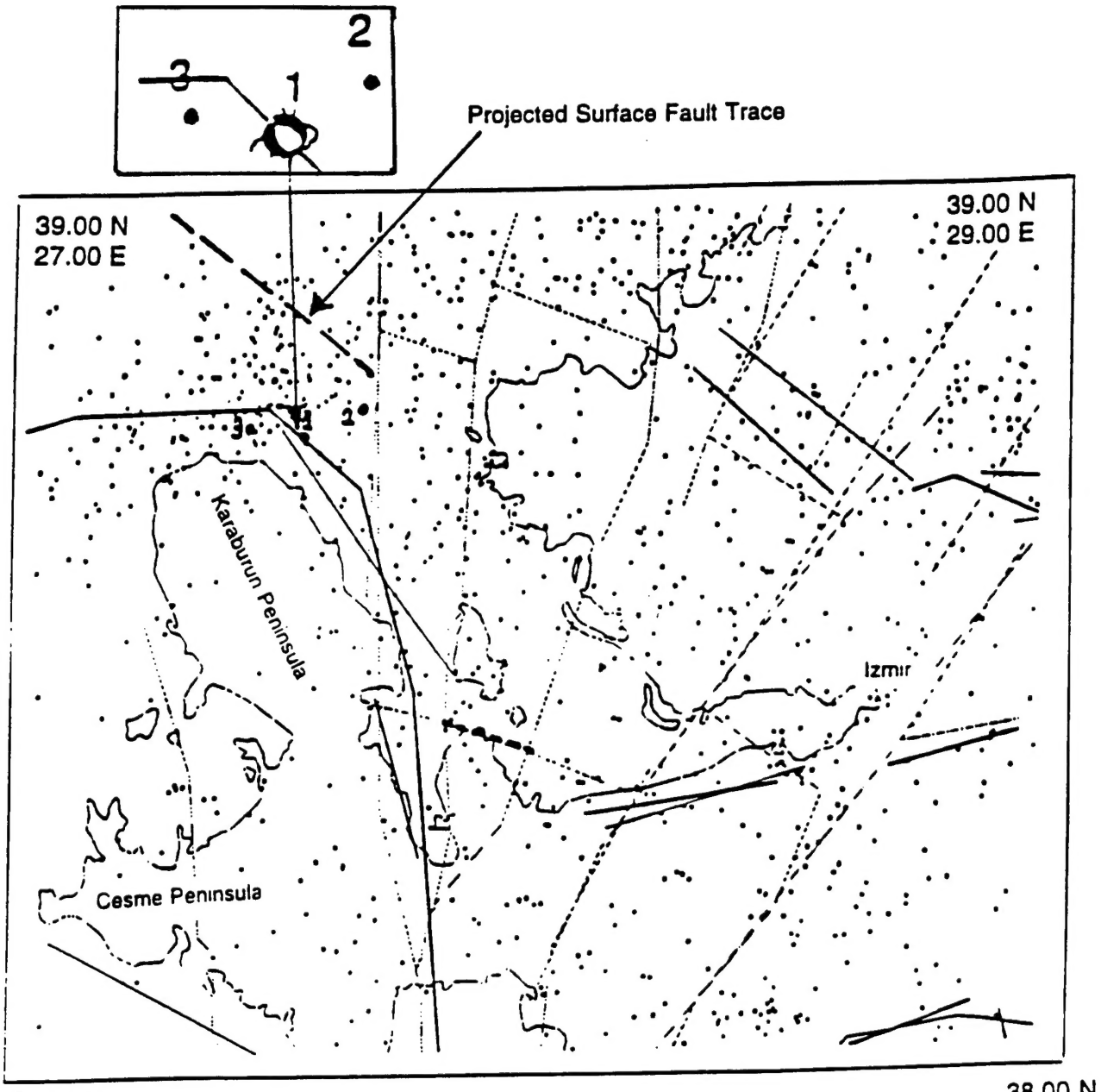

DEPTHS OF A MAINSHOCK AND TWO AFTERSHOCKS IN WESTERN TURKEY FROM CEPSTRAL STACKING

Event	Depth(Km)ISC	ISC (pP-P) (Km)	(pP-P) Cepst. Stack (Km)
1	10	16	17.0
2	10	13	7.5
3	0	11	16.0

Figure 4. Map showing location of the mainshock and two aftershocks in western Turkey and the projected surface fault trace. The table (bottom) shows a omparison of depth estimates for these events.

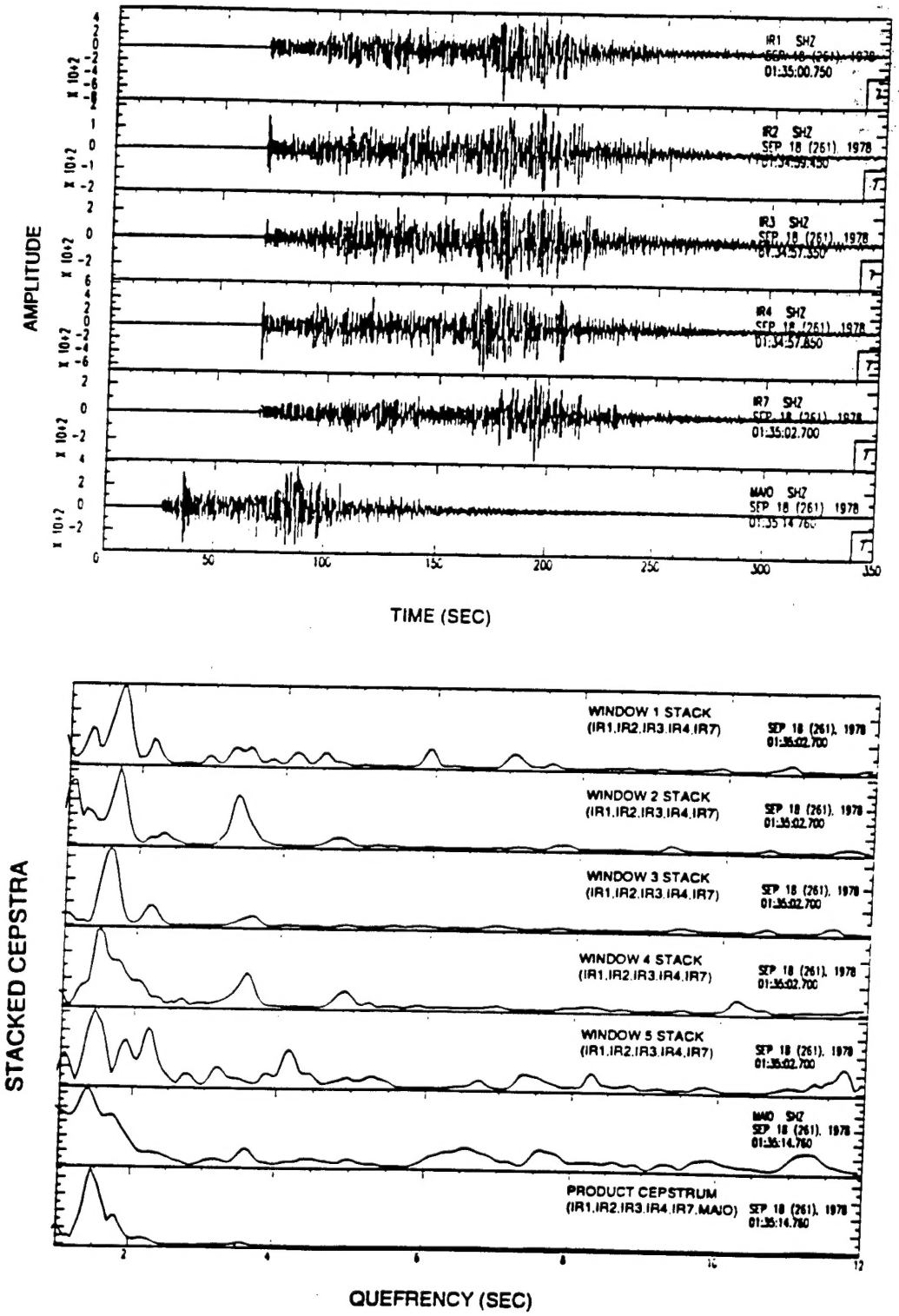

Figure 5. This example illustrates the combined cepstral stacking over the ILPA array and the SRO station MAIO for a regional event in Iran. The signals are shown in the top panel and the normalized, stacked cepstra are shown in the bottom panel. The last trace shows the composite product cepstrum for the ILPA array and MAIO; it has a prominent peak at a delay time of about 1.5 sec representing either the pP - P or sP - P time.